

**BOLU ABANT IZZET BAYSAL UNIVERSITY
THE GRADUATE SCHOOL OF NATURAL AND APPLIED
SCIENCES**



**SYNTHESIS, STRUCTURAL CHARACTERIZATION AND
OPTICAL PROPERTIES OF Ce, Eu AND Tb DOPED
STRONTIUM PYROBORATE NANOPARTICLES**

MASTER OF SCIENCE

FATMA YALÇIN

BOLU, SEPTEMBER 2019

BOLU ABANT IZZET BAYSAL UNIVERSITY
THE GRADUATE SCHOOL OF NATURAL AND APPLIED
SCIENCES
DEPARTMENT OF CHEMISTRY



SYNTHESIS, STRUCTURAL CHARACTERIZATION AND
OPTICAL PROPERTIES OF Ce, Eu AND Tb DOPED
STRONTIUM PYROBORATE NANOPARTICLES

MASTER OF SCIENCE

FATMA YALÇIN

BOLU, SEPTEMBER 2019

APPROVAL OF THE THESIS

SYNTHESIS, STRUCTURAL CHARACTERIZATION AND OPTICAL PROPERTIES OF Ce, Eu AND Tb DOPED STRONTIUM PYROBORATE NANOPARTICLES submitted by **Fatma YALÇIN** and defended before the below named jury in partial fulfillment of the requirements for the degree of **Master of Science in Department of Chemistry, The Graduate School of Natural and Applied Sciences of Bolu Abant İzzet Baysal University** in **9.09.2019** by

Examining Committee Members

Signature

Supervisor
Prof. Dr. Ayşe MORKAN
Bolu Abant İzzet Baysal University



Member
Prof. Dr. F. Devrim ÖZDEMİRHAN
Bolu Abant İzzet Baysal University



Member
Assoc. Prof. Dr. Mecit AKSU
Düzce University



Prof. Dr. Ömer ÖZYURT



Director of Graduate School of Natural and Applied Sciences ✓



To my beloved family

DECLARATION

I hereby declare that all information in this document has been obtained and presented in accordance with academic rules and ethical conduct. I also declare that, as required by these rules and conduct, I have fully cited and referenced all material and results that are not original to this work.

Fatma YALÇIN



ABSTRACT

SYNTHESIS, STRUCTURAL CHARACTERIZATION AND OPTICAL PROPERTIES OF Ce, Eu AND Tb DOPED STRONTIUM PYROBORATE NANOPARTICLES

MSC THESIS

FATMA YALÇIN

BOLU ABANT IZZET BAYSAL UNIVERSITY GRADUATE SCHOOL OF NATURAL AND APPLIED SCIENCES

DEPARTMENT OF CHEMISTRY

(SUPERVISOR: PROF. DR. AYŞE MORKAN)

BOLU, SEPTEMBER 2019

In this study, undoped and Ce, Eu and Tb ion doped Strontium Pyroborate nanoparticles were successfully synthesized by using Solution Combustion Synthesis (SCS), as well as the structural and optical properties of as-prepared products were comparatively characterized by Infrared spectroscopy (FTIR), X-Ray Powder Diffraction (PXRD), Ultraviolet-Visible (UV-VIS) Diffuse Reflectance Spectroscopy.

During the preparation process, $\text{Sr}(\text{NO}_3)_2$, H_3BO_3 , glycine, $\text{Tb}(\text{NO}_3)_3 \cdot 5\text{H}_2\text{O}$, $\text{Eu}(\text{NO}_3)_3 \cdot 5\text{H}_2\text{O}$, and $\text{Ce}(\text{NO}_3)_3 \cdot 6\text{H}_2\text{O}$ were used as the starting materials. The effect of temperature and dopant ion on the crystal structure of the products were examined. It was found that undoped and lanthanide element doped $\text{Sr}_2\text{B}_2\text{O}_5$ nanopowders obtained at 900°C were crystallized in monoclinic structure by examining XRD patterns.

The formation of $\text{Sr}_2\text{B}_2\text{O}_5$ was also confirmed with FT-IR spectroscopy by analyzing the vibrational modes belong to boron-oxygen bonds that occurred between 625 cm^{-1} to 1450 cm^{-1} .

Through UV-visible diffuse reflectance spectroscopic studies, the absorbance and reflectance spectra of the products were only observed in the ultraviolet region depending upon the host material, $\text{Sr}_2\text{B}_2\text{O}_5$. It was also detected that the optical band gap energies of the pyroborates synthesized were decreasing as the temperature increasing.

KEYWORDS: Solution Combustion Synthesis, Strontium pyroborate, lanthanide element, organic fuel, band gap

ÖZET

**Ce, Eu VE Tb KATKILI STRONSIYUM PİROBORAT
NANOPARÇACIKLARIN SENTEZİ, YAPISAL KARAKTERİZASYONU
VE OPTİK ÖZELLİKLERİ
YÜKSEK LİSANS TEZİ
FATMA YALÇIN
BOLU ABANT İZZET BAYSAL ÜNİVERSİTESİ
FEN BİLİMLERİ ENSTİTÜSÜ
KİMYA ANABİLİM DALI
(TEZ DANIŞMANI: PROF. DR. AYŞE MORKAN)**

BOLU, EYLÜL - 2019

Bu çalışmada, katkısız ve Ce, Eu ve Tb iyon katkılı $Sr_2B_2O_5$ nanoparçacıkları, Çözeltide Yanma Sentez Yöntemi kullanılarak başarılı bir şekilde sentezlenerek yapısal ve optik özellikleri Kızılötesi Spektroskopisi (FTIR), X-Işını Toz Kırınımı (PXRD), ve Ultraviyole-Görünür Bölge (UV-VIS) Diffüz Reflektans Spektroskopisi ile karakterize edildi.

Hazırlık sürecinde, başlangıç materyali olarak $Sr(NO_3)_2$, H_3BO_3 , glycine, $Tb(NO_3)_3 \cdot 5H_2O$, $Eu(NO_3)_3 \cdot 5H_2O$ ve $Ce(NO_3)_3 \cdot 6H_2O$ kullanıldı. Sıcaklık ve katkılanan iyonun ürünlerin kristal yapısı üzerindeki etkisi incelendi. $900^\circ C$ 'de katkısız ve lantanit elementleri katkılı $Sr_2B_2O_5$ nanotozların XRD desenleri incelendiğinde kristal yapının monoklinik olduğu bulundu.

$Sr_2B_2O_5$ 'ın oluşumu, 625 cm^{-1} ile 1450 cm^{-1} arasında meydana gelen bor-oksijen bağlarına ait titreşim modlarının FT-IR Spektroskopisi ile analiz edilmesiyle doğrulandı.

UV-Görünür Bölge Diffüz Reflektans Spektroskopisi çalışmaları sayesinde, ürünlerin soğurma ve yansıma spektrumları, ana malzeme olan $Sr_2B_2O_5$ 'a bağlı olarak sadece ultraviyole bölgede gözlemlendi. Sentezlenen piroboratların optik bant aralığı enerjilerinin sıcaklık arttıkça azaldığı tespit edildi.

ANAHTAR KELİMELEER: Çözeltide Yanma Sentez Yöntemi, Stronsiyum piroborat, lantanit elementi, organik yakıt, bant aralığı

TABLE OF CONTENTS

	<u>Page</u>
ABSTRACT	v
ÖZET	vi
TABLE OF CONTENTS	vii
LIST OF FIGURES	viii
LIST OF TABLES	x
LIST OF ABBREVIATIONS AND SYMBOLS	xi
1. INTRODUCTION	1
1.1 BORON	1
1.1.1 Boron Minerals and Reserves	2
1.1.2 Usage of Boron	3
1.2 BORATES	4
1.2.1 Classification of Borates	4
1.2.2 Pyroborates	5
1.2.3 Strontium Pyroborate	6
1.3 LANTHANIDE ELEMENTS	10
1.3.1 Properties of Lanthanide Elements	12
1.4 SYNTHESIS METHODS OF BORATES	21
1.4.1 Solution Combustion Synthesis	21
2. AIM AND SCOPE OF THE STUDY	22
3. MATERIALS AND METHODS	23
3.1 CHEMICALS	23
3.2 INSTRUMENTS	24
3.2.1 Fourier Transform Infrared Spectrophotometer	24
3.2.2 X-ray Powder Diffractometer	24
3.2.3 UV- VIS Spectrometer.....	24
3.2.4 Furnace.....	24
3.3 METHODS.....	25
3.3.1 Synthesis of Strontium Pyroborates.....	25
4. RESULTS AND DISCUSSION	27
4.1 Synthesis of Undoped and Doped Strontium Pyroborates	27
4.1.1 Structural Characterization of Undoped and Doped Sr ₂ B ₂ O ₅	29
4.1.1.1 FT-IR Spectroscopy Studies	29
4.1.1.2 Powder X-Ray Diffraction (PXRD) Studies	55
4.1.1.3 UV-VIS Spectroscopy Studies.....	67
5. CONCLUSION	79
6. REFERENCES	81
7. CURRICULUM VITAE	87

LIST OF FIGURES

	<u>Page</u>
Figure 1.1. Boron	1
Figure 1.2. The major industrial and domestic uses of boron minerals	3
Figure 1.3. Some borate structures. (i) Orthoborates. (ii) Pyroborates. (iii-v) Metaborates.	5
Figure 1.4. The crystal structure of strontium pyroborate.....	7
Figure 1.5. The worldwide usage of rare earth elements	11
Figure 1.6. Cerium Metal	13
Figure 1.7. Europium oxide under UV light	16
Figure 1.8. Tb ₂ (SO ₄) ₃ under UV light.....	18
Figure 4.1. Undoped Sr ₂ B ₂ O ₅ powder.....	27
Figure 4.2. FT-IR Spectra of Undoped Sr ₂ B ₂ O ₅	30
Figure 4.3. FT-IR Spectra of Ce ³⁺ Doped Sr ₂ B ₂ O ₅ at 400°C 10 minutes	32
Figure 4.4. FT-IR Spectra of Ce ³⁺ Doped Sr ₂ B ₂ O ₅ at 400°C.....	33
Figure 4.5. FT-IR Spectra of Ce ³⁺ Doped Sr ₂ B ₂ O ₅ at 500°C.....	34
Figure 4.6. FT-IR Spectra of Ce ³⁺ Doped Sr ₂ B ₂ O ₅ at 600°C.....	35
Figure 4.7. FT-IR Spectra of Ce ³⁺ Doped Sr ₂ B ₂ O ₅ at 700°C	36
Figure 4.8. FT-IR Spectra of Ce ³⁺ Doped Sr ₂ B ₂ O ₅ at 800°C.....	37
Figure 4.9. FT-IR Spectra of Ce ³⁺ Doped Sr ₂ B ₂ O ₅ at 900°C.....	38
Figure 4.10. FT-IR Spectra of Eu ³⁺ Doped Sr ₂ B ₂ O ₅ at 400°C 10 minutes	40
Figure 4.11. FT-IR Spectra of Eu ³⁺ Doped Sr ₂ B ₂ O ₅ at 400°C.....	41
Figure 4.12. FT-IR Spectra of Eu ³⁺ Doped Sr ₂ B ₂ O ₅ at 500°C	42
Figure 4.13. FT-IR Spectra of Eu ³⁺ Doped Sr ₂ B ₂ O ₅ at 600°C.....	43
Figure 4.14. FT-IR Spectra of Eu ³⁺ Doped Sr ₂ B ₂ O ₅ at 700°C.....	44
Figure 4.15. FT-IR Spectra of Eu ³⁺ Doped Sr ₂ B ₂ O ₅ at 800°C.....	45
Figure 4.16. FT-IR Spectra of Eu ³⁺ Doped Sr ₂ B ₂ O ₅ at 900°C.....	46
Figure 4.17. FT-IR Spectra of Tb ³⁺ Doped Sr ₂ B ₂ O ₅ at 400°C 10 minutes	48
Figure 4.18. FT-IR Spectra of Tb ³⁺ Doped Sr ₂ B ₂ O ₅ at 400°C.....	49
Figure 4.19. FT-IR Spectra of Tb ³⁺ Doped Sr ₂ B ₂ O ₅ at 500°C.....	50
Figure 4.20. FT-IR Spectra of Tb ³⁺ Doped Sr ₂ B ₂ O ₅ at 600°C.....	51
Figure 4.21. FT-IR Spectra of Tb ³⁺ Doped Sr ₂ B ₂ O ₅ at 700°C.....	52
Figure 4.22. FT-IR Spectra of Tb ³⁺ Doped Sr ₂ B ₂ O ₅ at 800°C.....	53
Figure 4.23. FT-IR Spectra of Tb ³⁺ Doped Sr ₂ B ₂ O ₅ at 900°C.....	54
Figure 4.24. PXRD Patterns of Undoped Sr ₂ B ₂ O ₅	56
Figure 4.25. PXRD Patterns of Ce ³⁺ Doped Sr ₂ B ₂ O ₅ at 400°C 10 minutes.....	57
Figure 4.26. PXRD Patterns of Ce ³⁺ Doped Sr ₂ B ₂ O ₅ at 800°C	58
Figure 4.27. PXRD Patterns of Ce ³⁺ Doped Sr ₂ B ₂ O ₅ at 900°C	59
Figure 4.28. PXRD Patterns of Eu ³⁺ Doped Sr ₂ B ₂ O ₅ at 400°C 10 minutes.....	60
Figure 4.29. PXRD Patterns of Eu ³⁺ Doped Sr ₂ B ₂ O ₅ at 800°C	61
Figure 4.30. PXRD Patterns of Eu ³⁺ Doped Sr ₂ B ₂ O ₅ at 900°C	62
Figure 4.31. PXRD Patterns of Tb ³⁺ Doped Sr ₂ B ₂ O ₅ at 400°C 10 minutes.....	63
Figure 4.32. PXRD Patterns of Tb ³⁺ Doped Sr ₂ B ₂ O ₅ at 800°C	64
Figure 4.33. PXRD Patterns of Tb ³⁺ Doped Sr ₂ B ₂ O ₅ at 900°C	65
Figure 4.34. UV-VIS Absorbance Spectra of Undoped Sr ₂ B ₂ O ₅	68
Figure 4.35. UV-VIS Reflectance Spectra of Undoped Sr ₂ B ₂ O ₅	68
Figure 4.36. UV-VIS Absorbance Spectra of Ce ³⁺ Doped Sr ₂ B ₂ O ₅ at 800°C	69

Figure 4.37.	UV-VIS Reflectance Spectra of Ce ³⁺ Doped Sr ₂ B ₂ O ₅ at 800°C	.69
Figure 4.38.	UV-VIS Absorbance Spectra of Ce ³⁺ Doped Sr ₂ B ₂ O ₅ at 900°C	.70
Figure 4.39.	UV-VIS Reflectance Spectra of Ce ³⁺ Doped Sr ₂ B ₂ O ₅ at 900°C	.70
Figure 4.40.	UV-VIS Absorbance Spectra of Eu ³⁺ Doped Sr ₂ B ₂ O ₅ at 800°C	.71
Figure 4.41.	UV-VIS Reflectance Spectra of Eu ³⁺ Doped Sr ₂ B ₂ O ₅ at 800°C	.71
Figure 4.42.	UV-VIS Absorbance Spectra of Eu ³⁺ Doped Sr ₂ B ₂ O ₅ at 900°C	.72
Figure 4.43.	UV-VIS Reflectance Spectra of Eu ³⁺ Doped Sr ₂ B ₂ O ₅ at 900°C	.72
Figure 4.44.	UV-VIS Absorbance Spectra of Tb ³⁺ Doped Sr ₂ B ₂ O ₅ at 800°C	.73
Figure 4.45.	UV-VIS Reflectance Spectra of Tb ³⁺ Doped Sr ₂ B ₂ O ₅ at 800°C	.73
Figure 4.46.	UV-VIS Absorbance Spectra of Tb ³⁺ Doped Sr ₂ B ₂ O ₅ at 900°C	.74
Figure 4.47.	UV-VIS Reflectance Spectra of Tb ³⁺ Doped Sr ₂ B ₂ O ₅ at 900°C	.74
Figure 4.48.	Optical Band Gap Energy of Ce ³⁺ Doped Sr ₂ B ₂ O ₅ at 800°C76
Figure 4.49.	Optical Band Gap Energy of Ce ³⁺ Doped Sr ₂ B ₂ O ₅ at 900°C76
Figure 4.50.	Optical Band Gap Energy of Eu ³⁺ Doped Sr ₂ B ₂ O ₅ at 800°C77
Figure 4.51.	Optical Band Gap Energy of Eu ³⁺ Doped Sr ₂ B ₂ O ₅ at 900°C77
Figure 4.52.	Optical Band Gap Energy of Tb ³⁺ Doped Sr ₂ B ₂ O ₅ at 800°C78
Figure 4.53.	Optical Band Gap Energy of Tb ³⁺ Doped Sr ₂ B ₂ O ₅ at 900°C78

LIST OF TABLES

	<u>Page</u>
Table 1.1. Commonly Used Boron Minerals Worldwide.....	2
Table 4.1. Observation During the Preparation of Ln Doped Sr ₂ B ₂ O ₅	28
Table 4.2. FT-IR band assignments of undoped Sr ₂ B ₂ O ₅	29
Table 4.3. FT-IR band assignments of Ce ³⁺ ion doped Sr ₂ B ₂ O ₅ at 900°C	31
Table 4.4. FT-IR band assignments of Eu ³⁺ ion doped Sr ₂ B ₂ O ₅ at 900°C	39
Table 4.5. FT-IR band assignments of Tb ³⁺ ion doped Sr ₂ B ₂ O ₅ at 900°C	47
Table 4.6. Crystallite Sizes of Undoped and Ln Doped Sr ₂ B ₂ O ₅	66
Table 4.7. Optical Band Gap Energy of Undoped and Ln Doped Sr ₂ B ₂ O ₅	75



LIST OF ABBREVIATIONS ANDSYMBOLS

EDS	: Energy Dispersive X-Ray Spectroscopy
FTIR	: Fourier-Transform Infrared Spectrophometer
ICDD	: International Centre for Diffraction Data
PXRD	: Powder X-Ray Diffractometer
RE	: Rare Earth
SAED	: Selected Area Electron Diffraction
SCS	: Solution Combustion Synthesis
TEM	: Transmission Electron Microscopy
UV-VIS	: Ultraviolet-Visible
W-LED	: White Light Emmision Diodes
EL	: Electro-Luminescence
XSL	: X-ray Stimulated Luminescence
DSC	: Differential Scanning Calorimetry
CTB	: Charge Transfer Band
TSL	: Thermally Stimulated Luminescence
3D	: Three Dimensional

ACKNOWLEDGEMENTS

I would like to express my deep and sincere gratitude to my supervisor Prof. Dr. Ayşe MORKAN for her support and professional guidance during my master studies, for useful critiques and important suggestions during research work, for her patience, motivation and immeasurable knowledge. I could not have imagined having a better thesis without her professional guidance.

I would also like to express my thanks to Prof. Dr. İzzet MORKAN for his support and moral motivation all the time.

I would like to thank to Seda KARABOĞA and Uzm. Nevin SOYLU for providing and informing TG/DTA and PXRD analysis.

Especially, I would like to thank to Gülden ÖZEN KAHVECİ and Umut KESKİN for their helps.

I would also like to thank my labmate and also my dearest friend, Liska FADLIYANI for helping and discussions about our work, for every time we were working together, and for all the fun we have had in the last two years.

There is special thanks to source of my happiness BTS that is Korean boy group has 7 members; Namjoon KIM, Seokjin KIM, Yoongi MIN, Hoseok JUNG, Jimin PARK, Taehyung KIM and Jeongguk JEON, for teaching me to love myself, inspiring me to find my dream, and helping me stay focused on my study with their music.

I would like to express my love to my friends Şeyda KASAP and Yasemin CEVİZOĞLU, who were of great support in deliberating over our problems and findings, as well as providing happy distraction to rest my mind outside of my research.

Last but not the least, I would like to express my thanks to my lovely parents, Zeki YALÇIN and Huriye YALÇIN, my brother, Onur YALÇIN for their wise counsel and sympathetic ear. You are always there for me.

1. INTRODUCTION

1.1 BORON

Boron is a metalloid that located between metals and nonmetals in group III B of the periodic table with relative atomic mass of boron is 10.81 and Atomic number is 5. Boron consists of two isotopes, which include 19.78% B^{10} that makes it a great neutron absorber and 80.22 B^{11} in its pure element. Unlike the elements around boron such as carbon and silicon, it has one less number of valence orbitals that known as “electron deficiency”. (Chatterjee, 2007) (Kar et al., 2006) (Kistler and Helvaci, 1994) (Greenwood and Earnshaw, 1997).

There are two types of boron namely crystalline boron and amorphous boron, which are black shiny solid and brown powder, respectively. The atoms in boron crystal form in a complex 3D arrangement, which are extremely hard and can be easily broken. Moreover, it is very stable in low temperature and can reacts with other chemicals in high temperature. (Beatty, 2005).

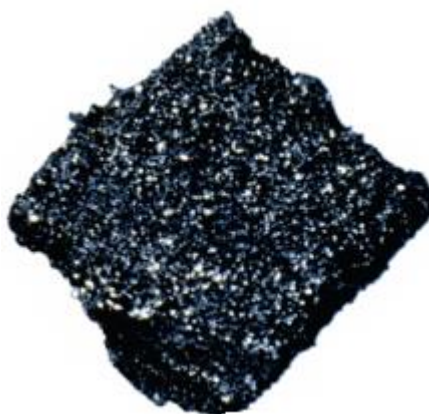


Figure 1.1. Boron

1.1.1 Boron Minerals and Reserves

Boron is a unique element that is found in rocks, soil, and water with concentration of boron 2-100 ppm, 10-20ppm and <0.01-9.6 ppm, respectively. The main deposits of boron minerals form in volcanic activity area and the waters of hot springs. The boron minerals contents in the world consist of Turkey 45%, USA 21%, Kazakhstan 17%, China 8.6% and Argentina 7.3%. In last decades, the production of boron minerals in Turkey has developed and surpassed that of the USA. In Turkey, the boron mineral's production is command by the national mining enterprise that is called Eti Maden. Its most common boron minerals such as ulexite, colemanite and borax are provided from mines in the Bigadic, Emet and Kirka Districts. (Kistler and Helvacı, 1994) (Greenwood and Earnshaw, 1997)

Table 1.1. Commonly Used Boron Minerals Worldwide.

Mineral	Formula	B ₂ O ₃ (%)	Regions of mineral
Kernite (Rasortie)	Na ₂ B ₄ O ₇ .4H ₂ O	51.0	Kırka, USA, and Argentina
Pandermite (Priceite)	CaB ₁₀ O ₁₉ .7H ₂ O	49.8	Sultancayır and Bigadic
Ulexite (Boronatrocaltite)	NaCaB ₅ O ₉ .8H ₂ O	43.0	Kırka, Bigadic, Emet, and Argentina
Colemanite	Ca ₂ B ₆ O ₁₁ .5H ₂ O	50.8	Emet, Bigadic, Kucukler, and USA
Probertite (Kramerite)	NaCaB ₅ O ₉ .5H ₂ O	49.6	Kestelek, Emet, and USA
Szaibelyite (Ascharite)	MgBO ₂ .2OH	41.4	Russia
Boraxs (Tincal)	Na ₂ B ₄ O ₇ .10H ₂ O	36.6	Kırka, Emet, Bigadic, and USA
Boracite (Stassfurite)	Mg ₆ B ₁₄ O ₂₆ C ₁₂	62.2	Germany
Hydroboracite	CaMgB ₆ O ₁₁ .6H ₂ O	50.5	Emet

1.1.2 Usage of Boron

As an industrial chemical element, boron is applied in large scale of area and is mostly used as ferroboron. Besides that, boron minerals also used as plant micronutrient, Fibre-reinforced metal matrix composites, nuclear reactor, optical fibre, semiconductor, Pyrotechnics, rocket igniter, neutron detecting instrument and permanent magnet. (Chatterjee, 2007)

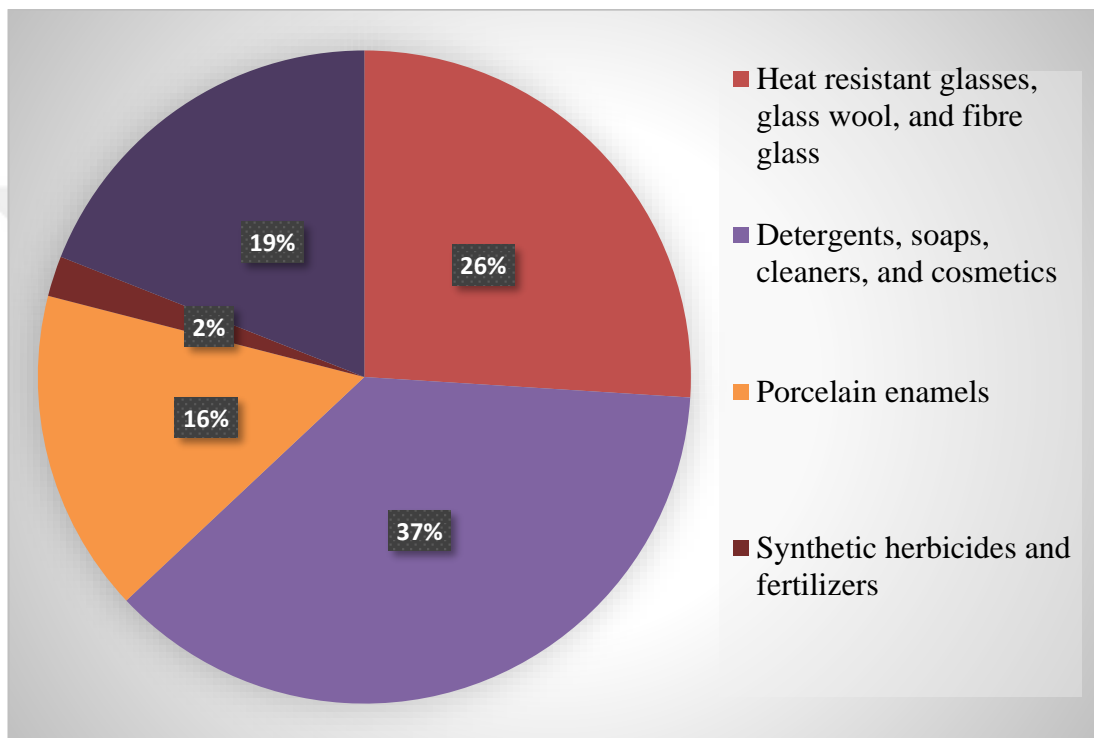


Figure 1.2. The major industrial and domestic uses of boron minerals

Borate minerals were utilized in many field since 8th century as a flux that uses to assay and refine gold and silver and these days they also applied in food preservatives, medicines, ceramic glazes. They use mainly as the insulation of glass fiber, detergents, textile glass fiber, ceramics, and borosilicate glass. (Travis and Cocks, 1984) (Kistler and Helvaci, 1994)

1.2 BORATES

Boron forms strong covalent boron-oxygen bonds in compounds due to its high affinity of oxygen which known as borates and it is also defined as salts of boric acid. The primary structural standards of crystalline metal borates are;

1. Boron can link either three oxygens to form trigonal BO_3 and tetrahedral BO_4
2. The cornersharing of triangles and tetrahedral boron-oxygen are resulted in Polynuclear anions
3. Protonatable oxygen atoms will be protonated in the hydrated borates,
4. The hydrated insular groups may polymerize in various ways by splitting out water; this process may be accompanied by the breaking of boron-oxygen bonds within the poly anion framework.
5. Complex borate polyanions may be modified by attachment of an individual side group, such as (but not limited to) an extra borate tetrahedron, an extra borate triangle, 2 linked triangles, an arsenate tetrahedron, and so on.
6. Isolated $\text{B}(\text{OH})_3$ groups, or polymers of these, may exist in the presence of other anions. (Greenwood and Earnshaw, 1997)

1.2.1 Classification of Borates

Borates are classified based on its structural anionic linking such as chain, sheet, and framework structures. The compounds that contains monomeric trigonal BO_3 units are known as the rare-earth orthoborates M_3BO_3 for instance $\text{CaSnIV}(\text{BO}_3)_2$ and $\text{Mg}_3(\text{BO}_3)_2$. The pyroborates are formed by the existence of binuclear trigonal planar BO_3 such as $\text{Mg}_2\text{B}_2\text{O}_5$, $\text{Co}_2\text{B}_2\text{O}_5$ and $\text{Fe}_2\text{B}_2\text{O}_5$. Furthermore, Trinuclear cyclic of BO_3 is found in metaborates, $\text{M}_3\text{B}_3\text{O}_6$ for example NaBO_2 and KBO_2 . Polynuclear linkage of BO_3 units includes infinite chains of BO_2

and 3D linkage of planar BO_3 units occurs in the $\text{Ca}(\text{BO}_2)_2$ and borosilicate mineral, respectively. (Greenwood and Earnshaw, 1997) (Helvacı, 2005)

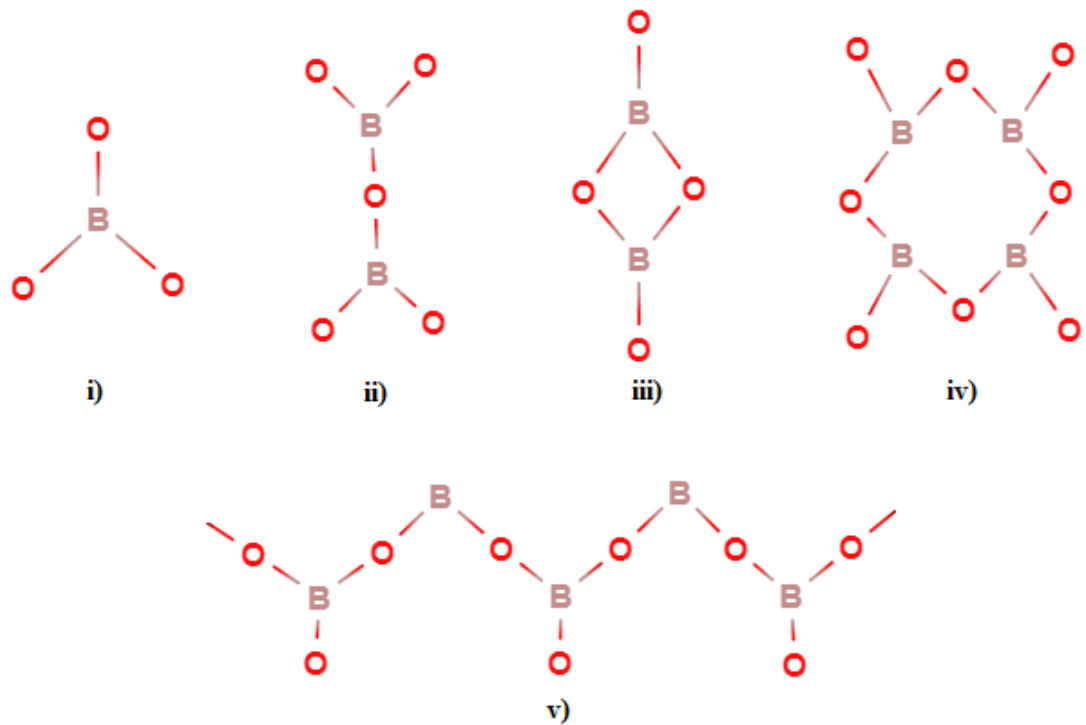


Figure 1.3. Some borate structures. (i) Orthoborates. (ii) Pyroborates. (iii-v) Metaborates.

1.2.2 Pyroborates

Crystals of Inorganic borate have been analyzed in many researches due to the coordinations of boron and oxygen atoms as triangular BO_3 and tetrahedral BO_4 that also can be polymerized into different formed B–O groups namely isolated B_2O_5 , two-four body, six-membered ring, and so on. The isolated B_2O_5 is also known as pyroborates that can be crystallized in various space groups such as $P21/c$, $Pbca$, etc. The complicated and unique structures of metal pyroborates give a valuable source for obtaining functional materials. (Wang and Liang, 2019) (Guo et al., 2014)

Metal pyroborates are a great mechanical ceramic material with good thermal properties and have high corrosion resistance. They also known for their attractive insulation properties, superb strength and elasticity, light weight, etc. (Elssfah et al.,

2007) (Li et al., 2004) According to their optical properties, range of short wavelength in metal pyroborates are higher transmittance of UV alongside thresholds damage. For these reason, they have been used in many applications such as optical and medical applications. (Malandrino et al., 2007)

There are many metal pyroborates that have been studied such as alkaline-earth metal pyroborates which are used as flame-retardants, matrix of luminescent and nonlinear optical matters. (Wang and Liang, 2019) The arrangement of B_2O_5 group of metal pyroborates are depends on the size of alkali-metal cations which are become more coplanar in higher size. The simplest triangular group in borates simplifies the pyroborates as anion, $B_2O_5^{4-}$ which are the coplanarity of terminal BO_2 torsion angles of terminal BO_2 lies between 1.6° to 67.0° and the angles of B-O-B in range of 111.8° - 138.7° . When combined with the cation, the pyroborates groups are paired with applicable polarizability coefficients resulting as effective materials for conversion of small threshold characteristics and for phase matching with small angular sensitivity. (Cheng et al., 2000)

In the past decades there are many studies about metal pyroborates for example $Mg_2B_2O_5$, $Ba_2B_2O_5$, $Ca_2B_2O_5$, $SrCdB_2O_5$ and $Sr_2B_2O_5$. (Guo et al., 2014)

1.2.3 Strontium Pyroborate

Metal borates have been studied in recent years because of their different types of structure and their properties such as great optical quality, good tolerance for laser damage and wavelength transparency in wide range. There are two types of hybridized borate atoms orbitals, which are sp^2 planar and 3D sp^3 , it form different kinds of B_xO_y complex group of anions by integrating three or four oxygen atoms. Strontium pyroborates have attracted many attentions due to their great stability, demand low cost raw materials for example H_3BO_3 for the reaction process, synthesizes at low temperature, simple synthesis, have an excellent thermal and chemical stability. Alkaline borates like strontium pyroborates have been studied in large area as nonlinear optical crystals such as Field Emission, Plasma Display Panels (PDPs), Electro-Luminescence (EL) panels and Displays (FEDs). (Yildiz and

Erdođmuş, 2018) Furthermore, the transfers of charged between oxygen and strontium atomic orbitals caused critical polarizability contributions. (Lin, 1999)

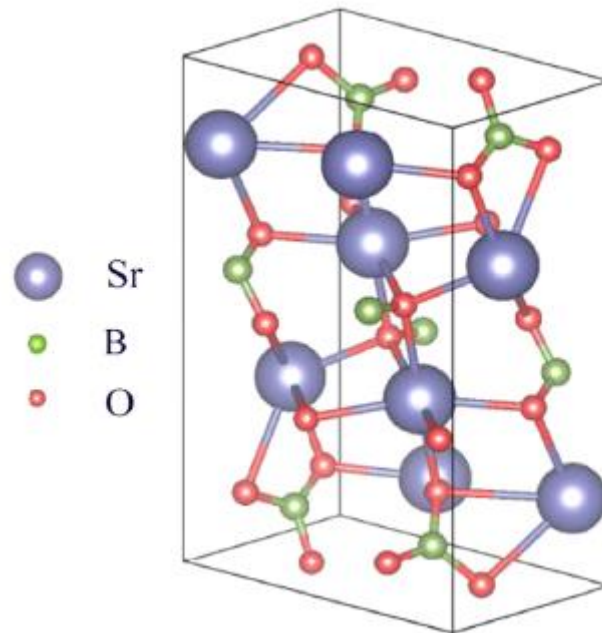


Figure 1.4. The crystal structure of strontium pyroborate

Alkaline earth borates are also favorable phosphor materials that known for their affordable cost, low synthesis different crystals structures and excellent stability. The phosphors materials are mainly focused on the inorganic compounds with oxygen such as oxides, aluminates, aluminoborates, silicates and borates. In luminescence, borates are used for host materials due to their transparency in UV region and higher optical threshold damage. They also have been applied in white light-emitting diode (LED) such as protection of environment, long lifetime and energy which is considered as solid-state light sources in incandescent lamps and fluorescent lamps. (Panse et al., 2016)

In recent years, strontium pyroborates have been studied by various methods due to their opportunity for being nonlinear optical material, white-light emitting diodes, phosphors and so on. In 1999, $\text{Sr}_2\text{B}_2\text{O}_5$ has synthesized by high temperature solution reaction method. Mixture of SrCO_3 , KFB_4 and H_3BO_3 was prepared and they were heated to 1193K for 15 hour, after that temperature quickly decreased to 1053K and slowly cooled to 973K in the rate of 0.011K in an hour. After getting 973K the temperature was decreased to room temperature. Colorless crystals of

$\text{Sr}_2\text{B}_2\text{O}_5$ were obtained. Its crystal structure was characterized as monoclinic by single-crystal X-ray diffraction techniques. Its electronic structure was also calculated by using INDO/S method. (Lin, 1999)

Cheng et al (2000) has studied optical properties and electronic structure of magnesium, calcium and strontium pyroborates. Their refractive indexes have compared, it is shown that refractive index increases when cation radius increases, but their energy gap decrease.

Using mixture of SrCO_3 , Tb_4O_7 , H_3BO_3 , and Li_2CO_3 , Tb^{3+} , Li^+ co-doped $\text{Sr}_2\text{B}_2\text{O}_5$ green phosphor has been synthesized by solid-state reaction method. Heating process has been carried out as at 400°C for 1 h, after that at 900°C for 3h. The structure of obtained crystals has been determined X-ray diffraction. In addition, photoluminescence excitation and emission spectra of crystals were measured by using Hitachi F-7000 spectrofluorometer. (Wang et al., 2012)

In 2012, Sun et al have synthesized Ce^{3+} and Tb^{3+} co-doped strontium pyroborate via solid-state method by using SrCO_3 , H_3BO_3 , CeO_2 and Tb_4O_7 as the starting materials. The luminescence and phase structure properties of resulted crystals were investigated by using photoluminescence emission and X-ray diffraction, respectively. Ce^{3+} , Tb^{3+} co-doped strontium pyroborate indicated blue emission by f-d transition of Ce^{3+} ions and green emission by f-f transition of Tb^{3+} ions. Due to calculation of energy transfer efficiency between Ce^{3+} and Tb^{3+} ions as 90%, this strontium pyroborate phosphor recognized as white LEDs. (Sun et al., 2012)

Liu et al have synthesized Eu^{2+} doped $\text{Sr}_2\text{B}_2\text{O}_5$ via high temperature solid-state method. The crystal structure of resulted product was determined by X-Ray diffraction as monoclinic. In unit cell volume and lattice parameters, decreasing was observed due to doping Eu^{2+} ion. (Liu et al., 2013)

Using solid-state reaction, Tm^{3+} , Na^+ co-doped strontium pyroborate was synthesized as white LEDs and the luminescence and crystal structure characteristics were determined. Effect of charge compensation of reagents was analyzed on luminescence and excellent blue emission of this phosphor was observed. (Cai et al., 2014)

Europium and sodium ions doped strontium pyroborate have been synthesized using solid-state reaction at high temperature. Eu_2O_3 , Na_2CO_3 , SrCO_3 , and H_3BO_3 have been used as starting materials. Mixing starting materials were heated at 400°C for 1 hour, and then continued to heat at 850°C for 3 hours. Phosphor with red emission was obtained as a resulted product, and characterized by X-Ray Diffraction, scanning electron microscope, and spectrofluorometer. (Ying et al., 2014)

Using SrCO_3 , boric acid, and Eu_2O_3 as raw materials, Eu^{3+} ion doped $\text{Sr}_2\text{B}_2\text{O}_5$ has been successfully synthesized by solid-state method at 1050°C for 2 hours. The structure of resulted phosphor product was investigated by XRD as monoclinic. Moreover, the luminescence analysis show that the phosphor product can be applied in white LED. (Liu et al., 2015)

In 2016, the luminescence properties and crystal structure of terbium and yttrium ions doped strontium pyroborate phosphors were investigated using solid-state reaction method by Zhi-Gang et al. X-Ray Diffraction studies show that these phosphors have pure monoclinic crystal structure.

Panse et al (2016) has reported the preparation of Tb^{3+} ion doped strontium pyroborate using combustion synthesis method by mixing SrNO_3 , H_3BO_3 , NH_2CONH_2 and Tb_4O_7 . The mixture was heated at 550°C for short time, and at 600°C for 12 hours. Green phosphor material was obtained and its crystal structure, morphology, and luminescence properties were investigated by XRD, SEM, infrared spectrometer, and fluorescence spectrometer.

Using impedance spectroscopy, X-ray diffraction, and differential scanning calorimetry, crystal structures of alpha, beta and gamma strontium pyroborates were investigated. Their phase transition is obtained at 378°C , 364°C , and 292°C , respectively. It is shown that alpha and gamma strontium pyroborates have monoclinic structures, however beta strontium pyroborate has triclinic structure. (Volkov et al., 2017)

Using SrCO_3 , boric acid, and PbCO_3 as starting materials, different concentration of lead ion doped strontium pyroborate has been studied by solid-state method at 400°C for 1h, and 900°C for 3h. After obtaining nice phosphors, their

monoclinic crystal structure has been investigated by XRD. By photoluminescence spectrometer, their emission intensities can be affected with increasing concentration. (Yildiz and Erdoğan, 2018)

Solid state and sol-gel synthesis methods were applied for the preparation of europium ion doped, SrB_4O_7 , $\text{Sr}_2\text{B}_2\text{O}_5$, and $\text{Sr}_3\text{B}_2\text{O}_6$. Their crystal structures and luminescence properties were studied by using X-Ray Diffraction, and fluorescence spectrometer. The luminescence analysis shows that these phosphor products have different emission properties. Europium ion doped strontium pyroborate and $\text{Sr}_3\text{B}_2\text{O}_6$ give red emission spectra, even though Eu^{3+} ion doped SrB_2O_4 gives orange emission spectra. (Wang et al., 2004)

1.3 LANTHANIDE ELEMENTS

Lanthanides are inner transition elements that are also known as rare earths because they exist in the mixture that is considered as earths which means could not be changed by heat in early Greece and they are discovered as oxides. The rare part assigned to the obstacle in finding the pure elements although they are more abundant than silver and lead. The compounds of lanthanide are identical which make them difficult to be compared. Ionic characteristics of lanthanide and alkaline earth metals are alike to each other with only differ in their oxidation states that are tripositive and dipositive, respectively. Individual lanthanides could be separated because they yielded oxidation states other than three. Thus the commonest lanthanide, cerium, exhibits oxidation states of +3 and +4. (Chambers and Holliday, 1975)

Lanthanides have 17 elements which included Sc, Y, The light lanthanides (LREEs); La, Ce, Pr, Nd, Pm, Sm, Eu and Gd that have no paired 4f electrons, heavy lanthanides (HREEs); Dy, Ho, Er, Tm, Yb and Lu. Sometimes, Geochemists exclude Eu because of its anomalous properties and classified as the middle lanthanides (MREEs) that consist of Nd, Pm, Sm, Eu, Gd and Tb. Due to its similar chemical properties with Dy-Ho, Yttrium can be included as heavy lanthanides. Besides, Scandium is not included in any group because of having different geochemical and chemical behaviors. Rare earths do not exist in nature as elements, but they oxidized in salts and minerals due to their electropositive nature. (Bünzli, 2013)

Lanthanides have specific chemical, magnetic and optical properties that affect their electronic structure. they play important role in many applications as catalysts for oil cracking, agriculture, high coercivity magnets used in motorization or audio applications, lighting devices, lasers, telecommunications, imaging, and biomedical analyses even though they used in small quantities. The uses area of rare earths have developed in daily life such as the petroleum industry, key technologies, television screens, and computer systems. They are also applied in the military and several governments as strategic materials and emerging clean technologies namely catalytic converters, energy-efficient lighting, wind power turbines, and electric vehicles. (Zhou et al., 2017) (Alonso et al., 2012)

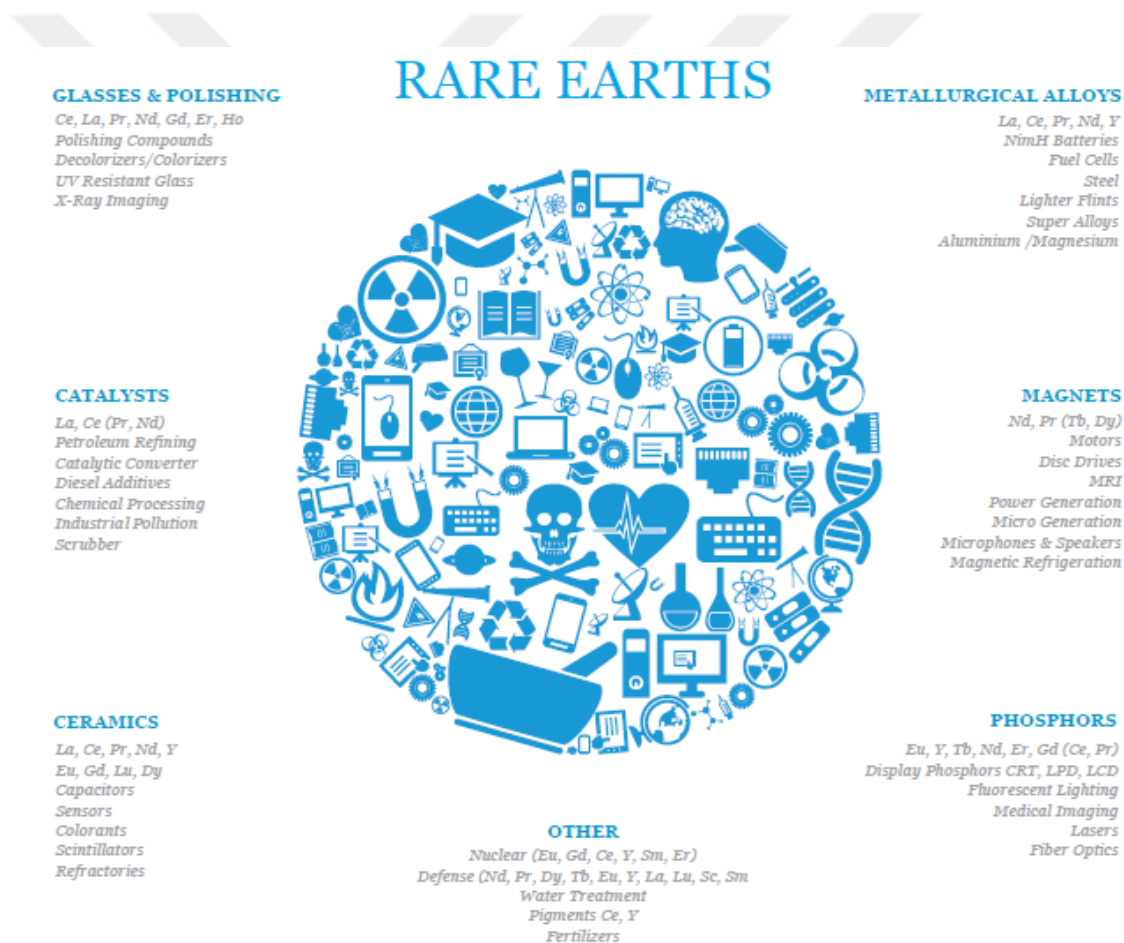


Figure 1.5. The worldwide usage of rare earth elements

1.3.1 Properties of Lanthanide Elements

Lanthanides devastate rapidly in air and a silvery white soft metals. The increase in atomic number increase their hardness while samarium remaining steel hard. The melting point of lanthanides are 1000 to 1200 K but the melting point of samarium is 1623 K. They are good heat and electricity conductors that have common metal structure. In the solid and solution form many lanthanide ions are colored. The color of these ions refer to existence of electrons of f orbital. Whereas, La^{3+} and Lu^{3+} ions give any color because of their narrow absorption bands within the excitation of f level. However the lanthanides ions are all paramagnetic while only *f* 0 type; La^{3+} and Ce^{4+} , and the *f* 14 type; Yb^{2+} and Lu^{3+} are diamagnetic. The maximum paramagnetism is in Nd. The other properties vary evenly except for Europium and Ytterbium and sometimes for Samarium and Thulium. (Hassan, 2011)

The characteristics of lanthanides are different from the d-block metals as follows;

1. A highly large range of coordination numbers.
2. The ligand steric factors are used to determine the coordination geometries
3. The labile ionic complexes are formed by the exchange of ligand.
4. Their magnetic and spectroscopic properties of lanthanides are not affected widely by the ligand.
5. In comparison, lanthanide metals have sharper electronic spectra and smaller crystal-field splittings than the d-block metals.
6. Lanthanides favor nonionic ligands with high electronegativity.
7. Lanthanides easily form hydrated complexes that cause the change in coordination numbers.
8. In the absent of complexing agents, insoluble hydroxides cannot be precipitated at neutral pH values.

9. Lanthanides have oxidation number that is +3 and usually in aqueous solution.

10. The multiple bonds of $\text{Ln}=\text{O}$ or $\text{Ln}\equiv\text{N}$, and stable carbonyls are not formed in lanthanide elements which also do not have 0 oxidation state.(Cotton, n.d.)

These studies are focused on doping effects of three lanthanides elements which are Cerium, Europium, and Terbium.

The most sufficient lanthanide element is Cerium that is discovered in many minerals such as monazite, samarskite, bastnasite, allanite, and certie. The most essential sources of cerium are Monazite and bastnasite which are found in Travancore, India, Brazil, and Southern California. Cerium is the most reactive metal that is shining iron-gray color, malleable, not radioactive, and oxidizes easily at room temperature. In some solutions such as alkali solutions, hot water, dilute and concentrated acid solutions, Cerium dissolves quickly, but dissolves slowly in cold water. It is located in the inner 4f level which make it required small amounts of energy to alter the relative occupancy that cause the increase to dual valency states. (Husted R, 2000)

Cerium is applied for production of cigarette lighters with pyrophoric alloy, and for self cleaning ovens it is used as a hydrocarbon catalyst. It is also applied as decolorizer and component in the glass manufacturing, carbon-arc lighting in picture industry, and as a catalyst.in nuclear applications, petroleum refining and metallurgical areas. (Husted R, 2000)

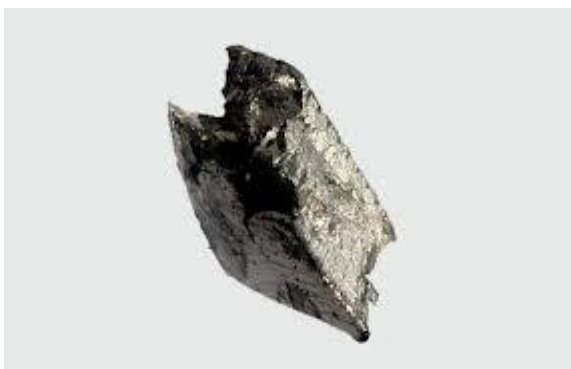


Figure 1.6. Cerium Metal

In 2001, Ce³⁺ doped LuAl₃(BO₃)₄ (Lu= Y, Gd) has been synthesized by solid state reaction. Characterization of resulted products has been investigated by X-ray diffraction, DTA-TG, MAS-NMR measurements. The results show that GdAl₃(BO₃)₄ has no structural transition and identical melting point. Cerium ion doped products give similar emission spectra in luminescent analysis. (Aloui-Lebbou et al., 2001)

Ternane et al (2002) has reported the preparation of cerium ion doped calcium borophosphate with formula as 10CaO_(6-x)PO_{2.5x}BO_{1.5}·tH₂O (x = 0, 0.3, 0.5) by using solid state reaction with reducing atmosphere. Characterization of the resulted product has been examined by X-ray diffraction, IR spectroscopy, and MAS-NMR analysis and they show that products have apatite structure.

Cerium ion doped lutetium orthoborate powders have been studied with using sol-gel synthesis. The resulted powders are characterized by X-ray diffraction, FT-IR spectroscopy, and SEM analysis. The results of analysis show that products have vaterite type even though calcination process are applied at 800°C, and cerium ion does not affect into structure of the product.(Mansuy et al., 2004)

Using BaCO₃, boric acid, and CeO₂ as a raw materials, undoped and cerium ion doped BaB₄O₇ products have been synthesized by a melting method. X-ray diffraction patterns of resulted materials show that they have monoclinic crystal structure. Thermoluminescence studies give that products have maximal efficiency and promise this phosphor for using in ionizing radiation dosimetry. (Yazici et al., 2006)

Jiang et al (2007) has studied cerium ion doped LiSr₄(BO₃)₃ phosphors via high temperature solid state reaction with using Li₂CO₃, SrCO₃, H₃BO₃, and CeO₂ as raw materials. Thermoluminescence and dosimetric characteristics of resulted products have been examined and show that 1% mol cerium ion doped borates have highest thermoluminescence intensity.

Afterwards, by using Czochralski method, single crystal of cerium ion doped Li₆Gd(BO₃)₃ has been investigated. Some macro defects and concave growth face problems have been observed. There is some solution about these problems like increasing the diameter of crucible for avoiding interface inversion. In order to avoid crystal cracking, the temperature cannot be too high. (Yang et al., 2009)

Yang et al (2010) has also studied cerium ion doped $\text{Li}_6\text{Lu}(\text{BO}_3)_3$ by Czochralski method. The characterization of resulted phosphors has been examined by X-ray diffraction, DSC, ultraviolet fluorescence spectrometer, and X-ray stimulated luminescence (XSL) spectrometer. Results of analysis show that the product has monoclinic system and decay time faster than cerium ion doped $\text{Li}_6\text{Gd}(\text{BO}_3)_3$. Due to these properties, the product can be considered as a promising scintillator.

Using glycothermal synthesis, cerium ion doped YBO_3 mesocrystals have been synthesized. The morphology and particle size of the products were characterized by XRD, TEM, SEM, the selected area electron diffraction (SAED) measurements, dynamic light scattering, and PLE. The results show that submicrometer sized particles of cerium ion doped YBO_3 blue-emitting phosphor has been obtained with hexagonal structure. Photoluminescence studies explain that higher concentration of cerium ion can cause lower PL lifetime. (Hara et al., 2013)

Using $\text{AlCl}_3 \cdot 6\text{H}_2\text{O}$, Y_2O_3 , H_3BO_3 , CeO_2 and NH_4NO_3 as raw material, cerium ion doped yttrium aluminium borate phosphors have been synthesized by modified solid state reaction. Their properties about purity and emission have been studied by XRD and photoluminescence spectroscopy. The results show that resulted products have rhombohedral structure and violet-blue emission. Also TGA study gives that the resulted phosphors have high thermal stability. (Kumar et al., 2014)

Polycrystalline cerium ion doped $\text{K}_3\text{YB}_6\text{O}_{12}$ phosphors have been synthesized by facile chemical sol-gel synthesis. The crystal structure and luminescence properties have been characterized by X-ray diffraction, and spectra of photoluminescence excitation (PLE). These phosphors have blue to yellowish green color emission and red shift with emission wavelength due to cerium ion doped. (Yang et al., 2016)

Chauhan et al (2017) have synthesized cerium ion doped $\text{LaBaB}_9\text{O}_{16}$ phosphor with using $\text{La}(\text{NO}_3)_3 \cdot 6\text{H}_2\text{O}$, $\text{Ba}(\text{NO}_3)_2 \cdot 2\text{H}_2\text{O}$, $\text{H}_3\text{BO}_3 \cdot 2\text{H}_2\text{O}$, $\text{Ce}(\text{NO}_3)_3 \cdot 6\text{H}_2\text{O}$, $\text{CO}(\text{NH}_2)_2$ (urea) and NH_4NO_3 as raw materials by solution combustion synthesis. The XRD results show that the phosphor has single phase with hexagonal structure. Due to high sintering temperature-agglomeration particle has

been observed in SEM images. The resulted phosphor can be efficient for UVA like UVB usage because of their broad emission.

Crystalline cerium ion doped yttrium aluminum borate phosphors have been synthesized by colloidal chemical synthesis. The characterization of obtained product has been applied by X-ray diffraction, TG, DTA and differential scanning calorimetry (DSC) analysis. The huntite like trigonal structure of the phosphor has been observed with XRD analysis. All results show that changing in local crystal structure around cerium ion causes changing optical properties. (Kichanov et al., 2018)

Europium is a silvery-white metal which is very ductile and hard. It is one of the most reactive lanthanide metals, which oxidizes readily and ignites at about 150°C to 180°C in air. The primary ores of Bastnasite and monazite include europium. Spectroscopically, it has been determined in specified stars and the sun. 17 isotopes of europium are known which are great absorbers of neutron and are studied for nuclear control uses. It also utilize in commercial area as a phosphor activator for example it is used in color television tube as a red phosphor. When Europium doped into plastic, it can be used as a laser material. (Husted R, 2000)



Figure 1.7. Europium oxide under UV light

In 1994, europium ions doped $\text{BaBe}_2(\text{BO}_3)_2$ has been prepared by solid state reaction. Its crystal structure has been investigated by X-ray diffraction as orthorhombic space group, and structure has two interpenetrating polyhedral frameworks. In emission spectra, the $4f^65d^1$ levels in silicate increasing in energy due to weaker crystal field at Ba part. The reduction of Eu^{3+} to Eu^{2+} by increasing sample temperature in air give relative high acidity of borate that have to maintain lower oxidation state. (Schaffers and Keszler, 1994)

Europium ions doped barium and strontium borates have been synthesized by using BaCO_3 , $\text{Sr}(\text{NO}_3)_2$ and B_2O_3 with heating at 873K for 30 minutes then heating 12 hour at 1273K. As a structural relationship showed that they are violet and blue emitting materials due to emitting at longer wavelength. The results show that containing oxygen atom bond with more than two strontium and barium atoms can cause blue Eu^{2+} ion emission. On the other hand, containing oxygen bond with three or more strontium and barium atoms can cause green or red emission. Because of that amount of distortion of oxygen atom environment is important for understanding Stokes shift. (Diaz and Keszler, 1996)

Lucas et al (2000) have reported europium ion doped strontium dialuminodiborate by flux method with using $\text{Sr}(\text{NO}_3)_2$, H_3BO_3 , $\text{Al}(\text{NO}_3)_3 \cdot 9\text{H}_2\text{O}$, and Eu_2O_3 as raw materials. Their characterization has been investigated by X-ray diffraction, and structure of resulted product has been determined as trigonal space group. Because of position of europium ion in SrB_4O_7 , emission band of europium as 5d to 4f has been observed longer wavelengths and small Stokes shift also observed. Due to decreasing of emission level, stability decreasing has been determined. Moreover, lower level of $4f^65d$ state in $\text{SrAl}_{12}\text{O}_{19}$ and SrAl_2O_4 has much higher stability. (Lucas et al., 2000)

In 2006, europium ion doped GdBO_3 phosphor materials which has great size and identical morphology have been synthesized by spray pyrolysis using spray solution containing citric acid and ethylene glycol. The characteristics of europium ion doped gadolinium borate phosphor have been investigated with changing preparation temperature by spray pyrolysis. 1400°C has been determined as optimum preparation condition for this synthesis. (Koo et al., 2006)

Europium doped orthoborates have been prepared by three synthesis methods that are microwave-assisted combustion method with using urea as a fuel, microwave-assisted sol-gel process with using glycine as a fuel, and microwave-assisted sol-gel process with using citric acid as a fuel. Particle size characterization shows that smallest size particles with citric acid and largest size particles with urea have been observed by SEM images. The resulted product, which is obtained with urea fuel, has strongest emission because of that this synthesis method would be better than the other methods. (Badan et al., 2012)

The conventional solid state reaction has been used for synthesizing europium ion doped $\text{Ba}_2\text{Mg}(\text{BO}_3)_2 - \text{Ba}_2\text{Ca}(\text{BO}_3)_2$ solid-solution by adding magnesium ions in $\text{Ba}_2\text{Mg}(\text{BO}_3)_2$ (BaMBO) with bigger calcium ions. The results of analysis give that lower symmetry for $\text{Ba}_2\text{Ca}(\text{BO}_3)_2$ as monoclinic, higher symmetry for $\text{Ba}_2\text{Mg}(\text{BO}_3)_2$ as trigonal. The emission spectra of resulted phosphors show different charge transfer band (CTB) energy for luminescence properties. Red shift higher lying charge transfer band energy and blue shift the lower lying charge transfer band energy are obtained by increasing calcium ion concentration. The ratio of electric and magnetic dipole of the components with emission in $^5\text{D}_0$ is smaller for barium calcium borate host, and decay time of luminescence takes longer than for barium magnesium borate host. Applying Judd-Ofelt analysis gives that not changing in $\Omega\lambda$ parameters with calcium ion concentration. (Bondzior and Dereń, 2019)

Terbium can be found together with other lanthanide elements in some minerals such as cerite, and gadolinite. Terbium is a silver-gray metal, malleable, stable in air, ductile, and soft. It has two crystal structures that transform at 1289°C . 21 isotopes of terbium have atomic masses in range between 145 and 165. The oxides of terbium have dark maroon color and use in color television tubes as a green phosphors activator. It also can be applied as a crystal stabilizer and in solid-state devices. (Husted R, 2000)



Figure 1.8. $\text{Tb}_2(\text{SO}_4)_3$ under UV light

Using solid state synthesis, terbium ion doped strontium borate phosphate phosphors have been synthesized. Cerium and terbium ion co-doped SrBPO_5 phosphors also have been studied. From their XRD analysis, hexagonal space group has been determined. Cerium and terbium ion co-doped borate phosphate has additional intense excitation because of transferring energy from cerium ion to terbium ion.

Resulted phosphors can be used as green emitting phosphors in tricolor lamps. (Lu et al., 2005)

Lu et al (2005) have also synthesized terbium and cerium ion co-doped BaBPO₅ phosphors by solid state reaction with using BaCO₃, Tb₄O₇, (NH₄)₂HPO₄, and H₃BO₃ Na₂HPO₄ and CeO₂ as raw materials. All XRD patterns show that phosphors have single phase and similar barium borophosphate. The energy transfer from cerium to terbium ions has been observed. These phosphors can be considered to apply in green phosphor applications such as tricolor lamps.

In 2006, europium ion and terbium ion doped LuBO₃ powders have been synthesized by sol-gel synthesis. The characterizations of resulted phosphors have been done by X-ray diffraction, FT-IR spectroscopy, scanning electron microscopy, thermogravimetric analysis, and afterglow measurements. Orthoborate LuBO₃ as vaterite form has been obtained. These two phosphors can be used in promising scintillators due to their morphology, crystallinity and purity and a homogeneous particle size. (Mansuy et al., 2007)

Terbium ion doped LiBO₂ phosphors have been prepared by conventional solid state synthesis method. Thermally stimulated luminescence (TSL), radioluminescence analysis and X-ray diffraction analysis have been studied and the results show that the phosphor has monoclinic crystal structure, strong green emission. (Dinçer and Ege, 2013)

Shyichuk et al (2013) have synthesized terbium ion doped strontium lanthanum borate by sol-gel Pechini method with using citric acid and ethylene glycol for gel formation. The XRD patterns show that this phosphor have similar crystal structure with strontium lanthanum borate. From TEM microphotographs, nanoscale sized and microscale sized particles have been observed. In the excitation spectra of phosphor, emission intensity changing have been observed by changing amount of terbium ion dopant, and also these phosphors have green emission. As a result of this study, the cell parameters of crystals decrease with increasing dopant concentration.

Using La₂O₃, Tb₄O₇, Na₂CO₃, H₃BO₃ and NaF as starting materials, terbium ion doped Na₃La₉O₃(BO₃)₈ crystals have been synthesized by the top-seeded solution growth method. The structure of Na₃La₉O₃(BO₃)₈ does not change with doping

terbium ion. Although terbium dopant has high concentration, the resulted crystals have long lifetime and high luminescence quantum efficiency with $^5D_4 \rightarrow ^7F_5$ transition, and also due to this transition, they can be used for green light applications. (Shan et al., 2015)

In 2018, undoped and terbium ion doped YBO_3 and Y_3BO_6 have been synthesized by co-precipitation method with using ethylene glycol at temperature between $100^\circ C$ and $800^\circ C$. Terbium doped YBO_3 has better resolving than terbium doped Y_3BO_6 by comparing transitions of the low spin, allowed spin $4f^8 \rightarrow 4f^7 5d^1$ and high spin, forbidden spin $4f^8 \rightarrow 4f^7 5d^1$. Terbium ion doped Y_3BO_6 has observed as green emission and has better color purity than terbium ion doped YBO_3 because of local environment around terbium ions in these two lattices. (Nair et al., 2018)

Cerium, europium and terbium ions doped $LiSr_4(BO_3)_3$ phosphors have been synthesized by solid state reaction method with using Li_2CO_3 , $SrCO_3$, H_3BO_3 , Eu_2O_3 , Tb_4O_7 , and CeO_2 as raw materials. Photoluminescence and UV analysis of resulted product have been done for characterization of materials. The cerium ion doped $LiSr_4(BO_3)_3$ phosphor give blue emission under UV due to $5d-4f$ transition of cerium ion. Europium ion doped products can be useful for solid-state lighting with phosphor converted because of its red emission under UV. Terbium ion doped products has strongest emission in $^5D_4 \rightarrow ^7F_5$. (Zhang et al., 2011)

Activated materials of RE ions have fascinating spectroscopic properties that allow them to be mostly used as cathode ray tubes, lamp and scintillator phosphors. Due to their $4f$ energy levels and transition properties, the luminescent materials have been applied in picture tubes, solid state lighting, color television sets and computer monitors. The commercial phosphors materials are usually formed by adding the rare earth or transitions metal ions into host materials. The rare earths ions such as Ce^{3+} , Tb^{3+} and Eu^{3+} owing the blue, green and red phosphors, respectively. Because of their usage in display and lightning application, Ce^{3+} and Tb^{3+} doped materials have drawn great attentions. Hence, the controllable color and great emission between $5d-4f$ electron transition of europium makes it a significant activator as strength and symmetry of crystal area are effected by band gap energy of $5d$ orbitals. (Panse et al., 2016) (Wang et al., 2008) (Liu et al., 2013)

1.4 SYNTHESIS METHODS OF BORATES

In organometallic and coordination chemistry, the synthesis of inorganic materials are based on the changing of ligands forming different molecules in solution-type reaction which done at low temperature with applicable solvents and have small activation energies. For these reasons, the reaction needs quite short time. On the other hand, high lattice energies are needed in the solid-based reactions resulting longer reaction time and higher temperatures.

Solid-state reaction method which is oldest, easy and most useful method for obtaining inorganic materials. Solid-state synthesis method takes long time due to their atomic level where they are not homogeneous. (Wieser and Coplen, 2010)

Sol-gel synthesis method which belongs to condensation and hydrolysis of alkoxides that contain metal. This method has two part that are sol and gel. Sol part involves nanoparticles in solid colloidal suspension, and gel part 3D network for interconnecting between obtained phases. (Ladj et al., 2013) (Boyer et al., 2003)

1.4.1 Solution Combustion Synthesis

Among the synthetic methods, Solution combustion synthesis is the most economical and effective methods because of its facile preparation, time efficient and form high purity products. This method is well-known as ‘self-propagating high-temperature synthesis’ and furnaceless process. The synthesis is based on the exothermic reduction-oxidation reaction of exchange between metals-nonmetals compounds. The combustion methods include the explosive reaction that forms a useful oxides and nonoxides materials such as phosphors, refractory oxides, catalyst, magnetics, insulators, sensors, semiconductors, dielectrics, nitrides, borides, carbides and silicides. Unique properties of metastable materials can be obtained by this high-temperature synthesis method which cause rapid cooling and heating. (Bai and Liu, 2010)

2. AIM AND SCOPE OF THE STUDY

The main purpose of this study is to synthesize and characterize undoped and cerium, europium and terbium ion doped strontium pyroborate nanoparticles using glycine as fuel by solution combustion synthesis method which is so convenient technique for synthesizing these materials. The reaction conditions were comparatively investigated by various concentrations of dopant ions at different heating temperatures. Additionally, the effect of various parameters on the crystal structure, crystallite size, and optical band gap energies of the pyroborates prepared in this thesis were examined.

3. MATERIALS AND METHODS

3.1 CHEMICALS

In this present work, the chemicals that were used are listed as follows;

Strontium nitrate, $\text{Sr}(\text{NO}_3)_2$: Merck, 99.00%

Terbium(III) nitrate pentahydrate, $\text{Tb}(\text{NO}_3)_3 \cdot 5\text{H}_2\text{O}$: Sigma-Aldrich, 99.9%

Europium nitrate pentahydrate, $\text{Eu}(\text{NO}_3)_3 \cdot 5\text{H}_2\text{O}$: Fluka Chemika, 98.5%

Cerium(III) nitrate hexahydrate, $\text{Ce}(\text{NO}_3)_3 \cdot 6\text{H}_2\text{O}$: Sigma-Aldrich, 99.0%

Boric acid, H_3BO_3 : Merck, 99.00%

Glycine, $\text{C}_2\text{H}_5\text{NO}_2$: Merck, 99.70%

Potassium Bromide, KBr, for IR Spectroscopy: Merck, 99.90%

3.2 INSTRUMENTS

3.2.1 Fourier Transform Infrared Spectrophotometer

Infrared spectra of the final products were recorded by Shimadzu Fourier Transform Infrared (FTIR) spectrophotometer in the region of 4000-400 cm^{-1} . The spectra of the product was obtained by preparing the pellets that are consisted of 0.1500:0.0010(wt/wt) of KBr:product ratio.

3.2.2 X-ray Powder Diffractometer

Rigaku miniflex and multiflex X-ray powder diffractometer were used to provide the structural properties of product using $\text{CuK}\alpha$ (30-40 kV, 10-20mA, $\lambda=1.54056 \text{ \AA}$) radiation. The data of each XRD pattern were obtained by using Rigaku programs and checked by using ICDD data card.

3.2.3 UV- VIS Spectrometer

Perkin Elmer Lambda 35 UV-VIS Spectroscopy was used to determine the optical properties of the samples. The spectra were recorded at wavelength range of 200-900nm. The data was plotted by using Data Processor WinLab.

3.2.4 Furnace

The reactions during the preparation of metal borates were carried out at heating range between 400-900°C by the aid of Nuve MF 120 furnace.

3.3 METHODS

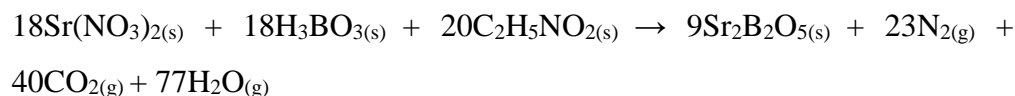
Strontium pyroborates ($\text{Sr}_2\text{B}_2\text{O}_5$) were synthesized by Solution Combustion Synthesis (SCS) using $\text{Sr}(\text{NO}_3)_2$, H_3BO_3 and glycine as starting materials. $\text{Sr}(\text{NO}_3)_2$ and H_3BO_3 were used as Sr and B source, respectively with 1:1 of Sr:B mole ratio. Glycine was used as fuel in this synthesis.

3.3.1 Synthesis of Strontium Pyroborates

Stoichiometric amount of $\text{Sr}(\text{NO}_3)_2$, H_3BO_3 and glycine were dissolved in distilled water. The homogeneous mixture was mixed using magnetic stirrer and was allowed to evaporate at 370°C until the gel-like residue was observed. Small amount of precursor-gel was collected for further thermal analysis determination and the rest of the gel was introduced in a furnace preheated at 400°C for 10 minutes. The as-prepared product was ground and the heating process was done at various temperatures in range between 400°C - 900°C for an hour. All the heated products of each temperature were kept for characterization studies.

The theoretical reaction for the preparation of undoped $\text{Sr}_2\text{B}_2\text{O}_5$ is considered as follows;

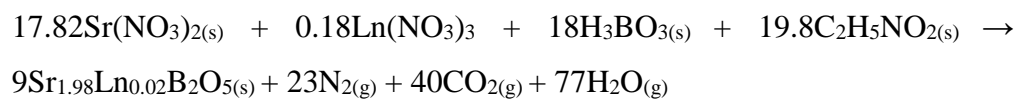
➤ Undoped $\text{Sr}_2\text{B}_2\text{O}_5$



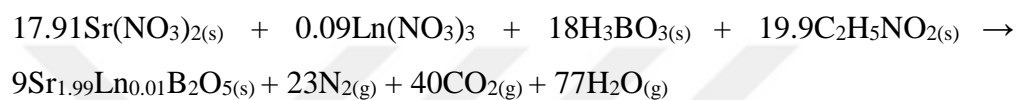
Lanthanide element doped strontium pyroborates given by the formula $\text{Sr}_{2-x}\text{Ln}_x\text{B}_2\text{O}_5$ ($\text{Ln} = \text{Ce}^{3+}, \text{Eu}^{3+}, \text{Tb}^{3+}$) were also synthesized by using the similar procedures with various concentrations of each lanthanide element ($x=0.005, 0.010, 0.020$).

The following reactions for the synthesis of doped pyroborates are predicted as follows;

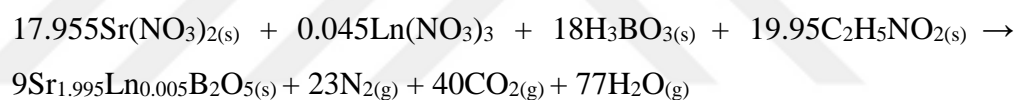
➤ **Ln 0.02mol Doped Sr₂B₂O₅ (Ln: Ce³⁺, Eu³⁺, Tb³⁺)**



➤ **Ln 0.01mol Doped Sr₂B₂O₅ (Ln: Ce³⁺, Eu³⁺, Tb³⁺)**



➤ **Ln 0.005mol Doped Sr₂B₂O₅ (Ln: Ce³⁺, Eu³⁺, Tb³⁺)**



4. RESULTS AND DISCUSSION

4.1 Synthesis of Undoped and Doped Strontium Pyroborates








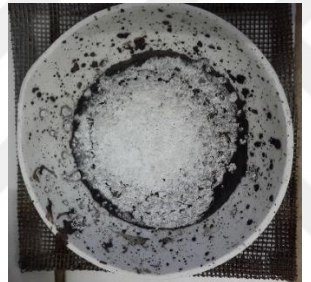

Strontium pyroborates, $\text{Sr}_2\text{B}_2\text{O}_5$ were synthesized via Solution Combustion Synthesis (SCS) by adjusting temperatures and concentrations of dopants. In order to examine its doped effect, Ce^{3+} , Eu^{3+} , and Tb^{3+} ions were used with Fuel:oxidizer ratio were applied in 1:1 mole ratio. Furthermore, reaction temperatures were also varied from 400°C to 900°C and the samples were heated for an hour.

During the preparations of undoped $\text{Sr}_2\text{B}_2\text{O}_5$ and lanthanide element doped $\text{Sr}_2\text{B}_2\text{O}_5$, similar behavior of solution was observed and the initial materials were quickly dissolved in solvent. The homogenized solution was colorless and produced a little amount of gas during the gel formation at 370°C and the precursor-gel was also colorless forming a fluffy light grey product after preheated at 400°C for 10 minutes. The prepared products were observed in the same appearances with black and white powder, which gave grey powder after grinding process.



Figure 4.1. Undoped $\text{Sr}_2\text{B}_2\text{O}_5$ powder

Table 4.1. Observation During the Preparation of Ln Doped $\text{Sr}_2\text{B}_2\text{O}_5$

%	Ce^{3+}	Eu^{3+}	Tb^{3+}
2.0			
1.0			
0.5			

4.1.1 Structural Characterization of Undoped and Doped Sr₂B₂O₅

The properties of undoped strontium pyroborate and lanthanide element doped (Ce³⁺, Eu³⁺, Tb³⁺) strontium pyroborates were heated at temperature between 400°C to 900°C by taking the synthesis products which were obtained at 400°C 10 minutes. The prepared products were characterized by using FT-IR to determine their vibrational modes, X-Ray Diffraction to characterize their crystal structures and size, and UV-Visible spectrometer were also used to examine their optical properties such as band gap energy.

4.1.1.1 FT-IR Spectroscopy Studies

The FT-IR spectra of undoped Sr₂B₂O₅ by using glycine as fuel were studied. The formation of undoped Sr₂B₂O₅ were confirmed by the following vibration modes between 625 to 1450 cm⁻¹. The stretching vibration of B-O bond in BO₃ was found at 1450 cm⁻¹, H-O-H bending vibrations were observed at 1376 cm⁻¹, the spectrum at 1150 cm⁻¹ belongs to BO₃ asymmetric stretching vibrations, and the BO₃ bending vibrations were indicated at 732 cm⁻¹ and 680 cm⁻¹. (Panse et al., 2016)

Given in Figure 4.2, the vibrational bands of Sr₂B₂O₅ FT-IR spectra were obtained at same wavenumbers and there is no additional peak were observed. These vibration modes were examined in all spectra starting from 400°C to 900°C and the same behavior were also summarize in Table 4.2.

Table 4.2. FT-IR band assignments of undoped Sr₂B₂O₅

Assignment	Bending BO ₃ (cm ⁻¹)	Asymmetric Stretching BO ₃ (cm ⁻¹)	Bending H-O-H (cm ⁻¹)	Symmetric Stretching BO ₃ (cm ⁻¹)
400°C 10mins	731, 680	1171	1385	1450
400°C 1 hour	731, 680	1171	1385	1450
500°C 1 hour	731, 680	1171	1385	1425
600°C 1 hour	727, 680	1173	1376	1443
700°C 1 hour	727, 680	1142	1376	1406
800°C 1 hour	727, 662	1138	1383	1456
900°C 1 hour	727, 660	1123	1385	1458

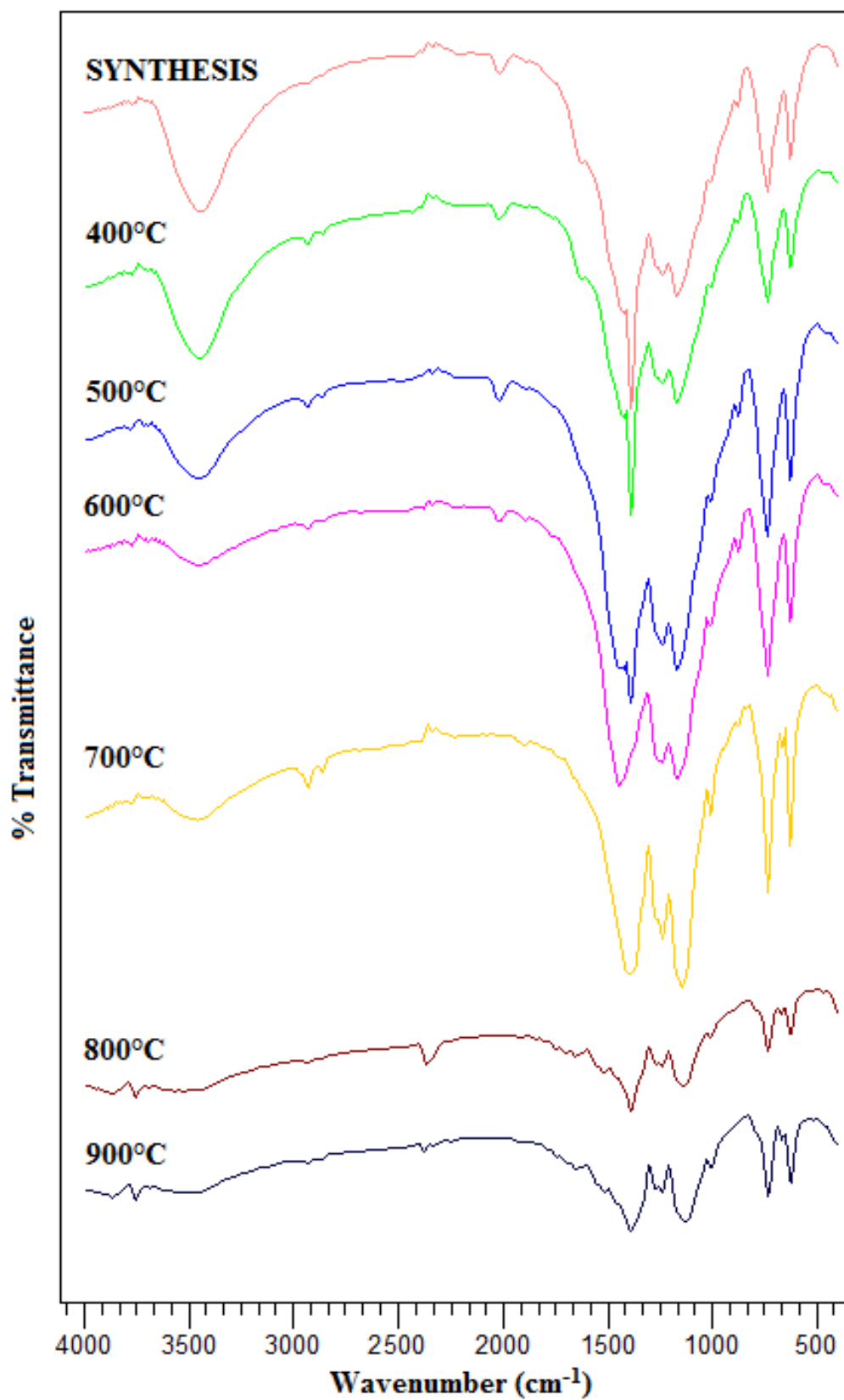


Figure 4.2. FT-IR Spectra of Undoped $\text{Sr}_2\text{B}_2\text{O}_5$

The FT-IR spectra of cerium ion doped strontium pyroborate were observed with similar wavenumbers in different temperature and concentration as shown from Figure 4.3 to Figure 4.6 which belong to the prepared products obtained at 400°C 10mins, 400°C, 500°C, and 600°C, respectively. The sharper peaks of resulted product were observed at higher temperatures as given in Figure 4.7, Figure 4.8, and Figure 4.9. Although different concentrations of cerium ion doped Sr₂B₂O₅ were applied, there was not much change of spectra were examined. Because of this reason, the wavenumbers of cerium ion doped strontium pyroborate that are obtained at 900°C were summarized in Table 4.3.

Table 4.3. FT-IR band assignments of Ce³⁺ ion doped Sr₂B₂O₅ at 900°C

Assignment	Bending BO₃ (cm⁻¹)	Asymmetric Stretching BO₃ (cm⁻¹)	Bending H-O-H (cm⁻¹)	Symmetric Stretching BO₃ (cm⁻¹)
2.0%	729, 663	1132	1364	1450
1.0%	727, 663	1136	1360	1450
0.5%	727, 663	1142	1395	1450

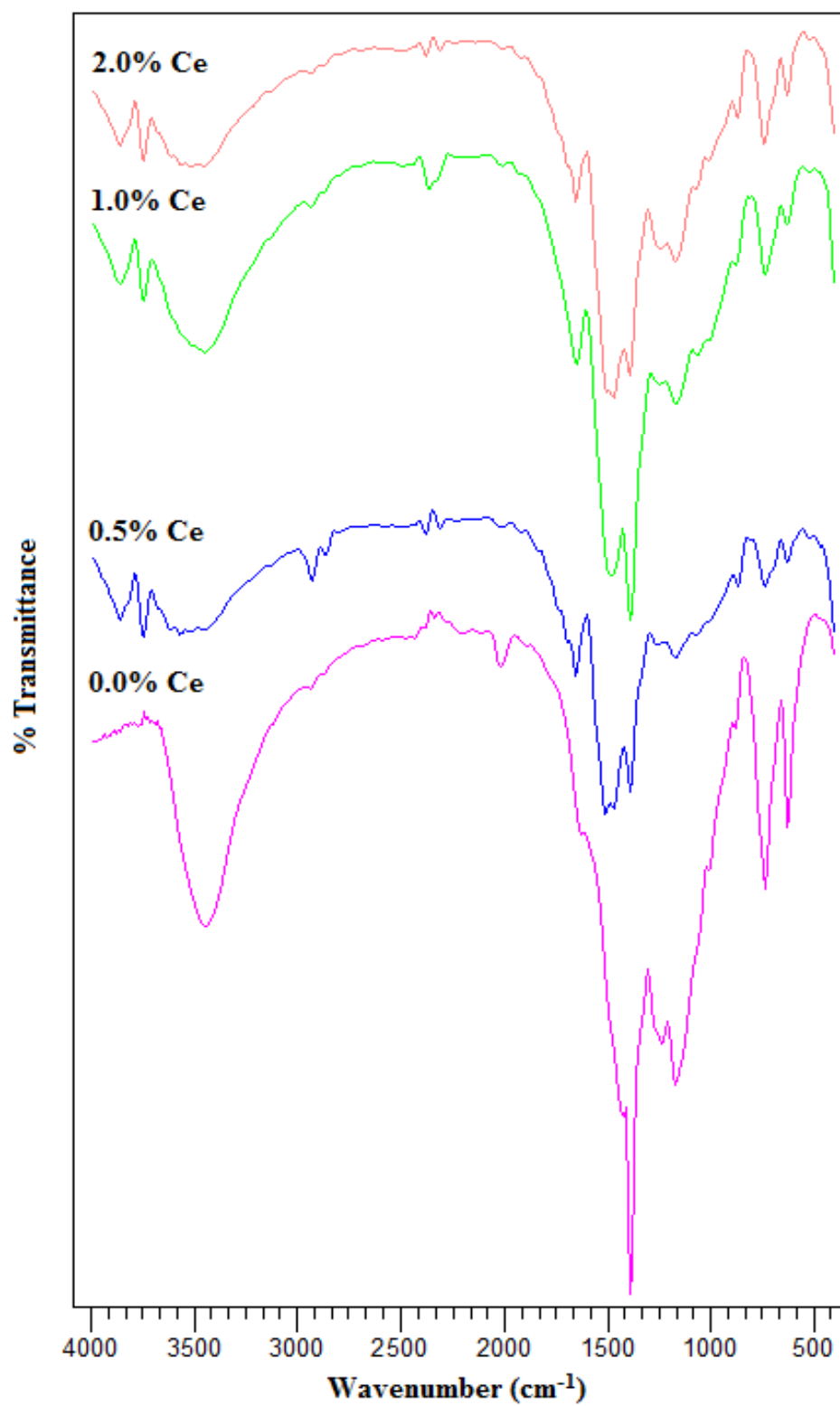


Figure 4.3. FT-IR Spectra of Ce^{3+} Doped $\text{Sr}_2\text{B}_2\text{O}_5$ at 400°C 10 minutes

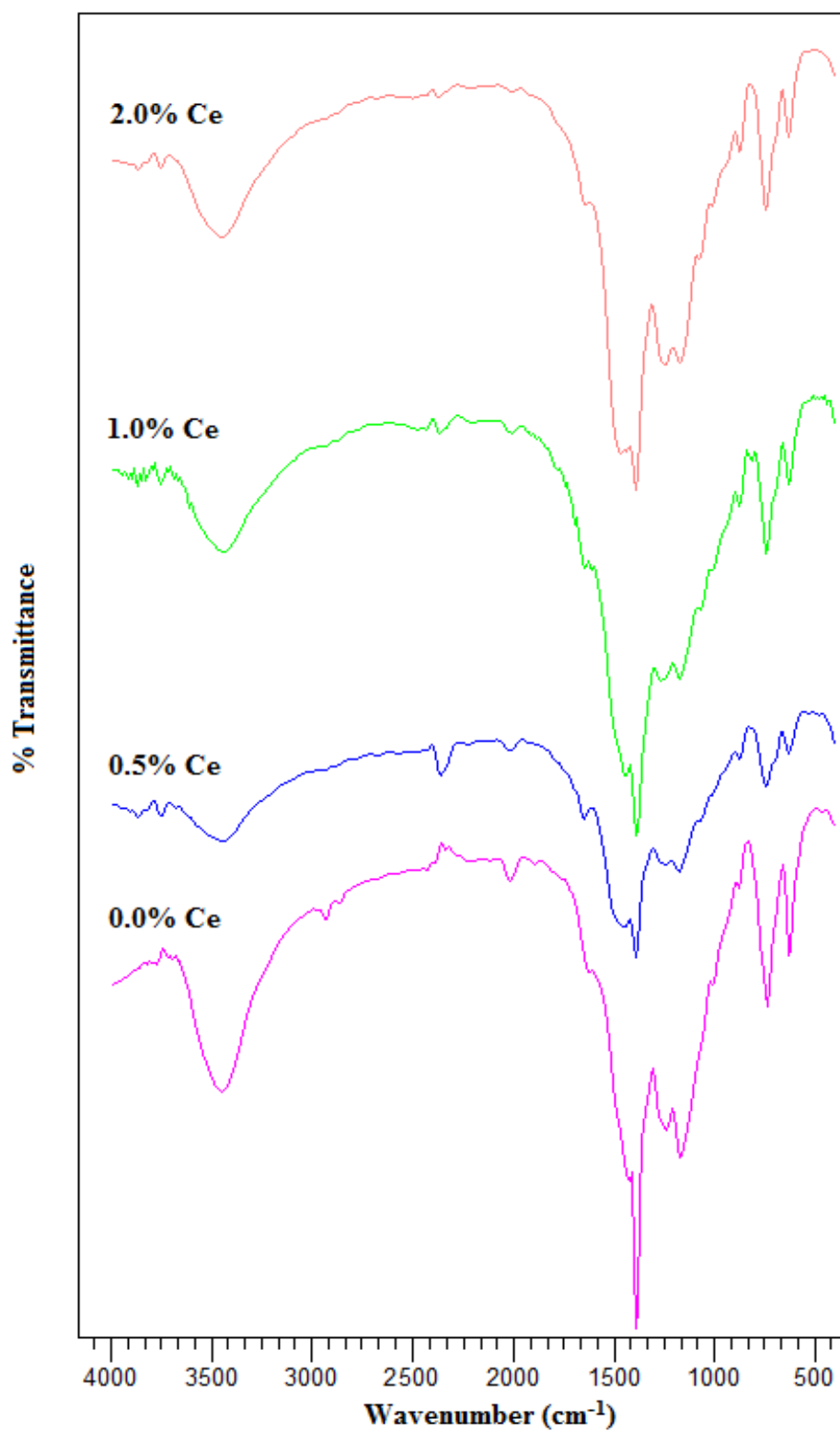


Figure 4.4. FT-IR Spectra of Ce^{3+} Doped $\text{Sr}_2\text{B}_2\text{O}_5$ at 400°C

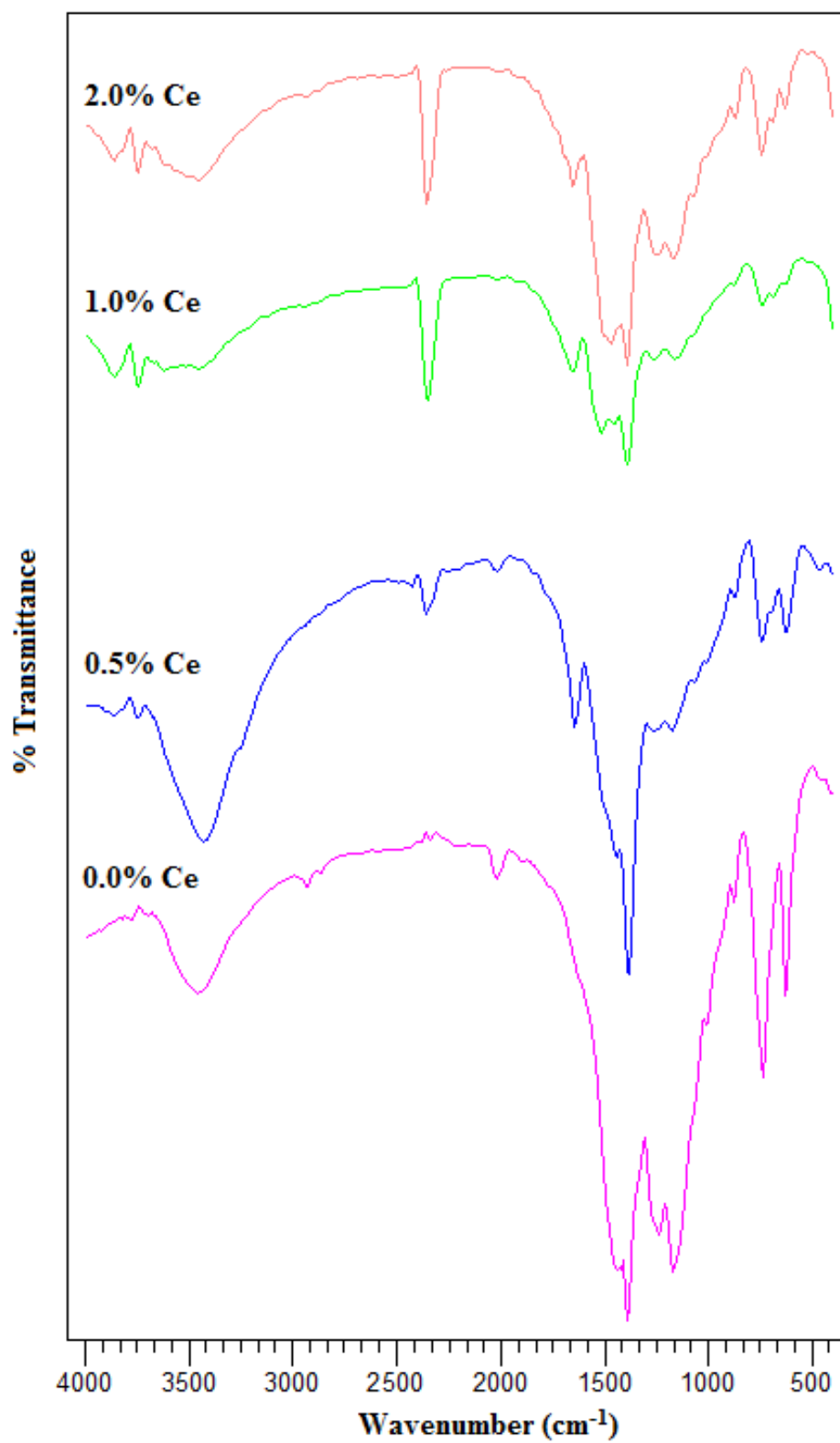


Figure 4.5. FT-IR Spectra of Ce^{3+} Doped $\text{Sr}_2\text{B}_2\text{O}_5$ at 500°C

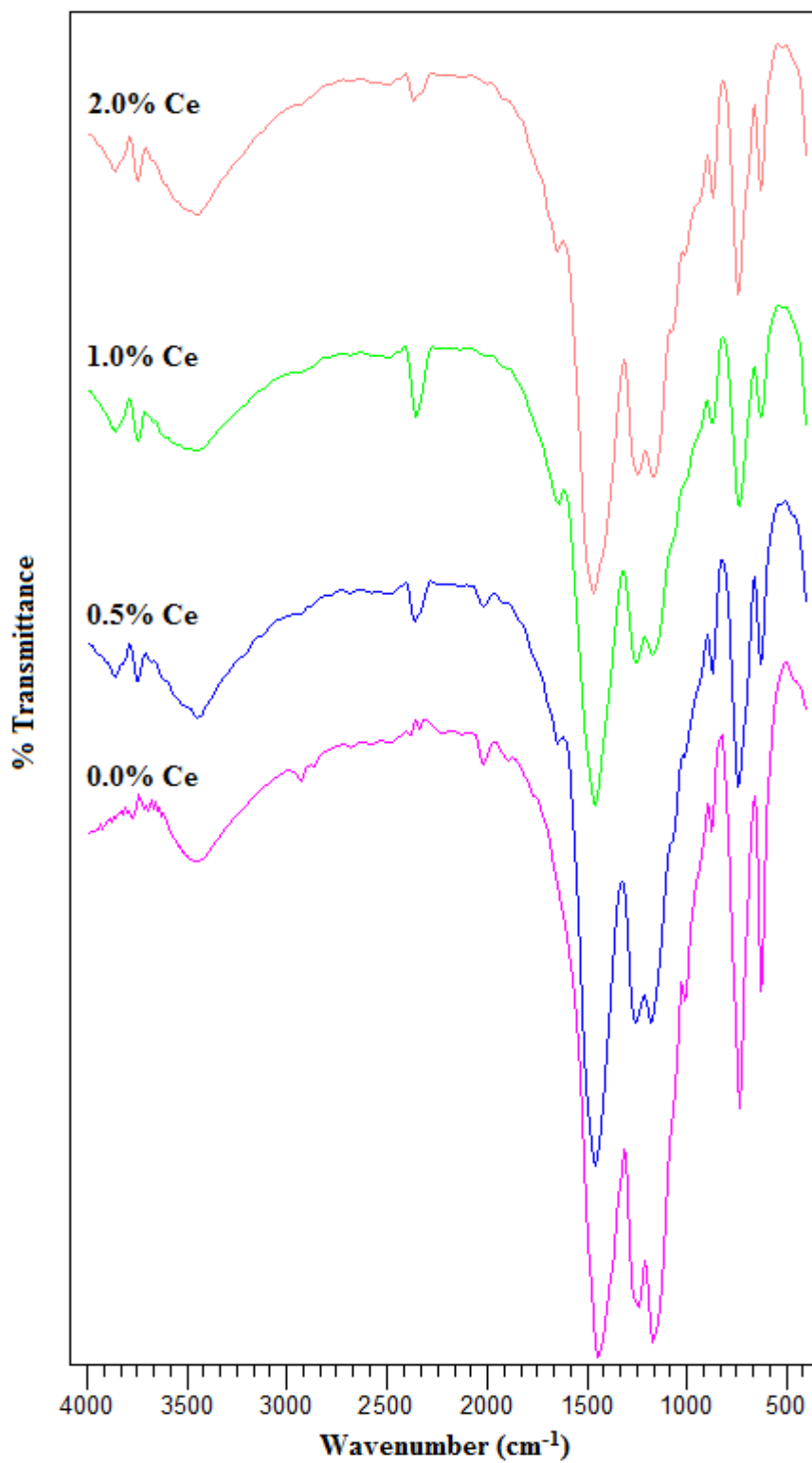


Figure 4.6. FT-IR Spectra of Ce^{3+} Doped $\text{Sr}_2\text{B}_2\text{O}_5$ at 600°C

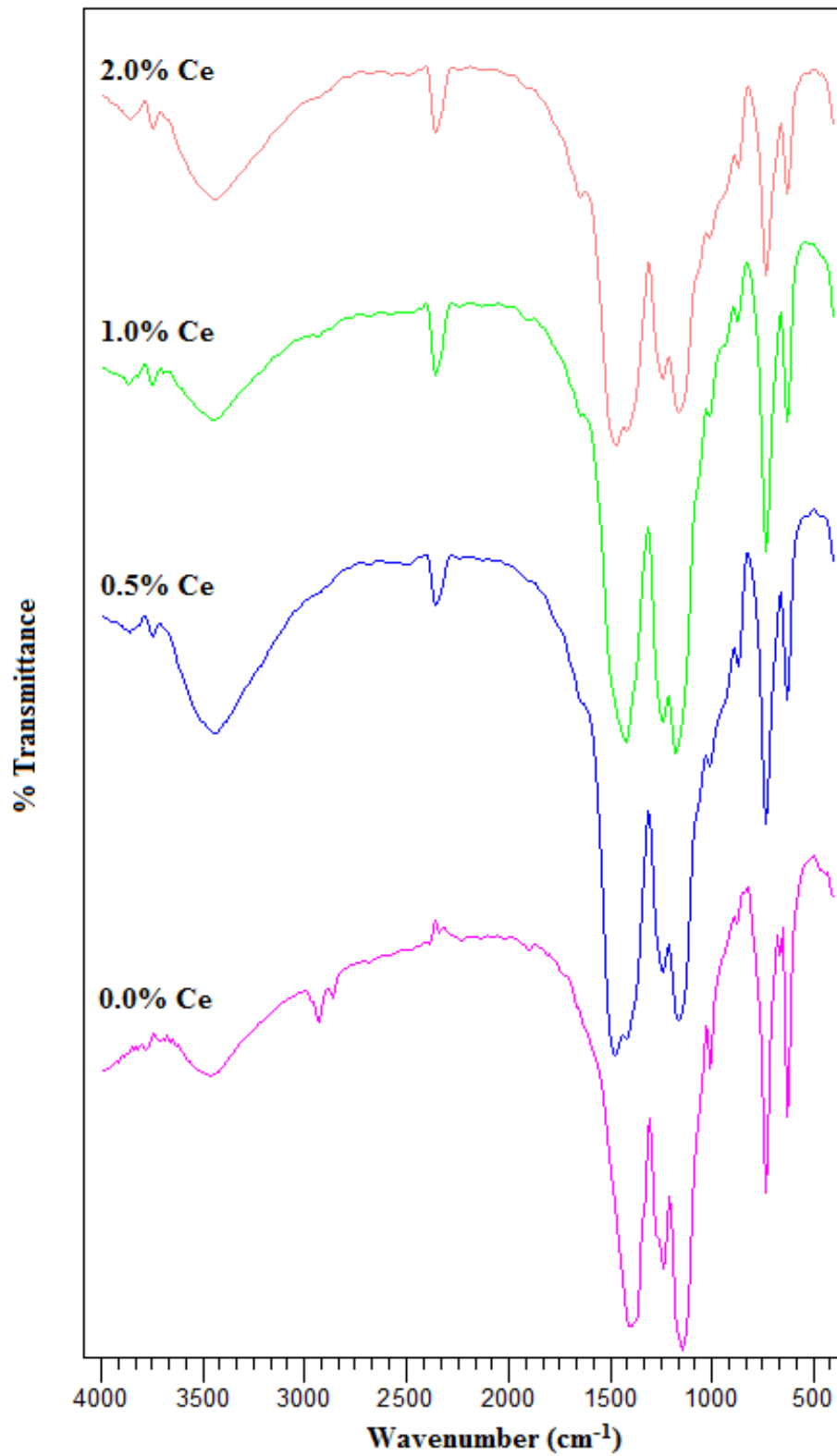


Figure 4.7. FT-IR Spectra of Ce^{3+} Doped $\text{Sr}_2\text{B}_2\text{O}_5$ at 700°C

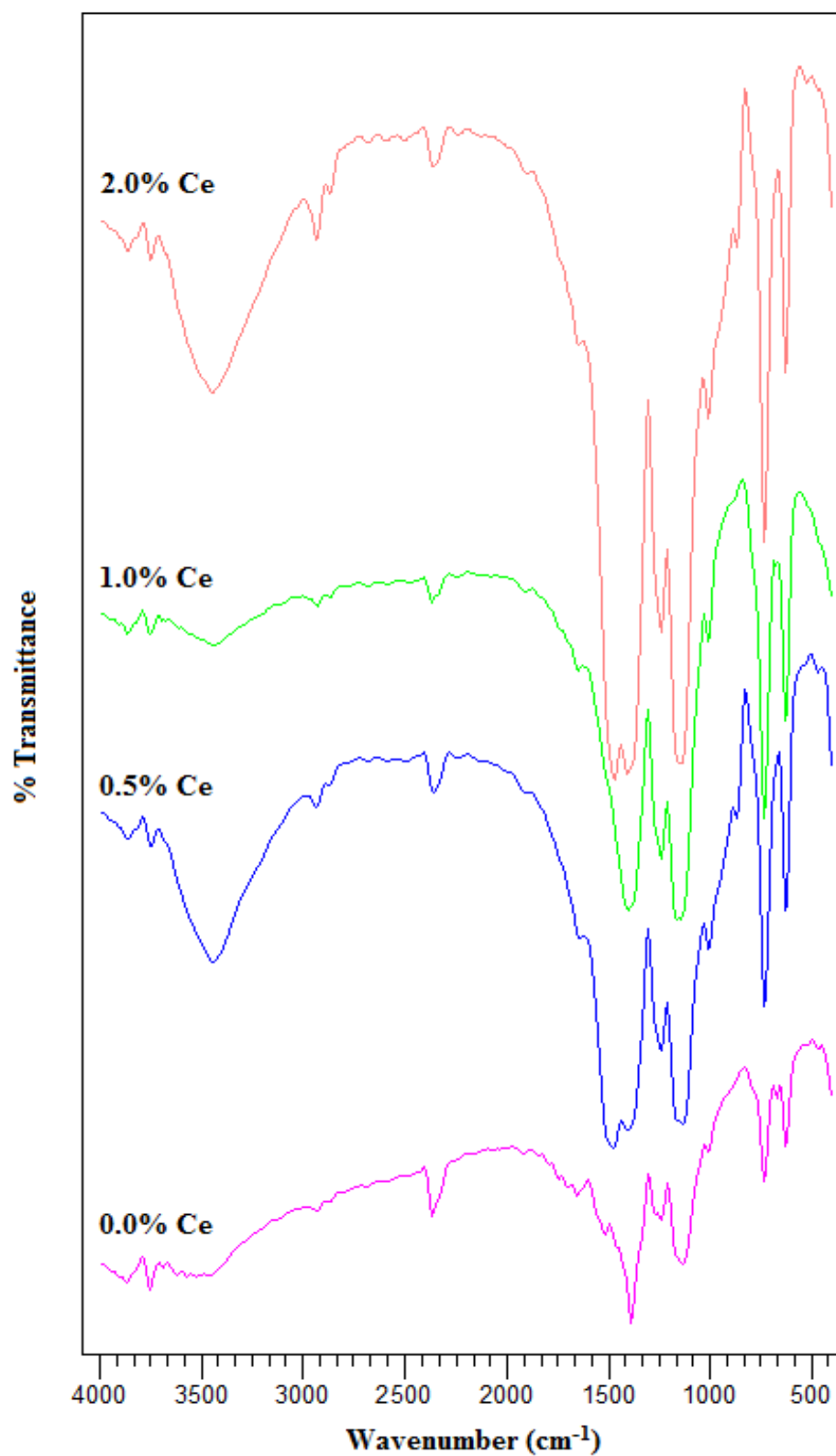


Figure 4.8. FT-IR Spectra of Ce^{3+} Doped $\text{Sr}_2\text{B}_2\text{O}_5$ at 800°C

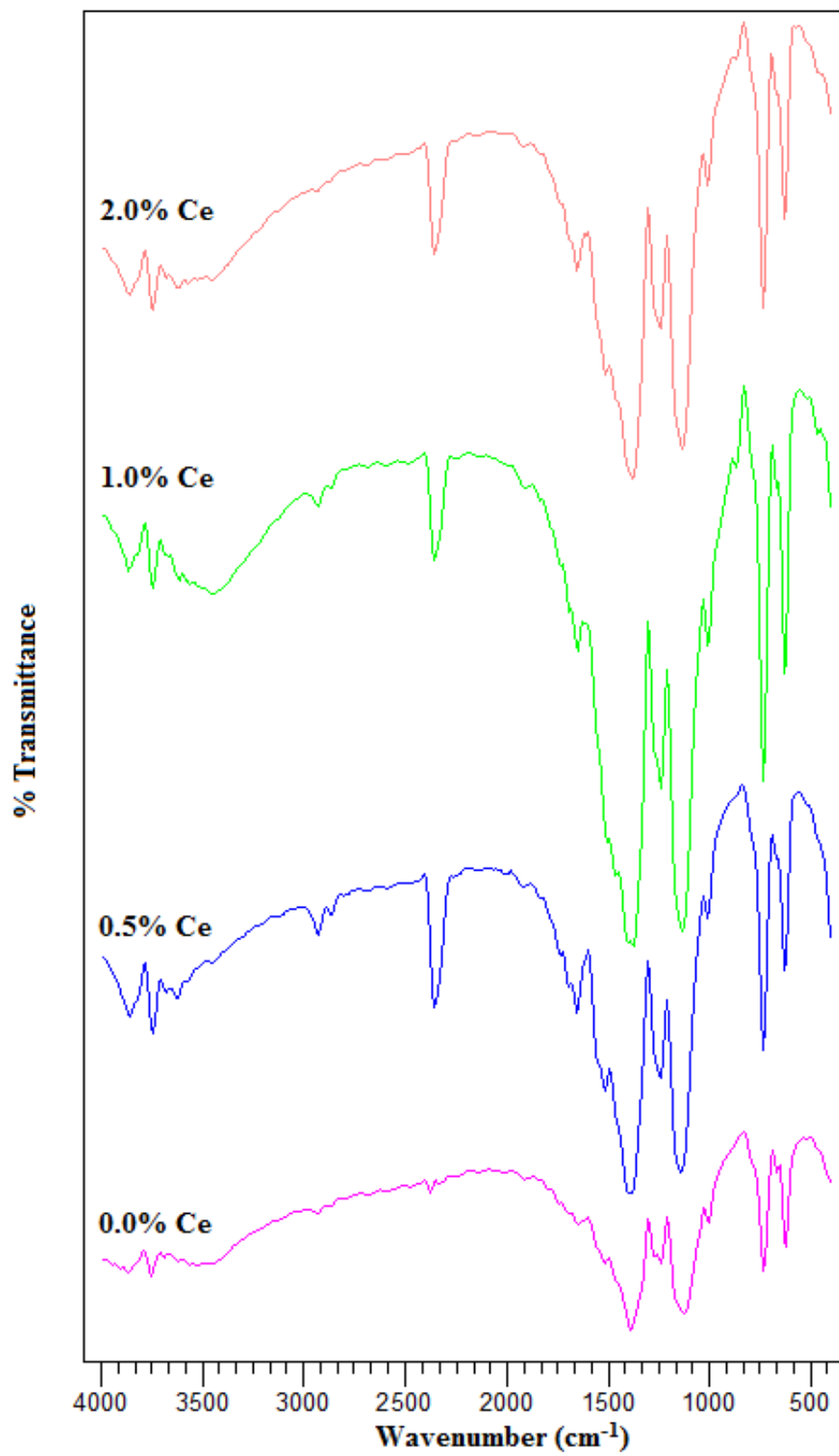


Figure 4.9. FT-IR Spectra of Ce^{3+} Doped $\text{Sr}_2\text{B}_2\text{O}_5$ at 900°C

Europium ion doped $\text{Sr}_2\text{B}_2\text{O}_5$ were also characterized by using FT-IR and the spectra showed similar behavior even though their concentration were varied as 0.02, 0.01, and 0.005 mol. Compared with the spectra of obtained product at 400°C 10mins (Figure 4.10), the spectra of product that was observed at 400°C (Figure 4.11) gave better result with 0.02mol concentration of europium. When heating temperature higher than 600°C , the spectra of the product showed excellent peaks as previous studies as shown in Figure 4.13, Figure 4.14, Figure 4.15, and Figure 4.16. Due to these similar results, the wavenumbers of $\text{Sr}_2\text{B}_2\text{O}_5$ with Eu^{3+} ion doped at 900°C were given in Table 4.4.

Table 4.4. FT-IR band assignments of Eu^{3+} ion doped $\text{Sr}_2\text{B}_2\text{O}_5$ at 900°C

Assignment	Bending BO_3 (cm^{-1})	Asymmetric Stretching BO_3 (cm^{-1})	Bending H-O-H (cm^{-1})	Symmetric Stretching BO_3 (cm^{-1})
2.0%	727, 665	1136	1360	1452
1.0%	729, 665	1136	1360	1452
0.5%	729, 665	1136	1360	1452

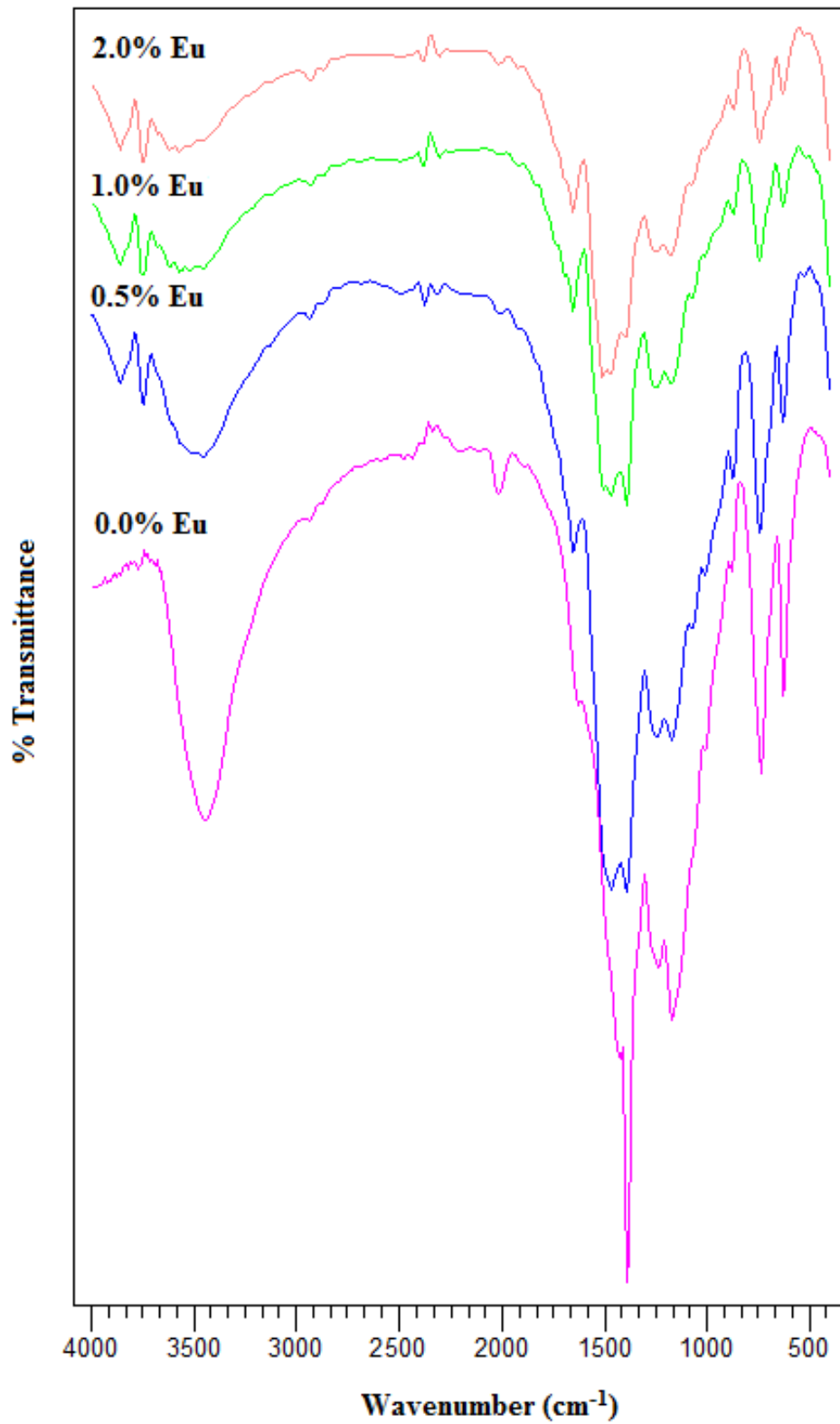


Figure 4.10. FT-IR Spectra of Eu³⁺ Doped Sr₂B₂O₅ at 400°C 10 minutes

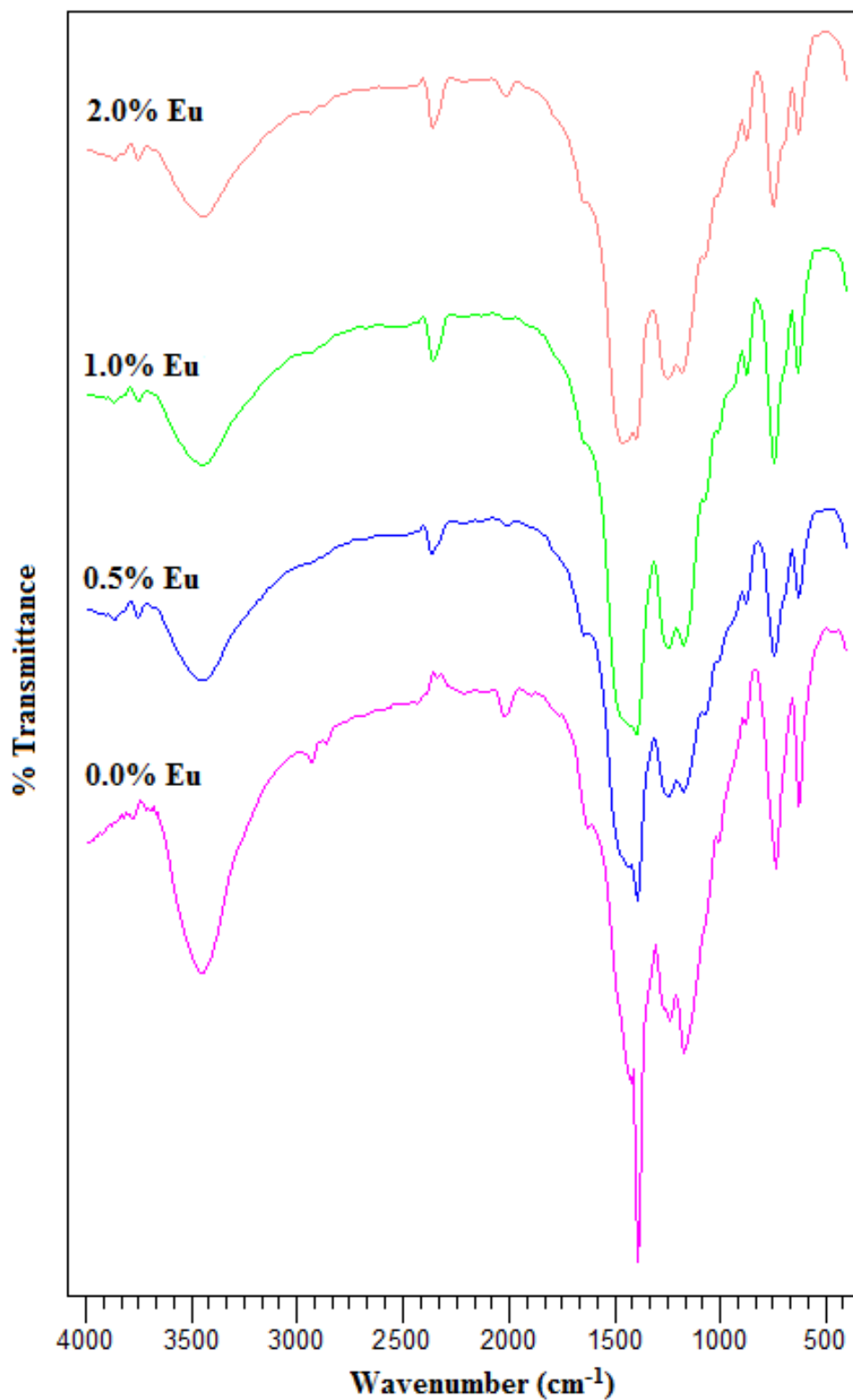


Figure 4.11. FT-IR Spectra of Eu³⁺ Doped Sr₂B₂O₅ at 400°C

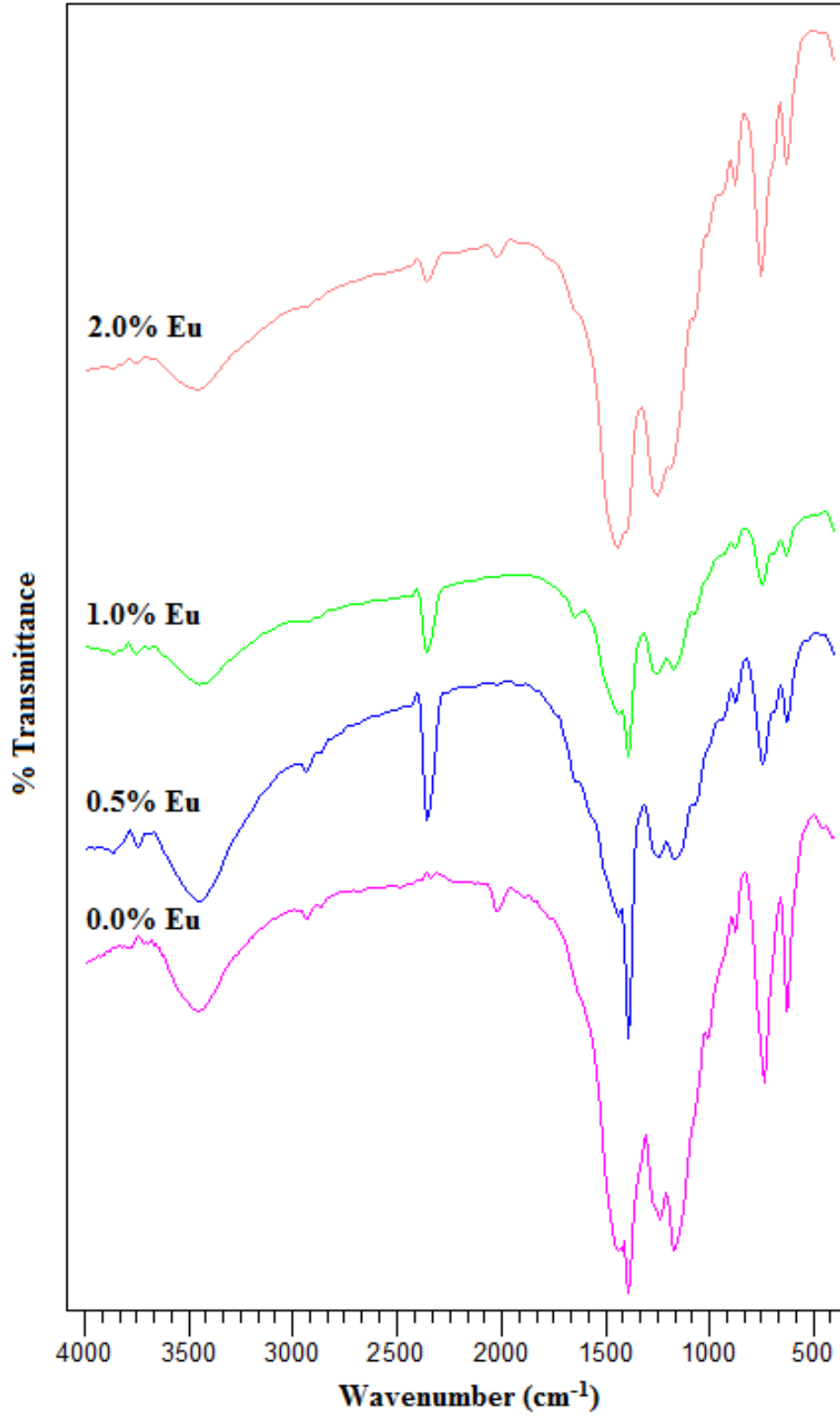


Figure 4.12. FT-IR Spectra of Eu³⁺ Doped Sr₂B₂O₅ at 500°C

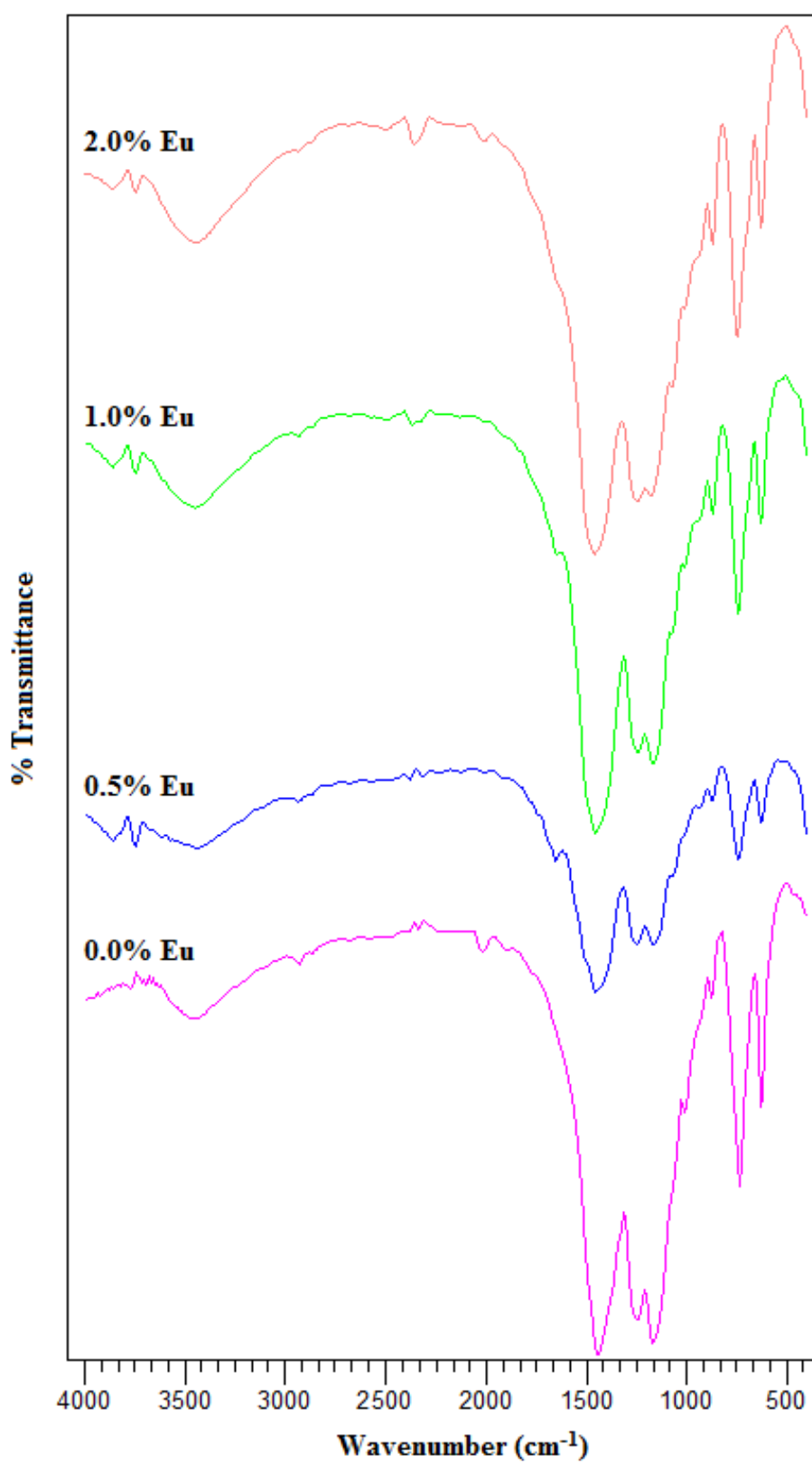


Figure 4.13. FT-IR Spectra of Eu^{3+} Doped $\text{Sr}_2\text{B}_2\text{O}_5$ at 600°C

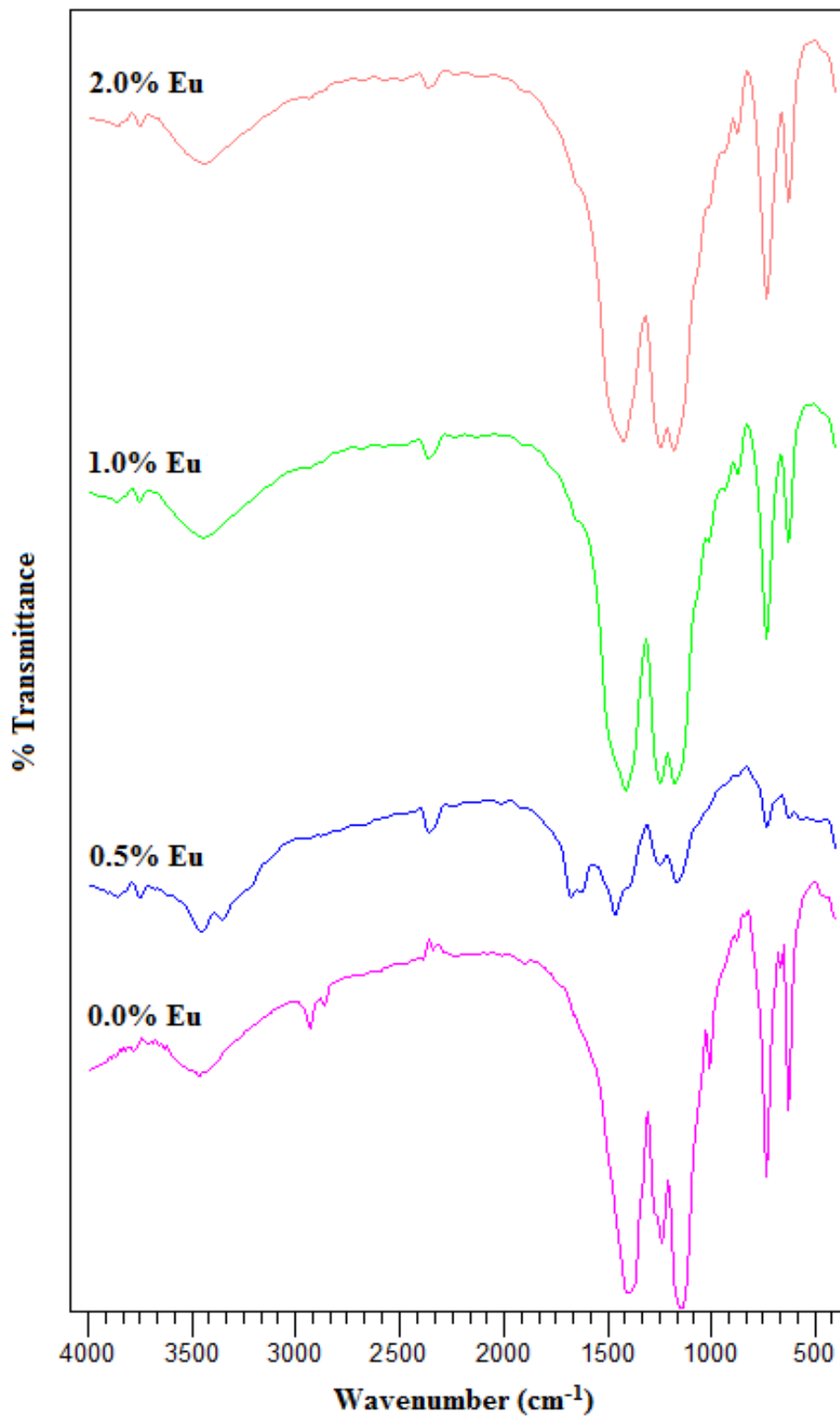


Figure 4.14. FT-IR Spectra of Eu³⁺ Doped Sr₂B₂O₅ at 700°C

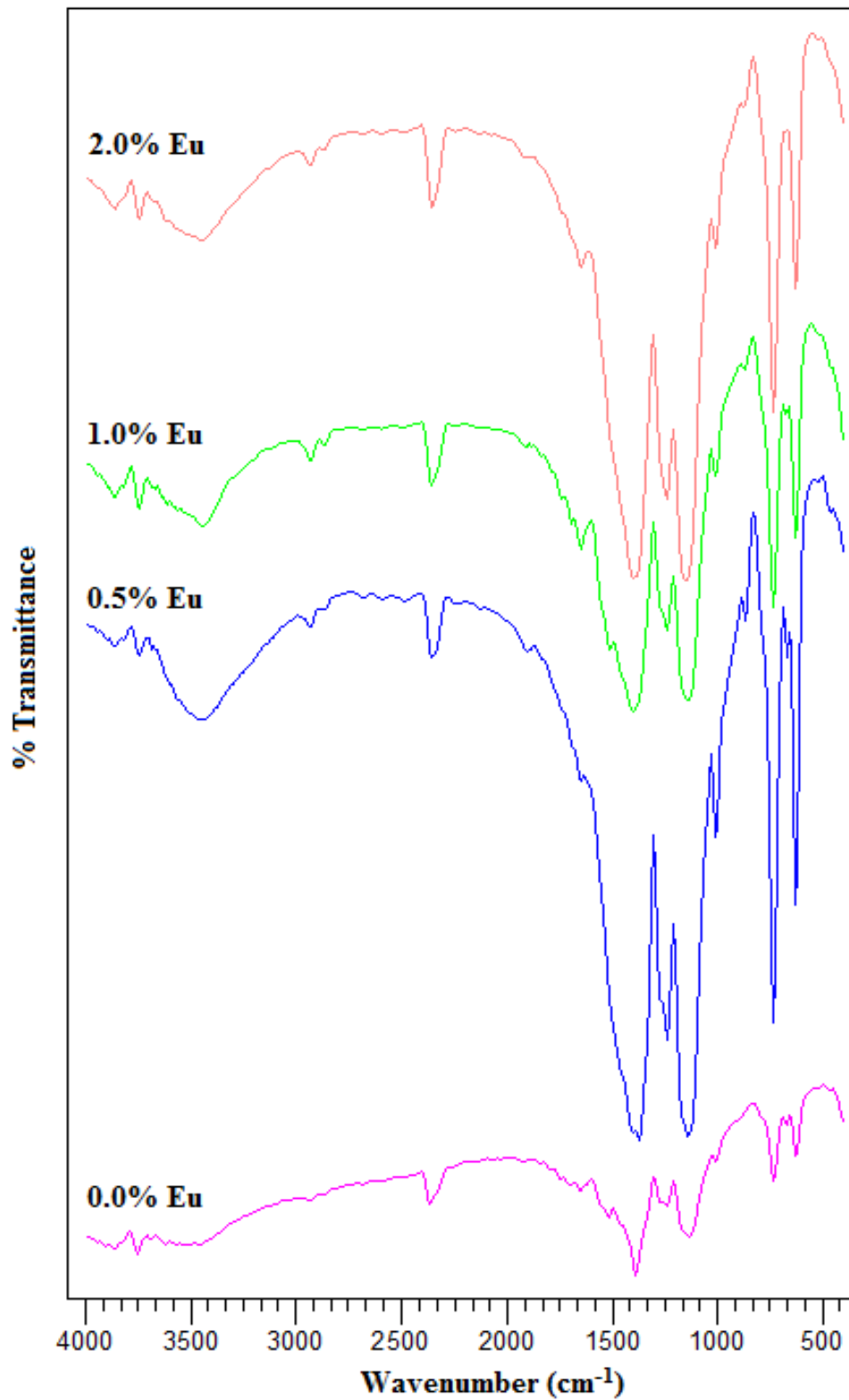


Figure 4.15. FT-IR Spectra of Eu³⁺ Doped Sr₂B₂O₅ at 800°C

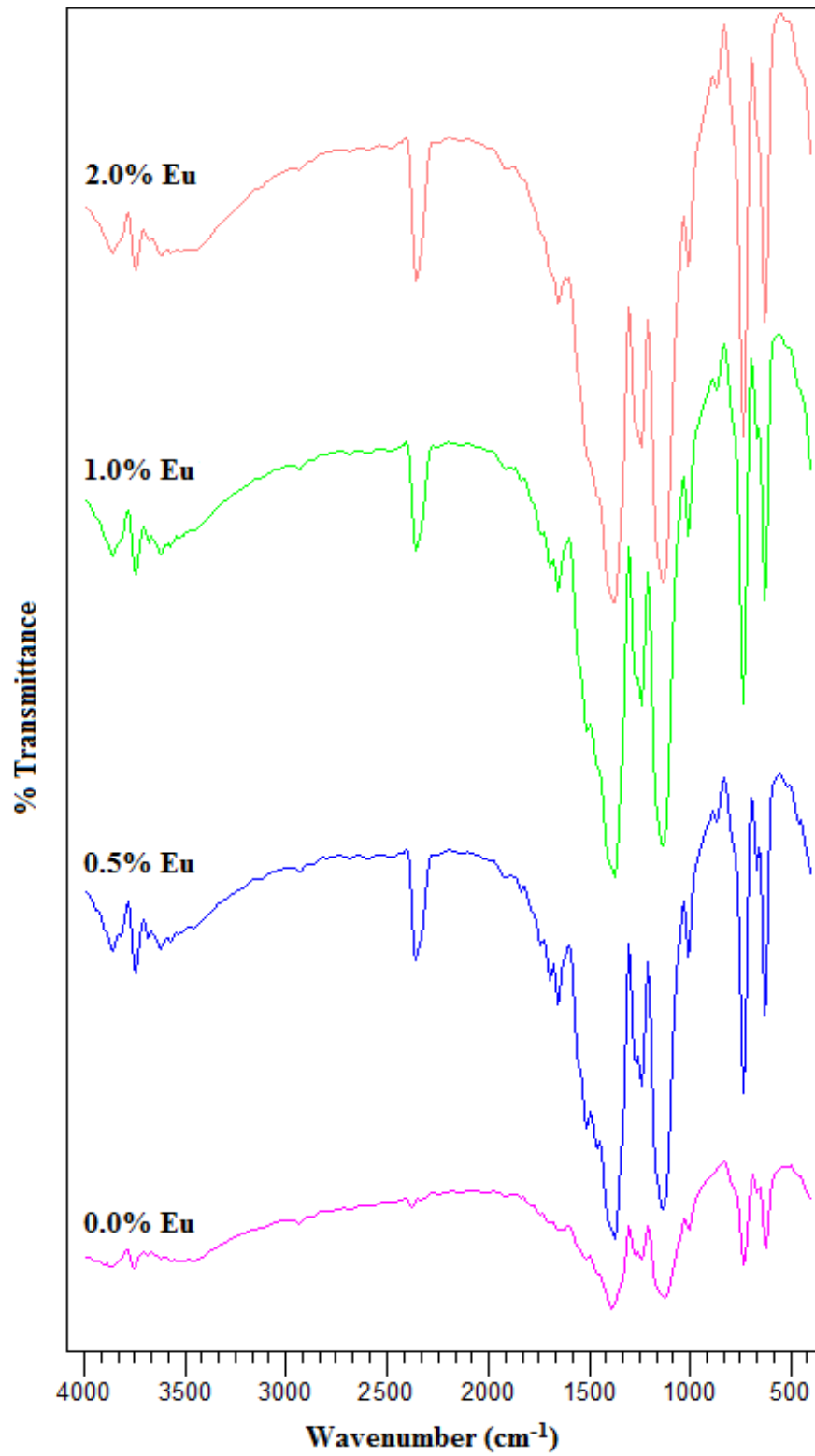


Figure 4.16. FT-IR Spectra of Eu³⁺ Doped Sr₂B₂O₅ at 900°C

Similar with cerium and europium doped $\text{Sr}_2\text{B}_2\text{O}_5$, the FT-IR spectra of terbium ion doped $\text{Sr}_2\text{B}_2\text{O}_5$ of each concentrations (0.02, 0.01, and 0.005 mol) gave a better peaks at higher temperature starting from 600°C to 900°C given in Figure 4.20, Figure 4.21, Figure 4.22, and Figure 4.23. All the vibrational modes of $\text{Sr}_2\text{B}_2\text{O}_5$ were observed and there is no additional peaks were examined, except for the peaks at around 2500 cm^{-1} , which belongs to background of FT-IR instrument. The best results were summarized in Table 4.5, which belongs to the terbium ion doped $\text{Sr}_2\text{B}_2\text{O}_5$ products obtained at 900°C.

Table 4.5. FT-IR band assignments of Tb^{3+} ion doped $\text{Sr}_2\text{B}_2\text{O}_5$ at 900°C

Assignment	Bending BO_3 (cm^{-1})	Asymmetric Stretching BO_3 (cm^{-1})	Bending H-O-H (cm^{-1})	Symmetric Stretching BO_3 (cm^{-1})
2.0%	727, 663	1136	1364	1455
1.0%	727, 663	1138	1360	1455
0.5%	727, 663	1138	1360	1455

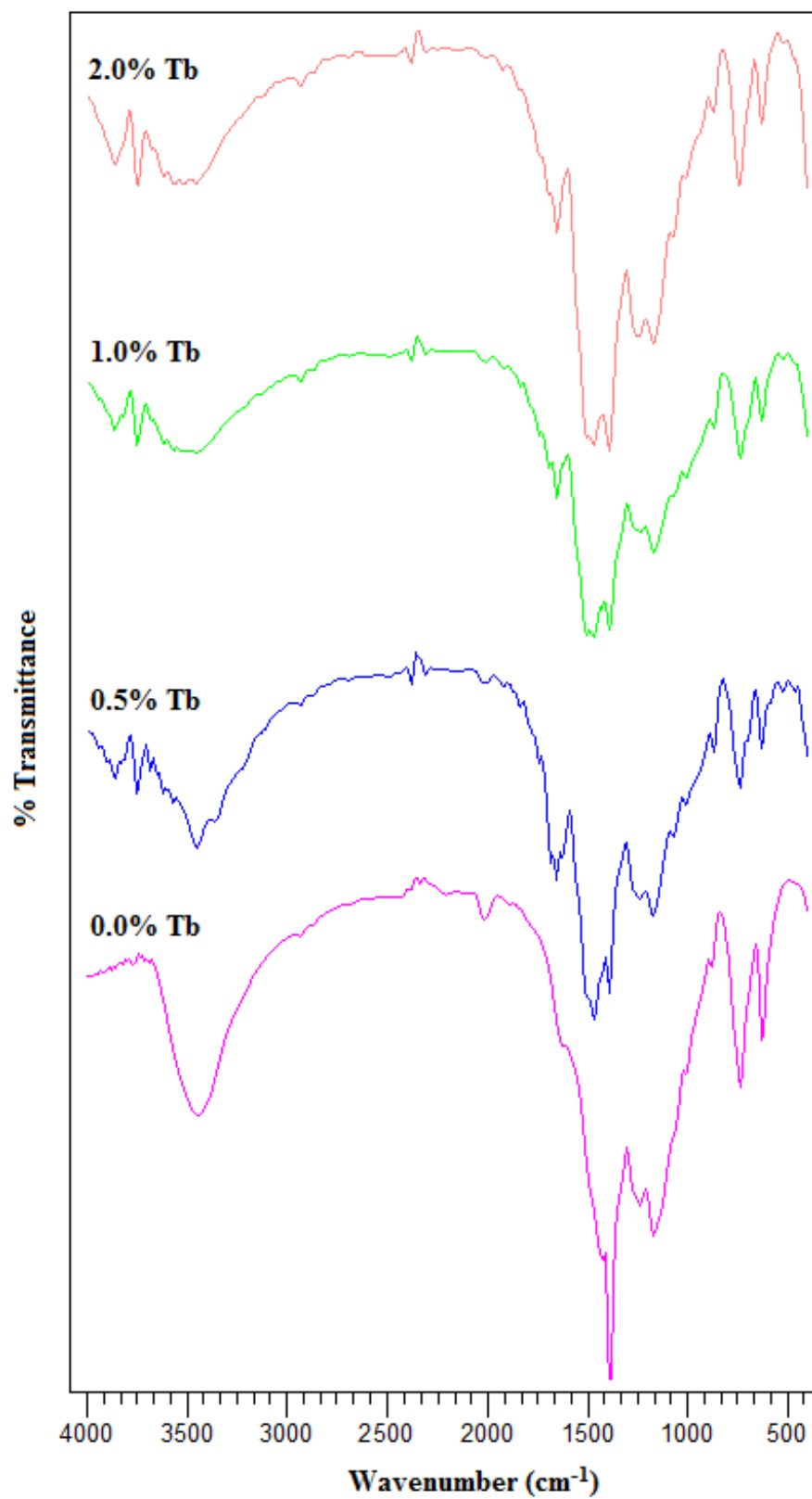


Figure 4.17. FT-IR Spectra of Tb^{3+} Doped $\text{Sr}_2\text{B}_2\text{O}_5$ at 400°C 10 minutes

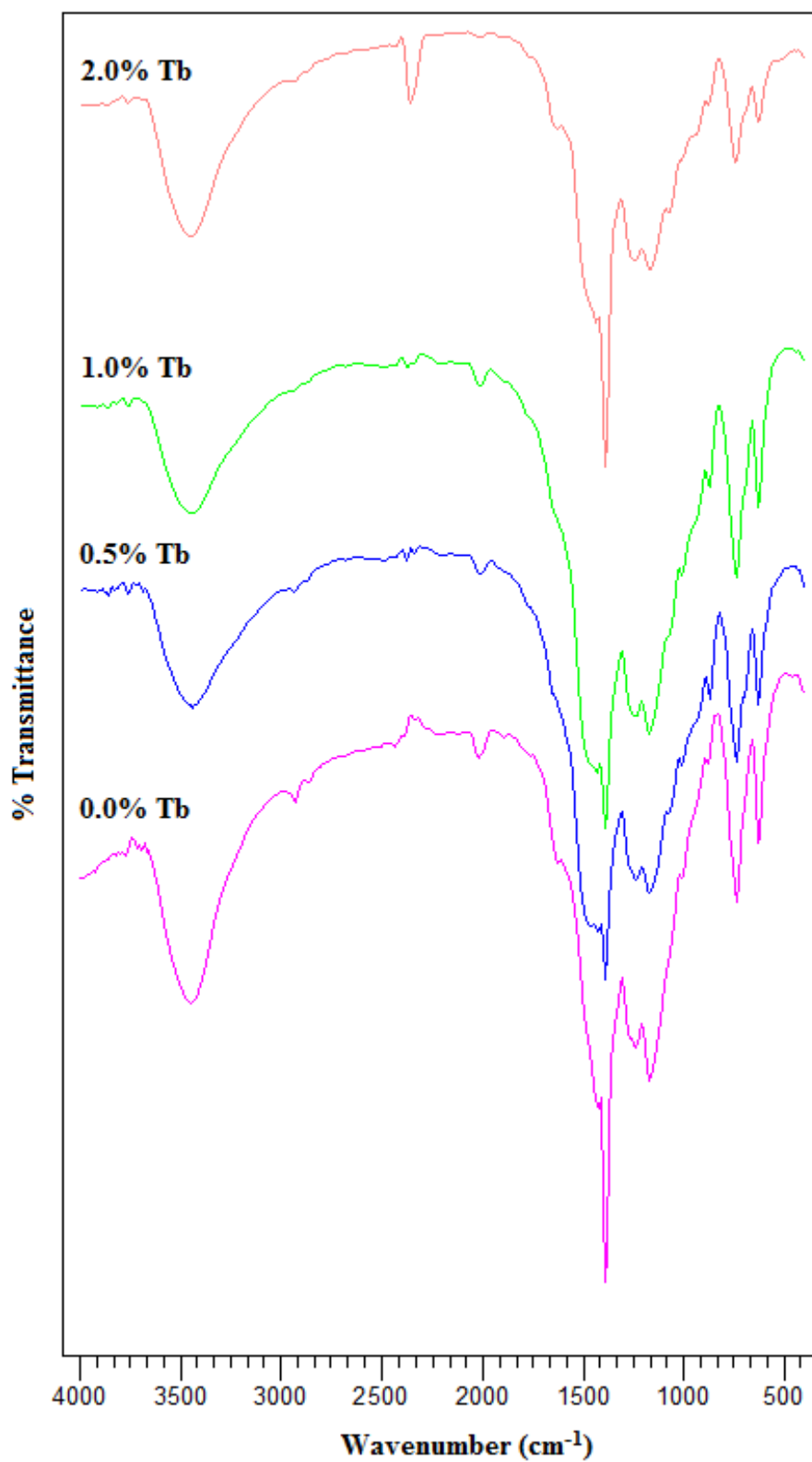


Figure 4.18. FT-IR Spectra of Tb^{3+} Doped $\text{Sr}_2\text{B}_2\text{O}_5$ at 400°C

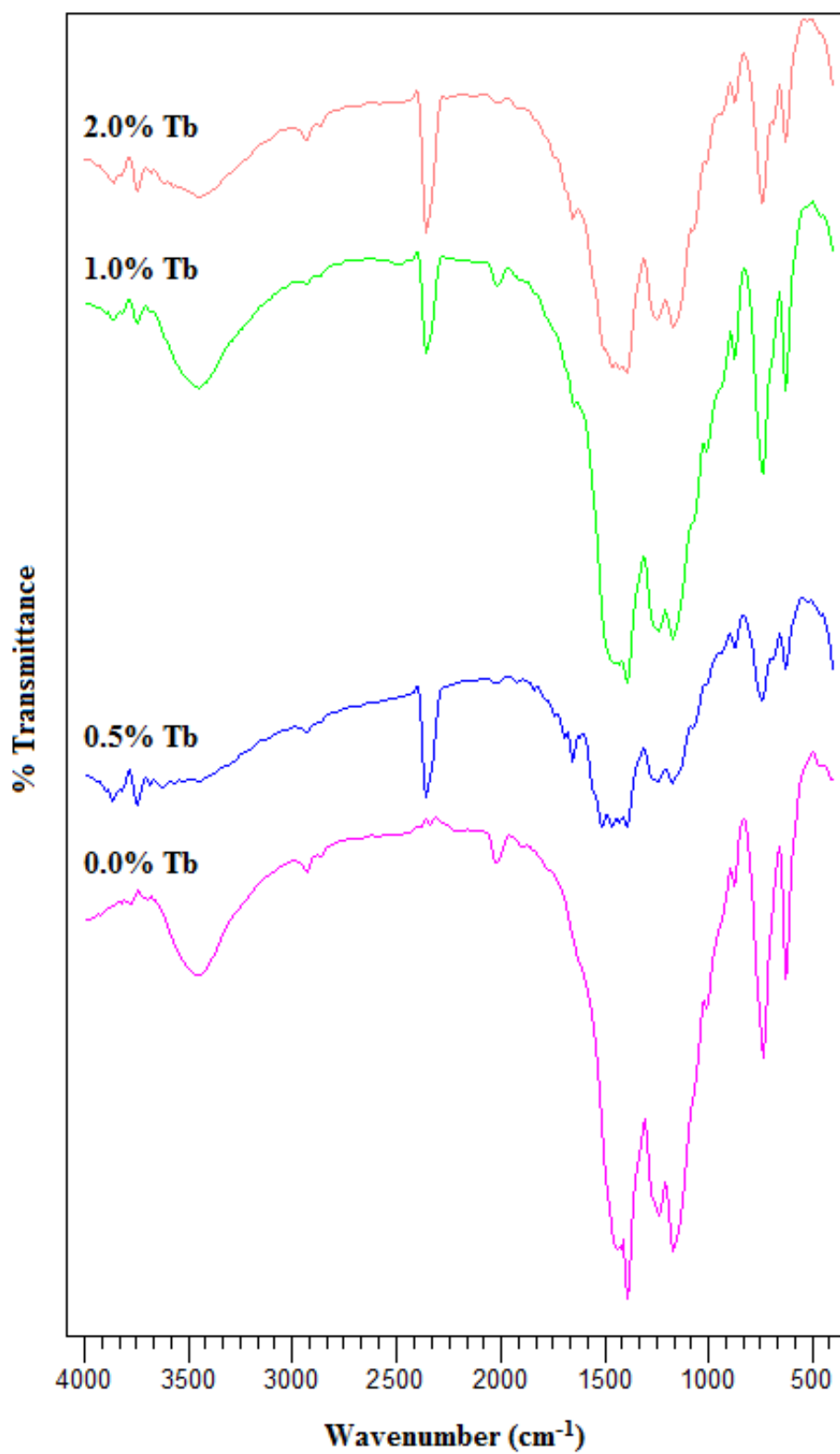


Figure 4.19. FT-IR Spectra of Tb^{3+} Doped $\text{Sr}_2\text{B}_2\text{O}_5$ at 500°C

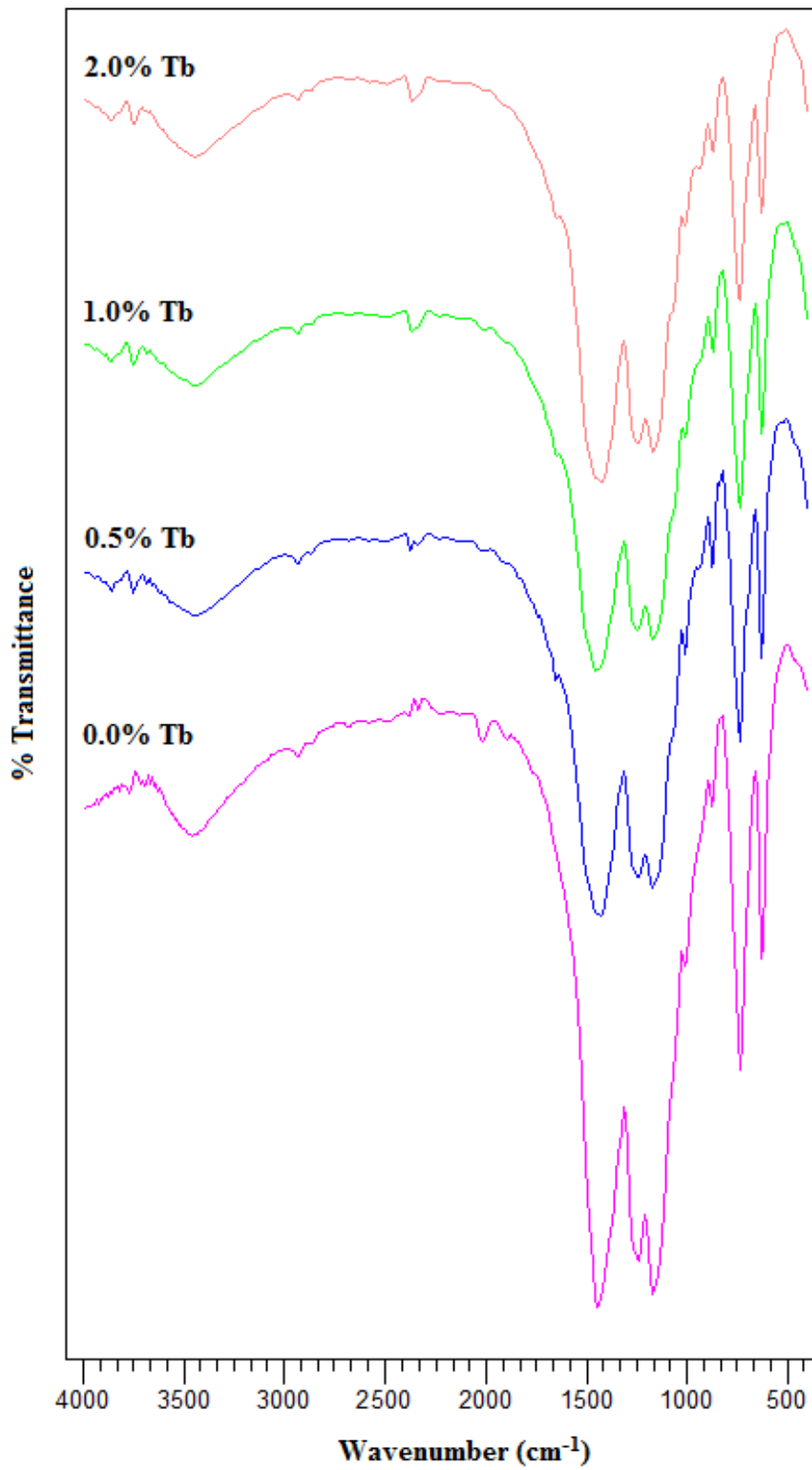


Figure 4.20. FT-IR Spectra of Tb^{3+} Doped $\text{Sr}_2\text{B}_2\text{O}_5$ at 600°C

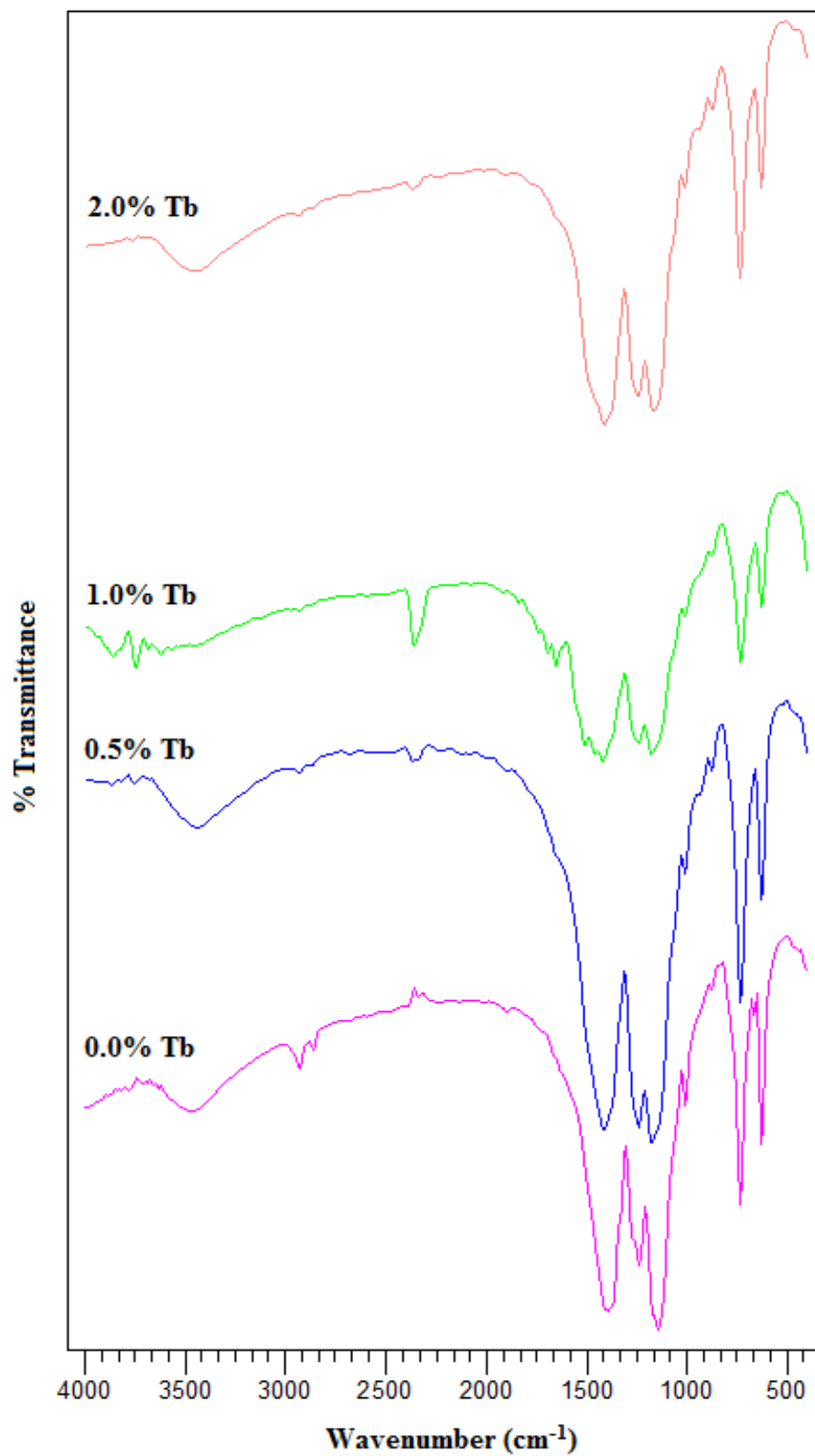


Figure 4.21. FT-IR Spectra of Tb^{3+} Doped $\text{Sr}_2\text{B}_2\text{O}_5$ at 700°C

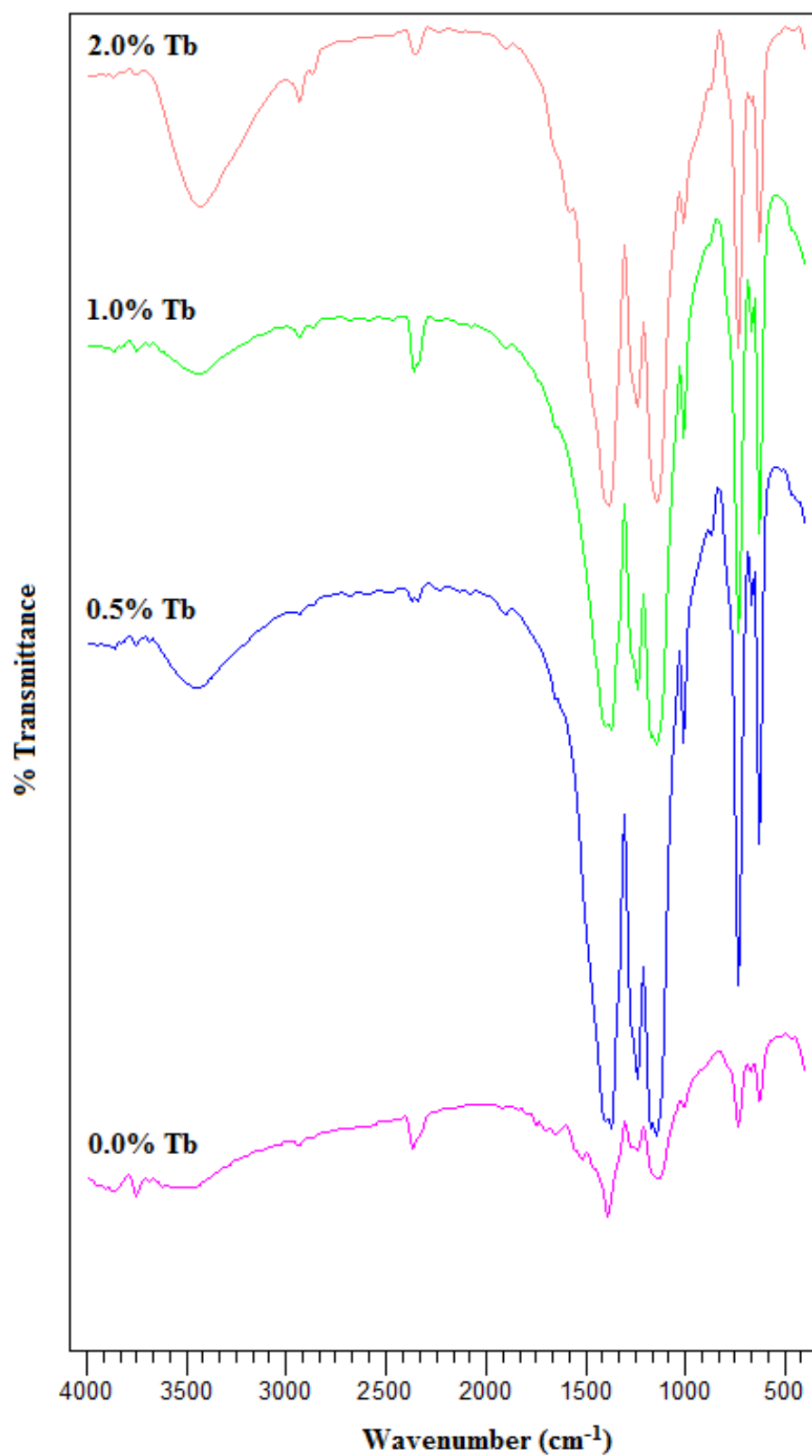


Figure 4.22. FT-IR Spectra of Tb^{3+} Doped $\text{Sr}_2\text{B}_2\text{O}_5$ at 800°C

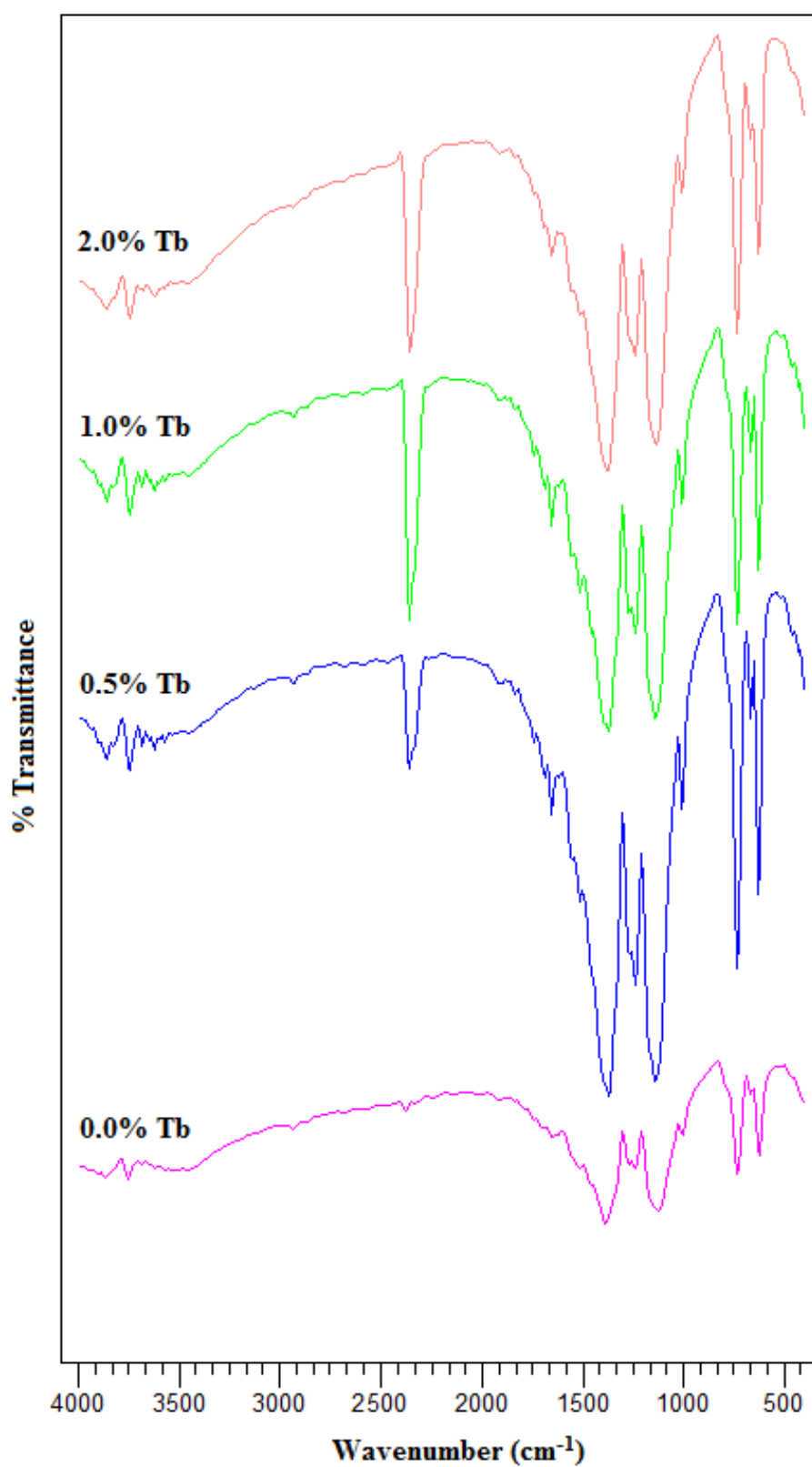


Figure 4.23. FT-IR Spectra of Tb^{3+} Doped $\text{Sr}_2\text{B}_2\text{O}_5$ at 900°C

4.1.1.2 Powder X-Ray Diffraction (PXRD) Studies

The X-ray powder diffraction patterns of the undoped $\text{Sr}_2\text{B}_2\text{O}_5$ that was synthesized by using glycine fuel obtained at various temperature were shown in Figure 4.24. The XRD patterns of the products are similar to that of $\text{Sr}_2\text{B}_2\text{O}_5$ form that given in ICDD card No.89-4488. It observed that, the color of products became lighter from grey to white by increasing the heating temperature. According to ICDD card No.89-4488 the crystal structure of $\text{Sr}_2\text{B}_2\text{O}_5$ is monoclinic phase. Hence, through these patterns it also observed that small impurity lines were observed at lower temperature at $2\theta = \sim 20^\circ$ and single phase monoclinic $\text{Sr}_2\text{B}_2\text{O}_5$ started to form at 600°C .

High crystallinity products were obtained at higher temperature, 900°C as it has highest intensity about 3000 a.u. Comparing the intensity of their XRD patterns, the intensity value of products increase with increasing the heating temperature which lead to the changed in crystallite size of the resulted products.

The XRD patterns of lanthanide element doped $\text{Sr}_2\text{B}_2\text{O}_5$ were also characterized and their XRD patterns that were obtained at 800°C and 900°C were compared by varying their dopant concentrations. Given in Figure 4.25, the XRD patterns reflections of Ce^{3+} doped $\text{Sr}_2\text{B}_2\text{O}_5$ synthesis products were characterized and the impurities were observed. The XRD patterns of all dopant concentrations showed sharp peak at $2\theta = \sim 20^\circ$ which indicate the existence of impurities. This impurity reflection is also observed in the XRD patterns of synthesis undoped $\text{Sr}_2\text{B}_2\text{O}_5$.

By increasing the temperature to 800°C , the impurities are starting to disappear (Figure 4.26) and pure $\text{Sr}_2\text{B}_2\text{O}_5$ was obtained at 900°C with the highest intensity value (Figure 4.27). The intensity value of 1.0% Cerium doped $\text{Sr}_2\text{B}_2\text{O}_5$ that are obtained at 800°C is similar with pure $\text{Sr}_2\text{B}_2\text{O}_5$ whereas the other concentrations have lower intensities. However, the patterns of the products of each concentrations showed similar behaviors with pure $\text{Sr}_2\text{B}_2\text{O}_5$ at 900°C .

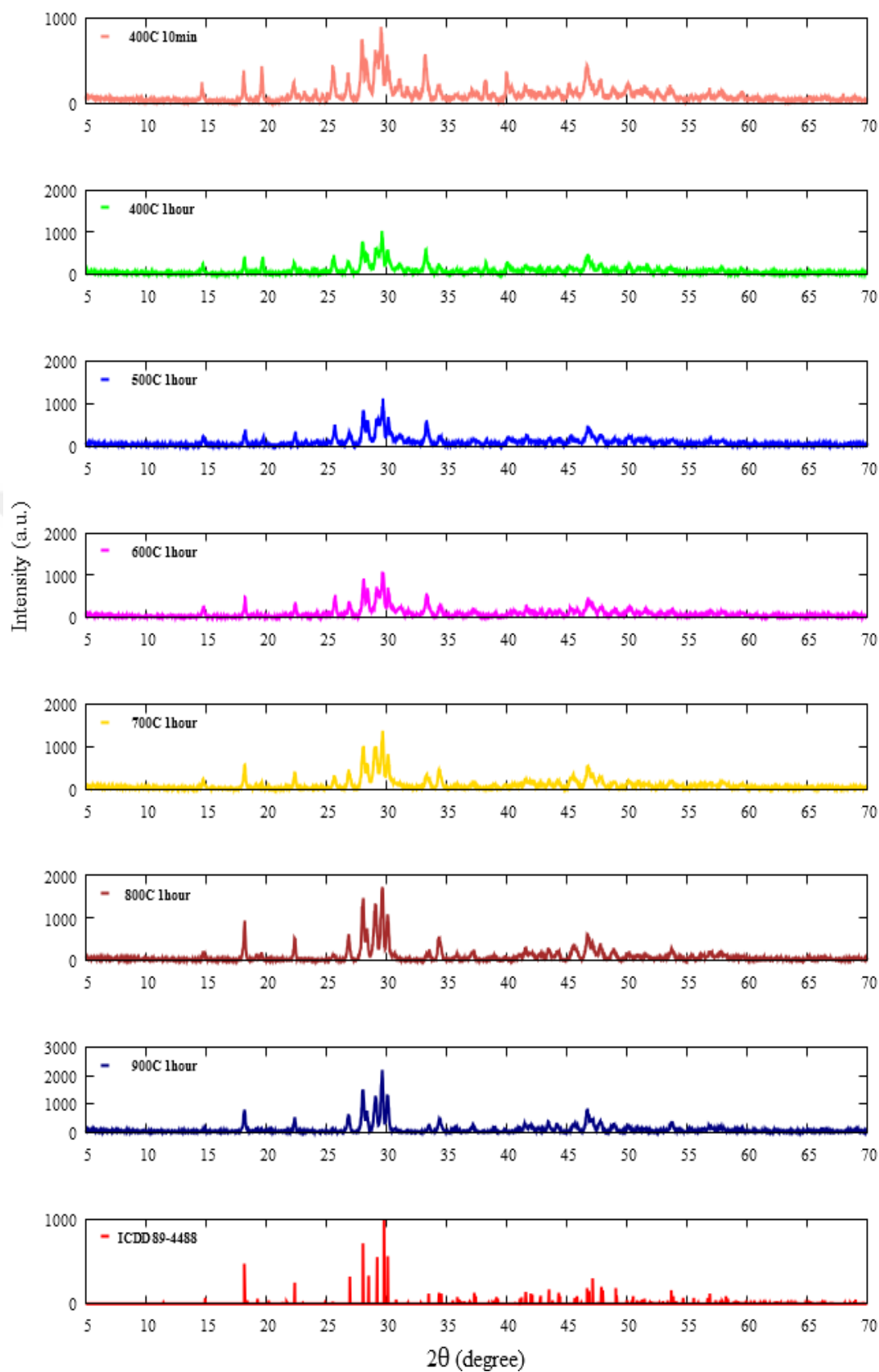


Figure 4.24. PXRD Patterns of Undoped $\text{Sr}_2\text{B}_2\text{O}_5$

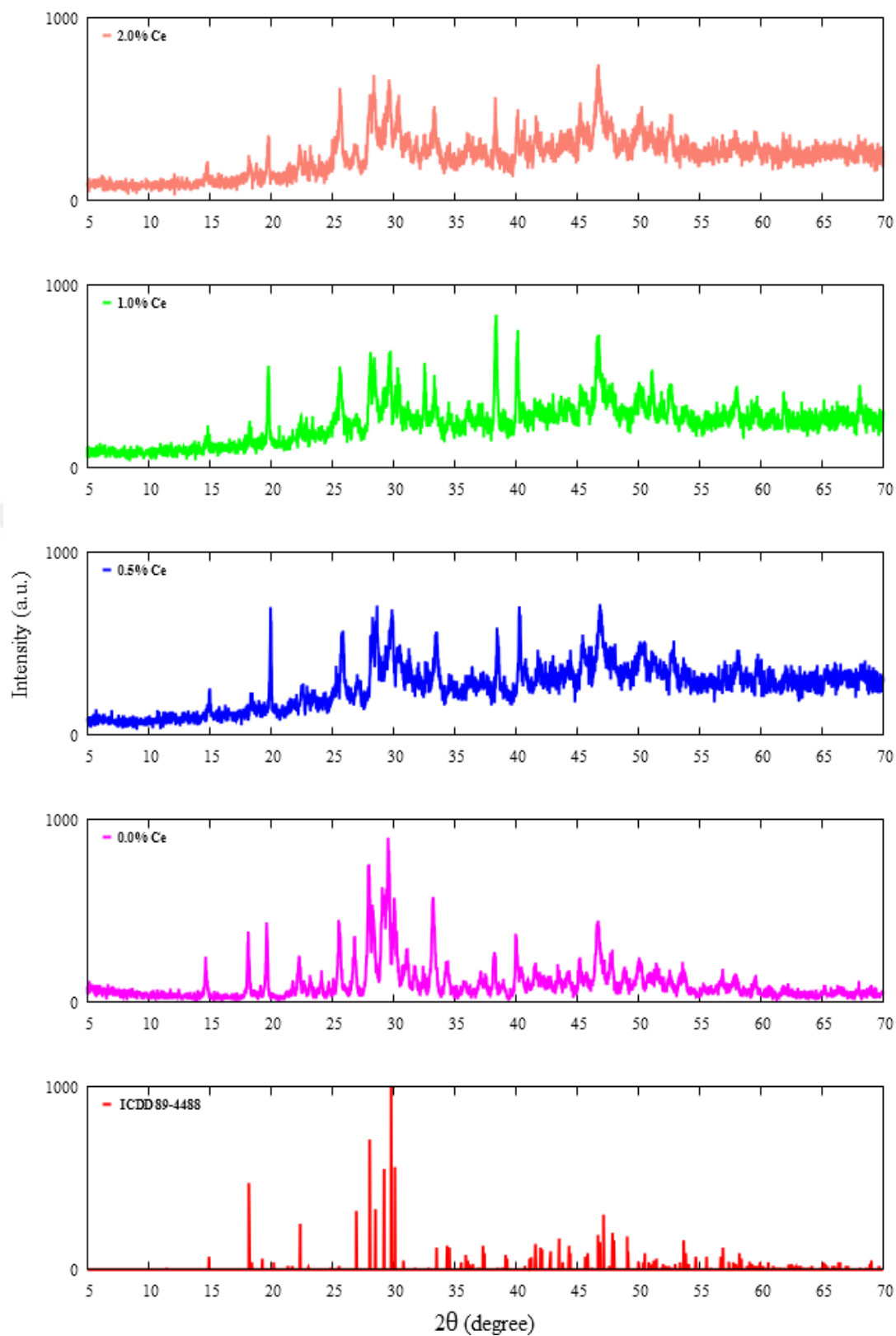


Figure 4.25. PXRD Patterns of Ce^{3+} Doped $\text{Sr}_2\text{B}_2\text{O}_5$ at 400°C 10 minutes

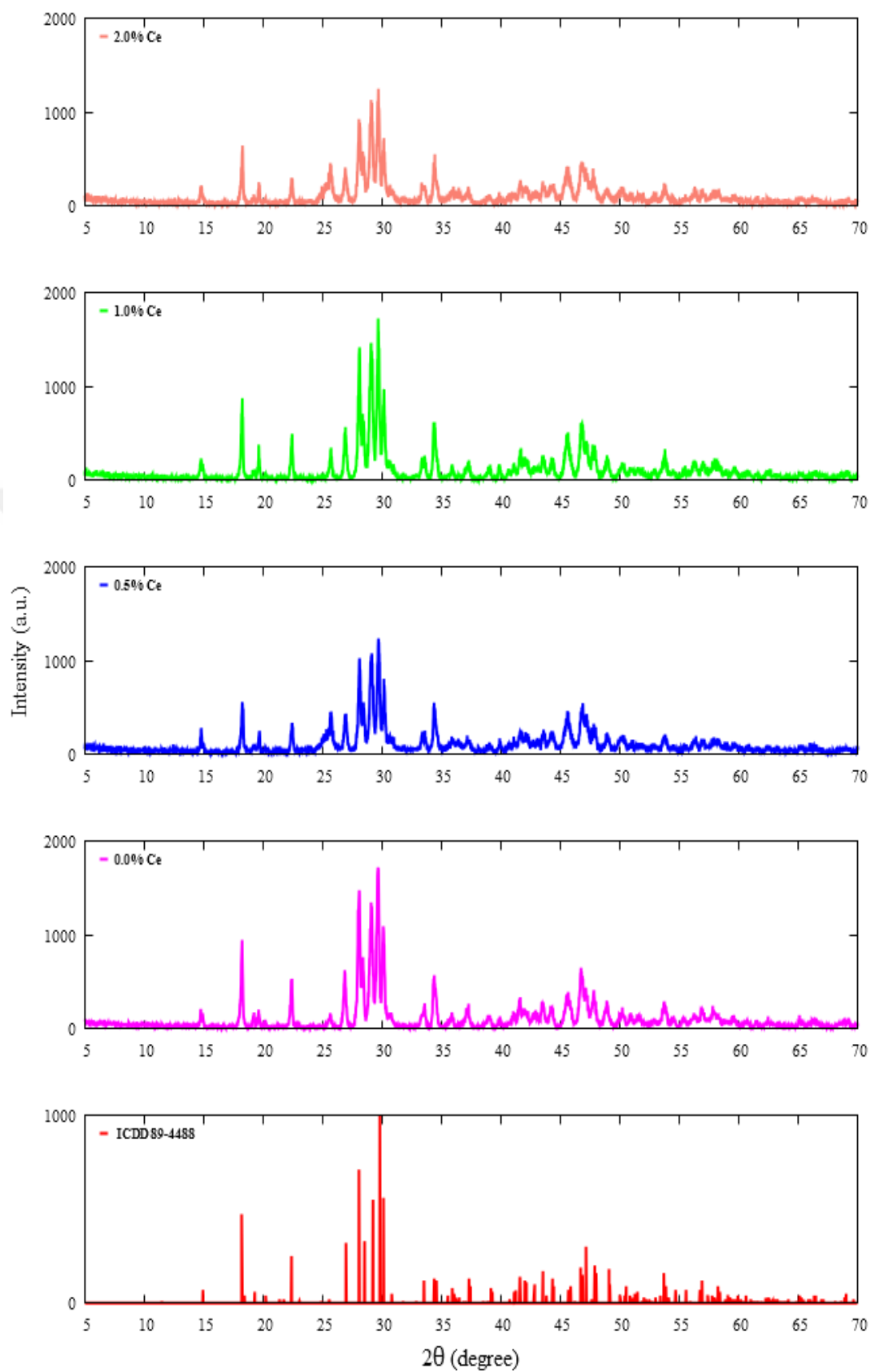


Figure 4.26. PXRD Patterns of Ce^{3+} Doped $\text{Sr}_2\text{B}_2\text{O}_5$ at 800°C

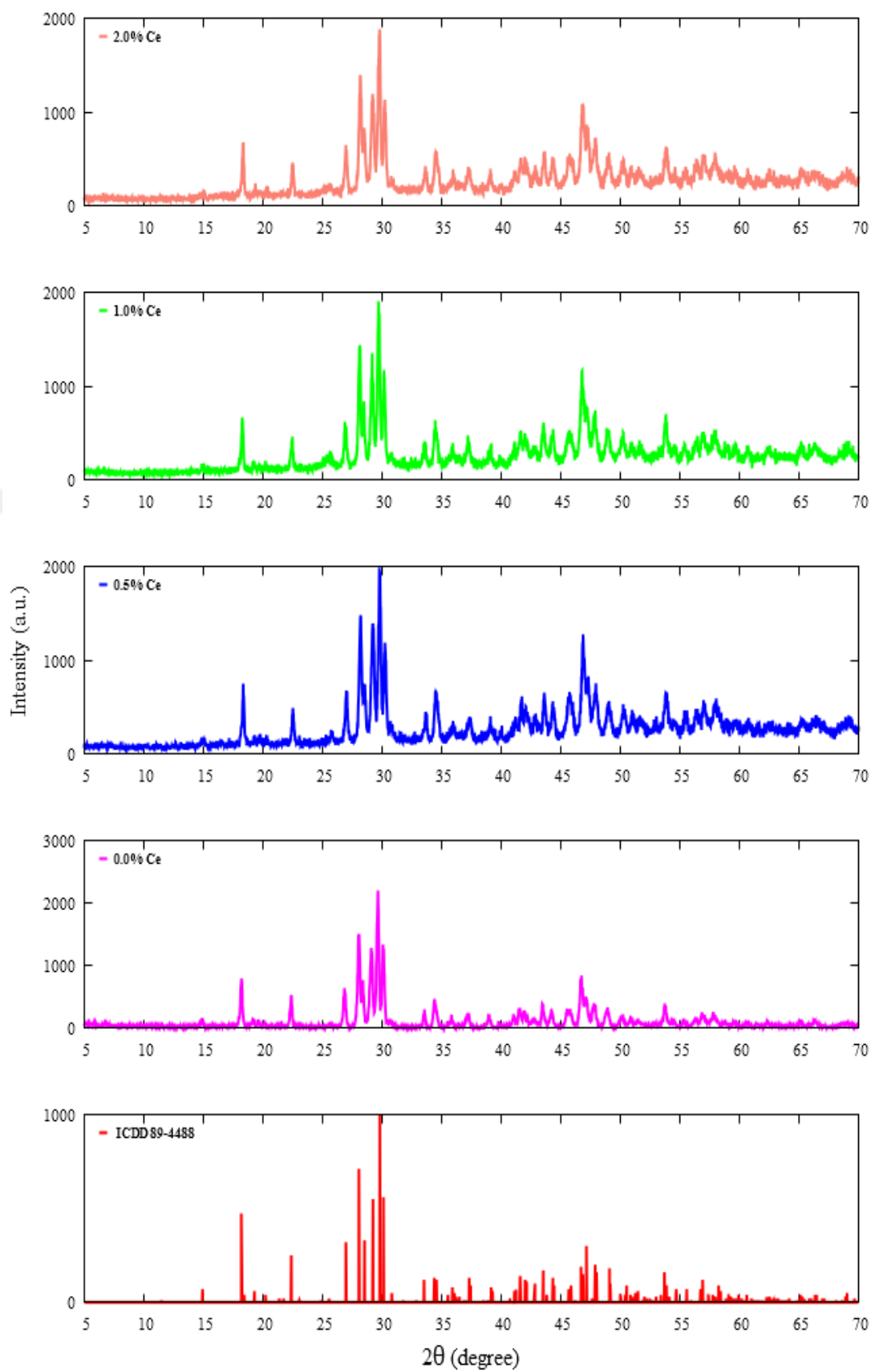


Figure 4.27. PXRD Patterns of Ce^{3+} Doped $\text{Sr}_2\text{B}_2\text{O}_5$ at 900°C

The XRD patterns of Eu^{3+} doped $\text{Sr}_2\text{B}_2\text{O}_5$ with all concentrations were characterized and were compared with undoped $\text{Sr}_2\text{B}_2\text{O}_5$. Similar to Ce^{3+} doped $\text{Sr}_2\text{B}_2\text{O}_5$, the additional peak was observed at $2\theta \approx 20^\circ$ in the synthesis products which indicate the presence of impurities. It observed that, the impurities are starting to disappear at 800°C (Figure 4.29) and 900°C (Figure 4.30). Moreover, the intensity value of products at these temperatures are decreasing by increasing the dopants concentrations.

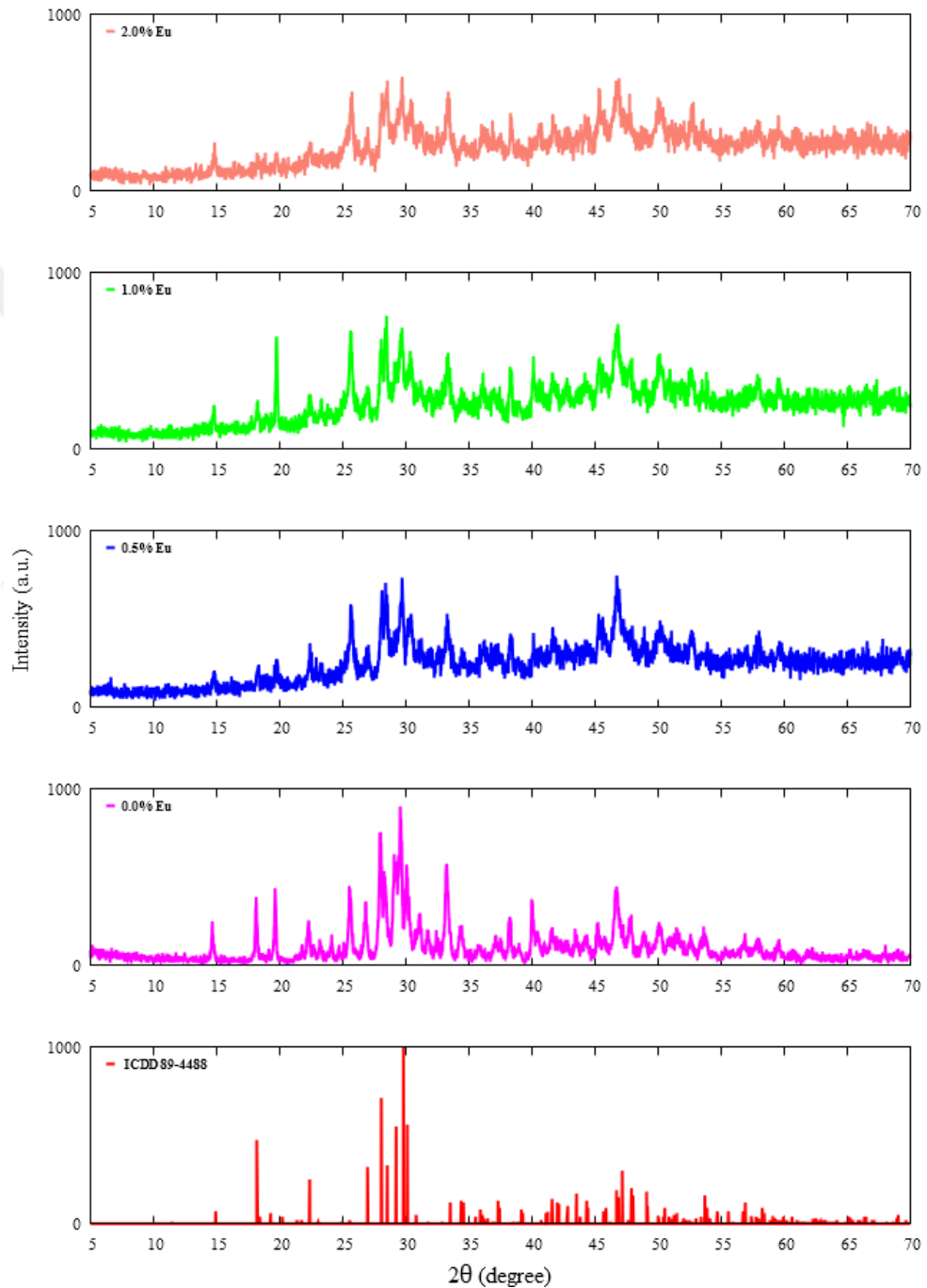


Figure 4.28. PXRD Patterns of Eu^{3+} Doped $\text{Sr}_2\text{B}_2\text{O}_5$ at 400°C 10 minutes

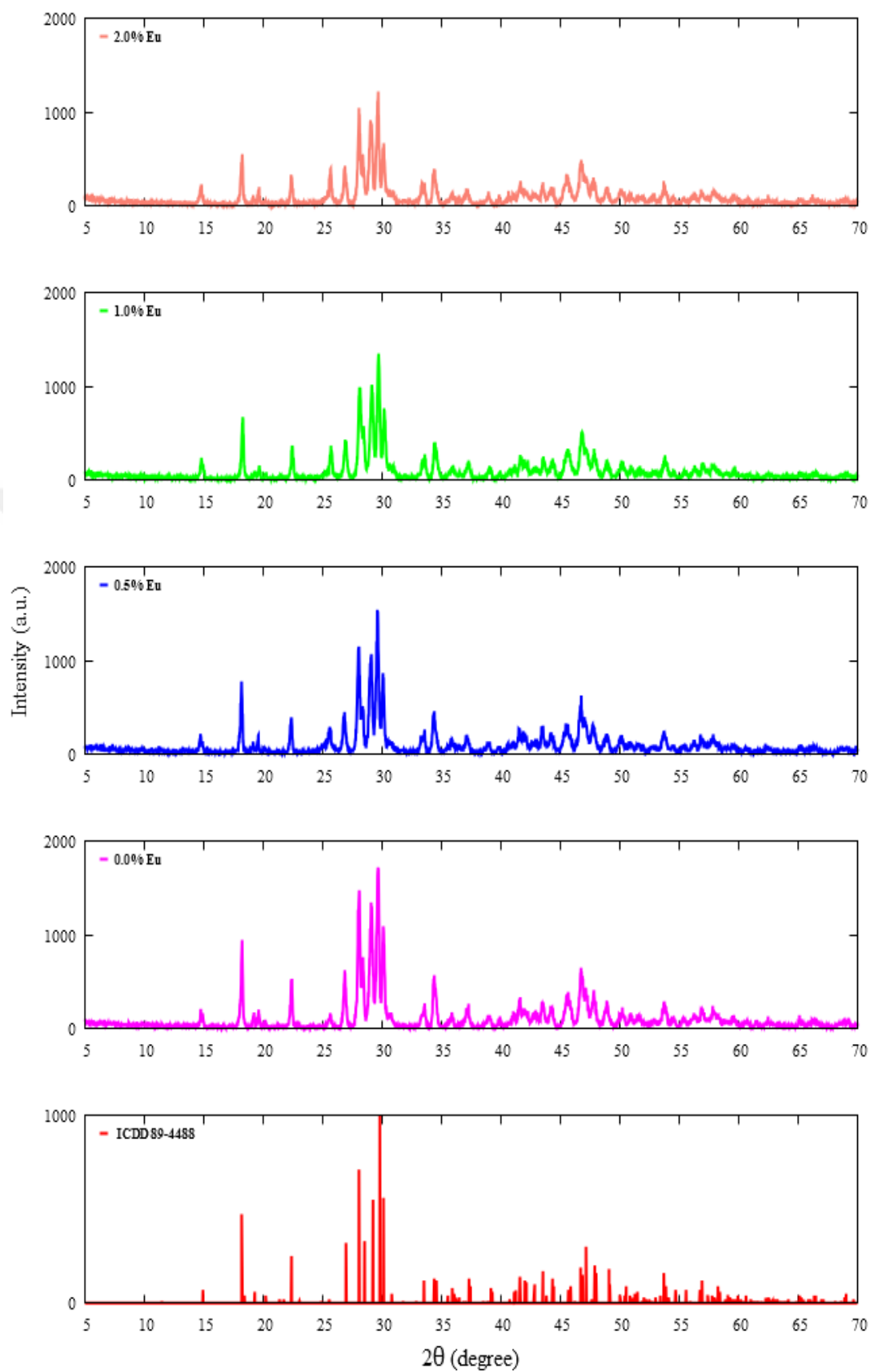


Figure 4.29. PXRD Patterns of Eu^{3+} Doped $\text{Sr}_2\text{B}_2\text{O}_5$ at 800°C

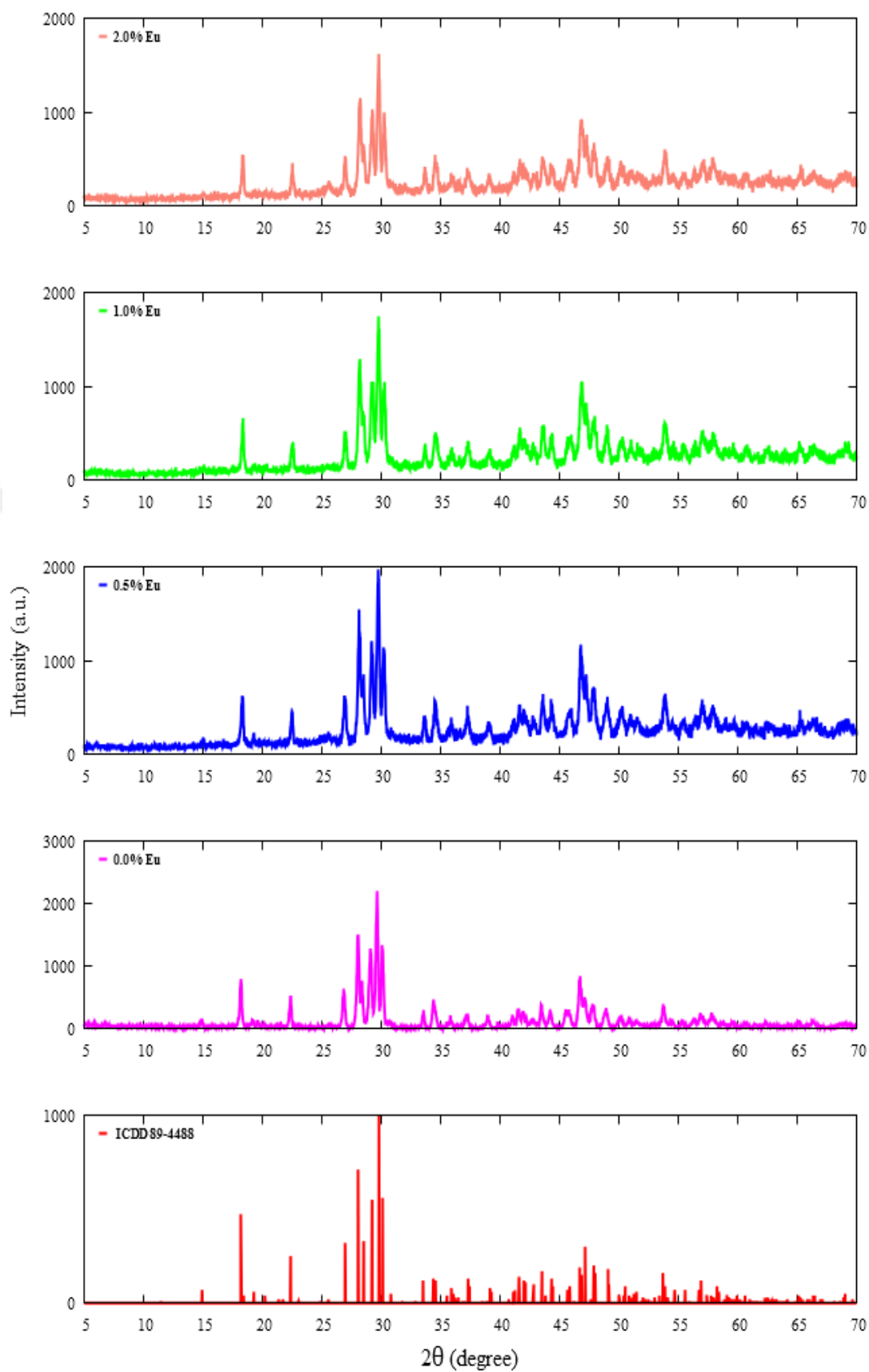


Figure 4.30. PXRD Patterns of Eu^{3+} Doped $\text{Sr}_2\text{B}_2\text{O}_5$ at 900°C

Tb³⁺ doped Sr₂B₂O₅ with all concentrations were characterized by X-Ray Diffraction (XRD) and were compared with undoped Sr₂B₂O₅. The impurity that were observed at 2θ = ~20° in the synthesis products (Figure 4.31) were starting to disappear at higher temperature as 800°C (Figure 4.32) and 900°C (Figure 4.33). The changed in intensity value were also examined in XRD patterns of Tb³⁺ doped Sr₂B₂O₅. Unlike the patterns of Europium ion doped Sr₂B₂O₅, the intensity value of 1.0% Tb³⁺ doped Sr₂B₂O₅ was observed lower that the others concentrations.

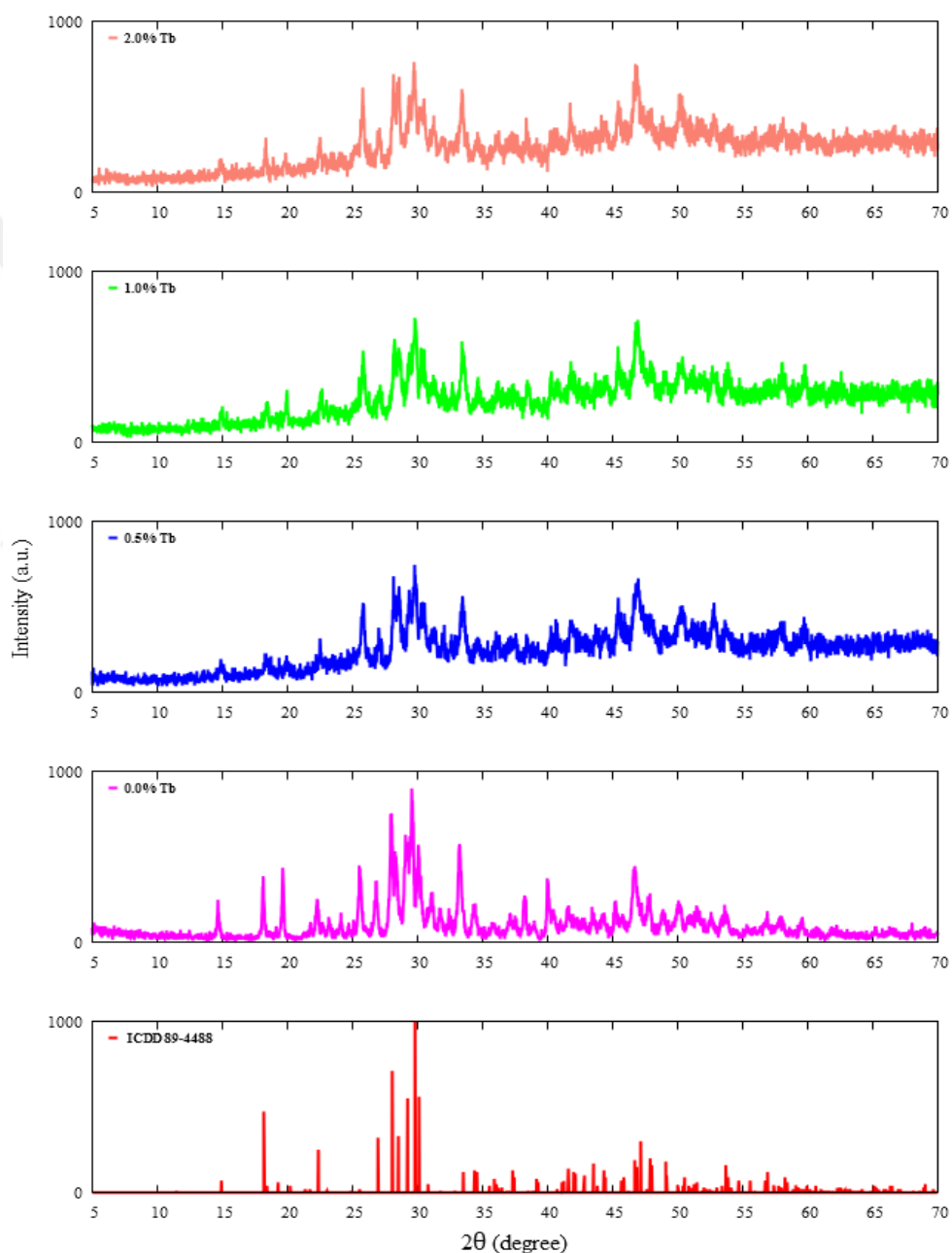


Figure 4.31. PXRD Patterns of Tb³⁺ Doped Sr₂B₂O₅ at 400°C 10 minutes

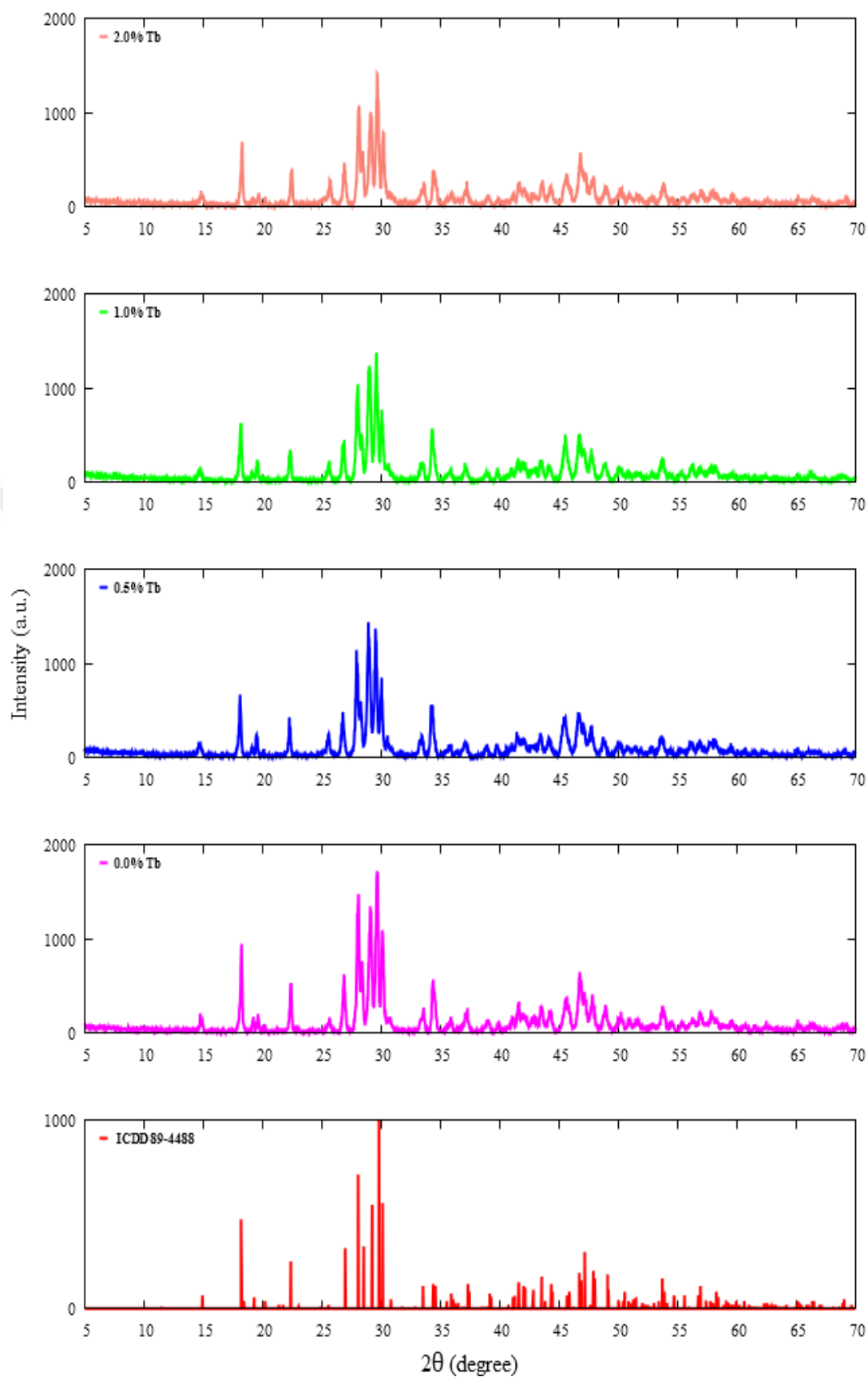


Figure 4.32. PXRD Patterns of Tb³⁺ Doped Sr₂B₂O₅ at 800°C

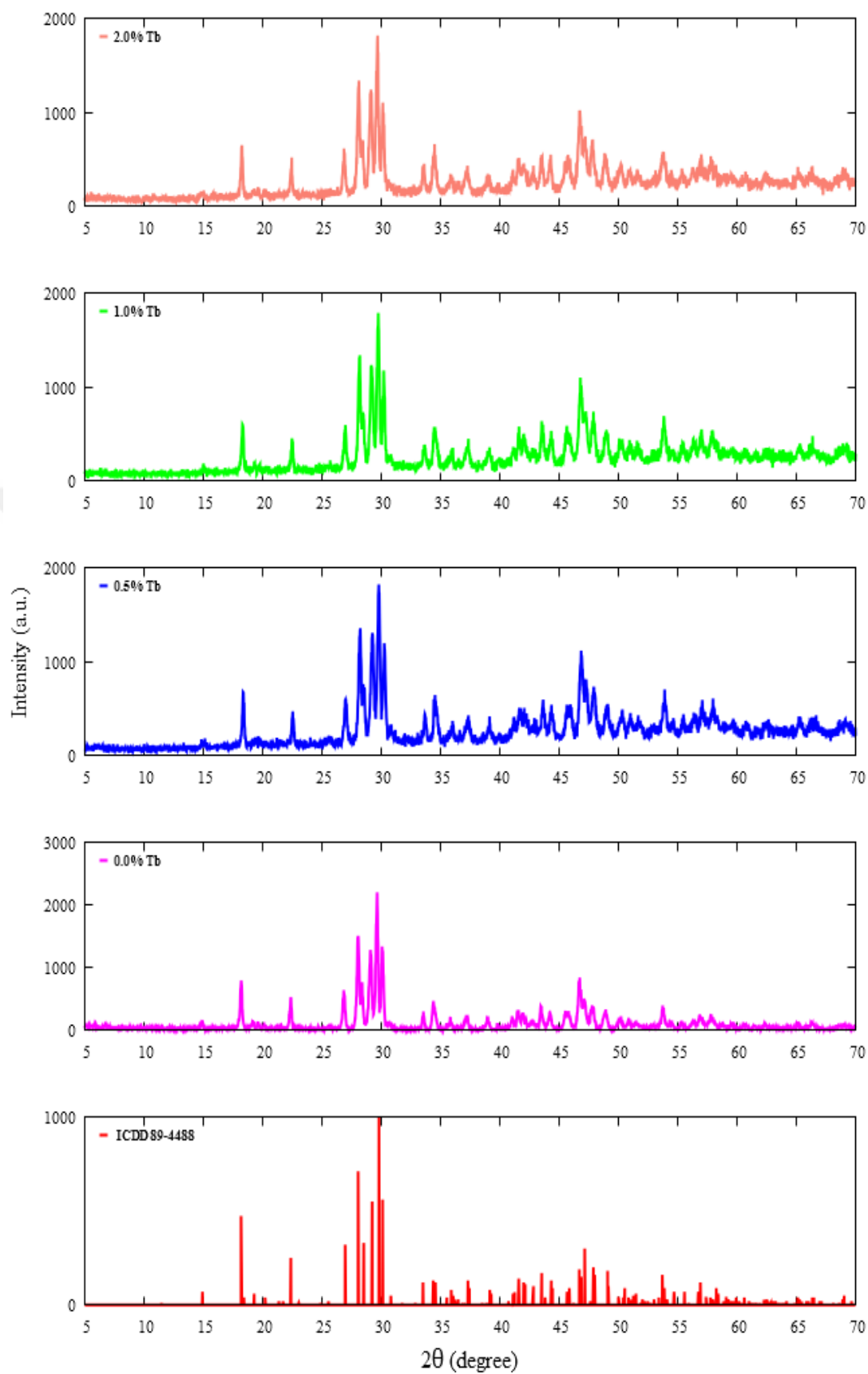


Figure 4.33. PXRD Patterns of Tb^{3+} Doped $\text{Sr}_2\text{B}_2\text{O}_5$ at 900°C

The crystallite sizes of the undoped and lanthanide element doped Sr₂B₂O₅ were determined by using Debye-Scherrer's Equation.

$$D = \frac{K\lambda}{\beta \cos\theta}$$

Where D is the average crystallite size (nm), K is constant, the shape factor which is generally taken as 0.90, λ is the radiation wavelength (CuK α) which is λ equal to 1.54056 Å, β is the full width at half of the maximum (radians) and θ is the diffraction angle. (Langford and Wilson, 1978; Scherrer, 1918)

Table 4.6. Crystallite Sizes of Undoped and Ln Doped Sr₂B₂O₅

Strontium Pyroborates	Crystallite size (nm)	
	800°C	900°C
Undoped	41.82	40.94
2.0% Ce³⁺	36.18	33.24
1.0% Ce³⁺	41.67	34.73
0.5% Ce³⁺	35.93	35.59
2.0% Eu³⁺	40.50	31.88
1.0% Eu³⁺	33.01	29.33
0.5% Eu³⁺	36.56	31.59
2.0% Tb³⁺	37.34	34.92
1.0% Tb³⁺	34.36	34.17
0.5% Tb³⁺	41.66	32.82

Given in Table 4.6, the effect of temperatures and dopants concentrations on the crystallite size of Sr₂B₂O₅ were investigated. It showed that, the crystallite size are decreasing with increasing the heating temperature and the crystallite sizes are also affected by various dopant concentrations. Crystallite sizes of Ce³⁺ ion doped Sr₂B₂O₅ products are decreasing by increasing the concentrations. On the other hand, the crystallite sizes of Tb³⁺ ion doped Sr₂B₂O₅ products are increasing by decreasing the concentrations. Furthermore, the Eu³⁺ ion doped Sr₂B₂O₅ products gave different values of crystallite size which the lowest belongs to 1.0% Eu³⁺ ion doped.

4.1.1.3 UV-VIS Spectroscopy Studies

The optical characteristics of undoped $\text{Sr}_2\text{B}_2\text{O}_5$ were also determined by using UV-VIS Spectrophotometer in the range of wavelength 900-200 nm. The optical band gap energy of prepared products were examined by plotting the $(\alpha h\nu)^2$ versus energy which also known as tauc plot. The graph was plotted by using the UV-VIS absorbance data and the optical band gap energy was attained by taking the intercept of the curve on the energy in the x-axis.

The absorbance and reflectance spectra of undoped strontium pyroborate at all temperatures are shown in Figure 4.34 and Figure 4.35, respectively. According to the absorbance spectra of undoped $\text{Sr}_2\text{B}_2\text{O}_5$, the blue shift was observed due to the decreasing in the wavelength with increasing temperature. It also observed that the absorbance of the undoped $\text{Sr}_2\text{B}_2\text{O}_5$ products decrease with increasing temperature.

The UV-Visible spectra of Ce^{3+} ion doped $\text{Sr}_2\text{B}_2\text{O}_5$ are shown in Figure 4.36 and Figure 4.37 for heated products at 800°C. Because of the increasing in the wavelength with increasing the concentration, the red shift was observed at 800°C, and this behavior was also observed at 900°C which is given in Figure 4.38 and Figure 4.39 for absorbance and reflectance, respectively.

Unlike cerium ion doped $\text{Sr}_2\text{B}_2\text{O}_5$, blue shift was examined in europium ion doped strontium pyroborate as the wavelength decreasing with increasing the concentrations. The absorbance and reflectance spectra of Eu^{3+} ion doped products were obtained at 800°C shown in Figure 4.40 and Figure 4.41, respectively. At 900°C, blue shift was also observed by investigating the absorbance and reflectance spectra (Figure 4.42 and Figure 4.43).

Terbium ion doped $\text{Sr}_2\text{B}_2\text{O}_5$ products gave very similar behavior with Cerium ion doped products because their wavelength values increasing by increasing concentration which indicate the red shift behavior. The red shift behavior was observed from 800°C in Figure 4.44 and Figure 4.45 as absorbance and reflectance spectra. In more addition, the absorbance spectra (Figure 4.46) and reflectance spectra (Figure 4.47) were also obtained at 900°C.

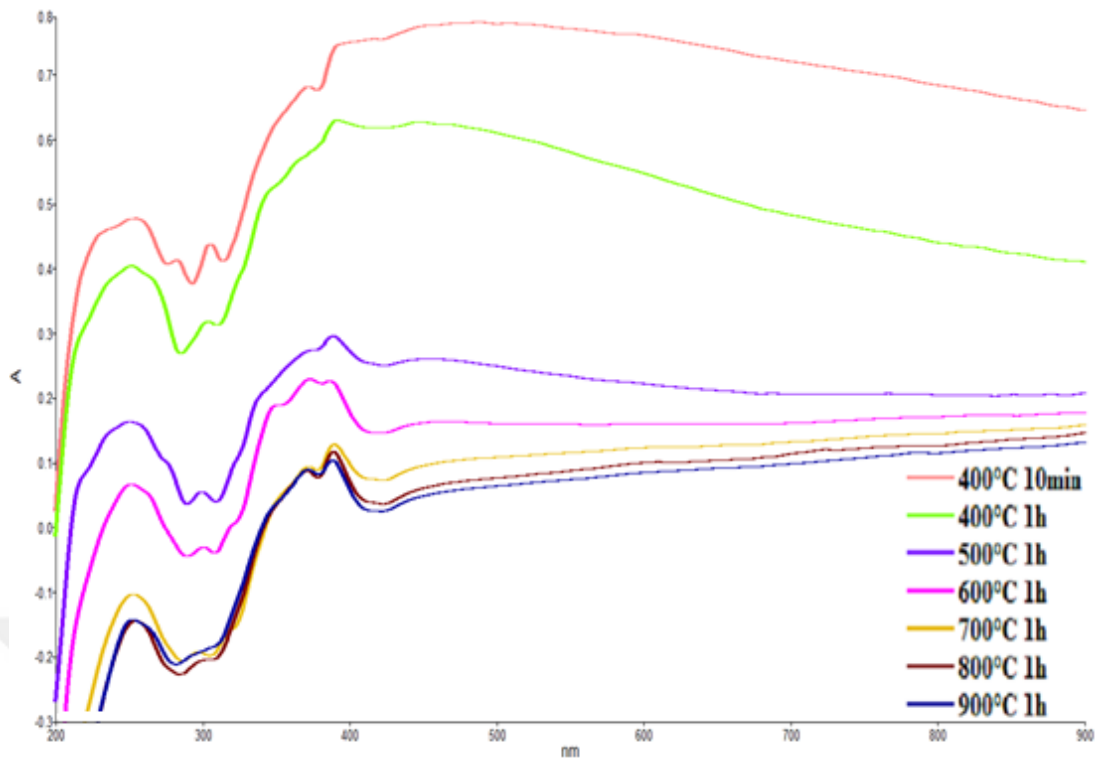


Figure 4.34. UV-VIS Absorbance Spectra of Undoped $\text{Sr}_2\text{B}_2\text{O}_5$

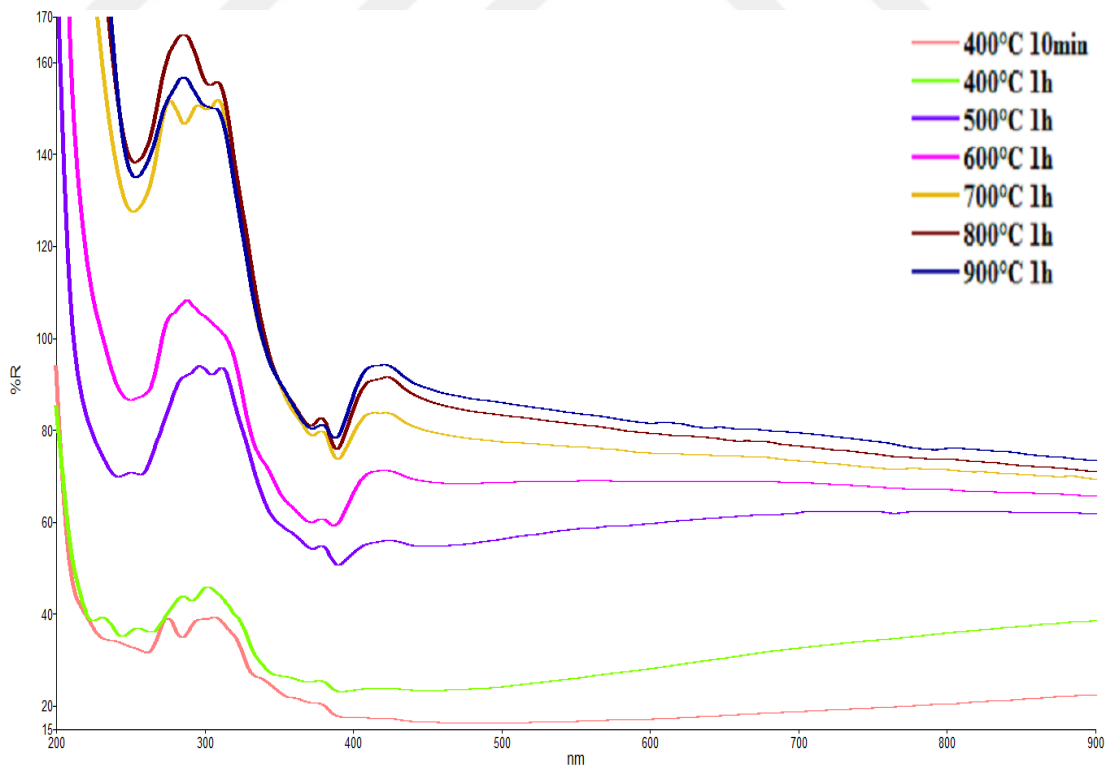


Figure 4.35. UV-VIS Reflectance Spectra of Undoped $\text{Sr}_2\text{B}_2\text{O}_5$

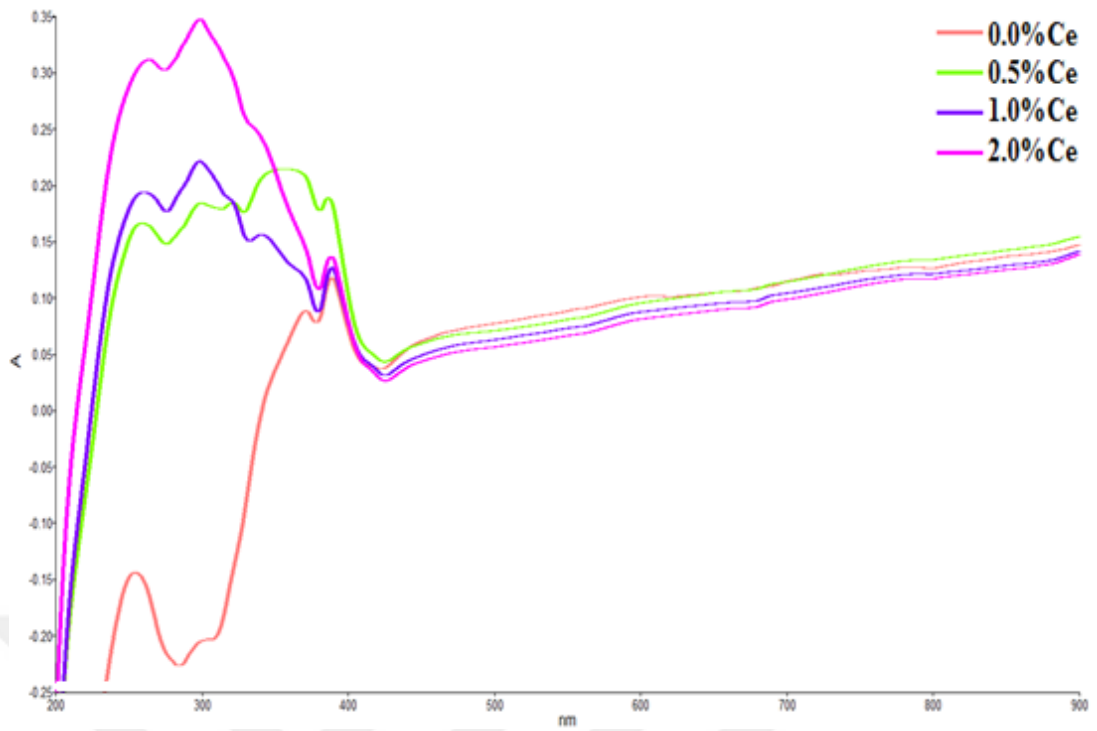


Figure 4.36. UV-VIS Absorbance Spectra of Ce^{3+} Doped $\text{Sr}_2\text{B}_2\text{O}_5$ at 800°C

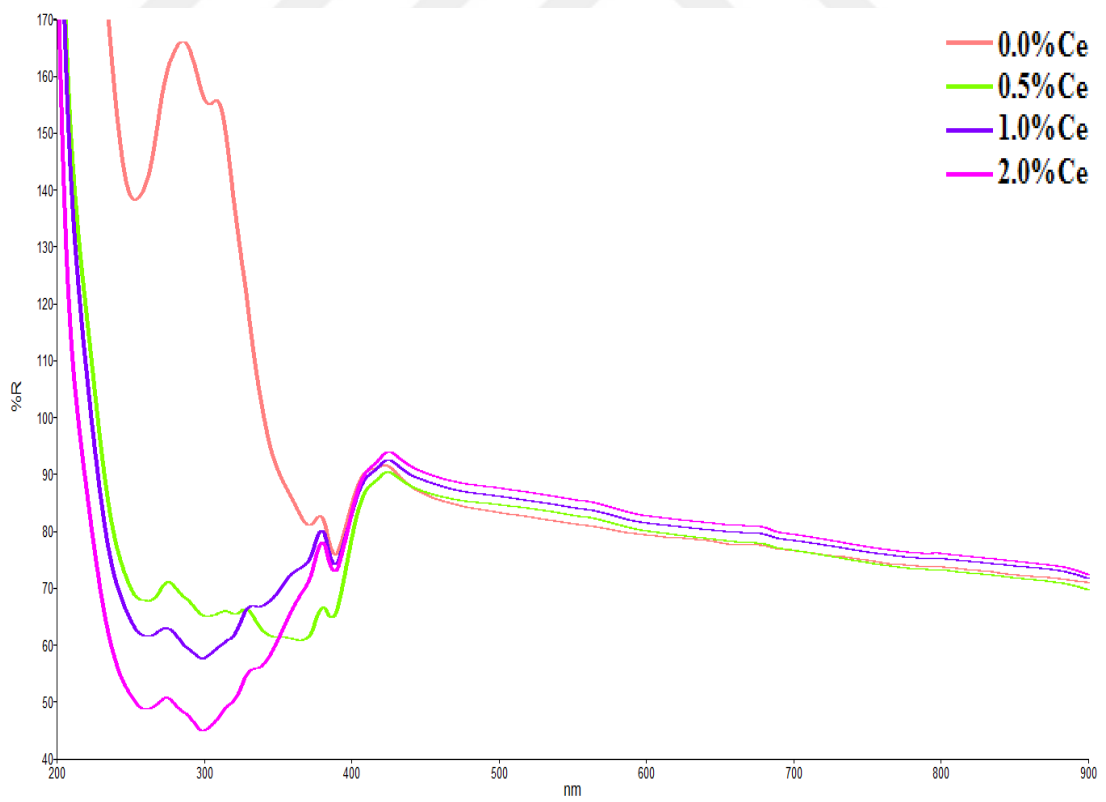


Figure 4.37. UV-VIS Reflectance Spectra of Ce^{3+} Doped $\text{Sr}_2\text{B}_2\text{O}_5$ at 800°C

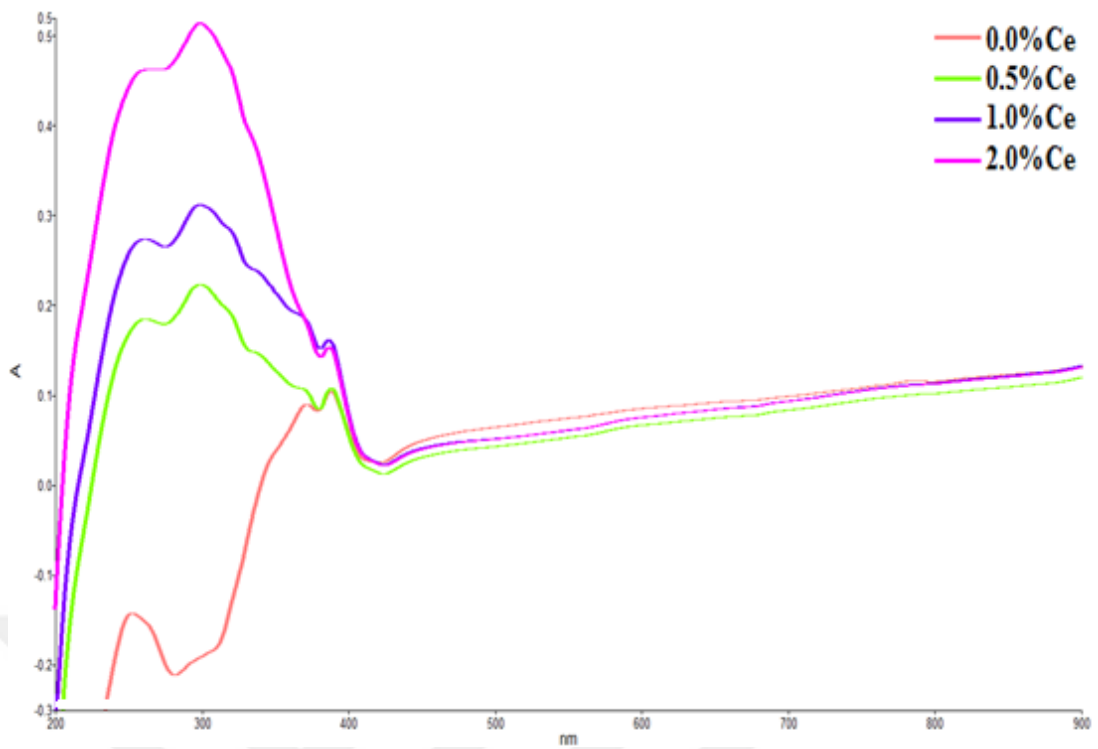


Figure 4.38. UV-VIS Absorbance Spectra of Ce^{3+} Doped $\text{Sr}_2\text{B}_2\text{O}_5$ at 900°C

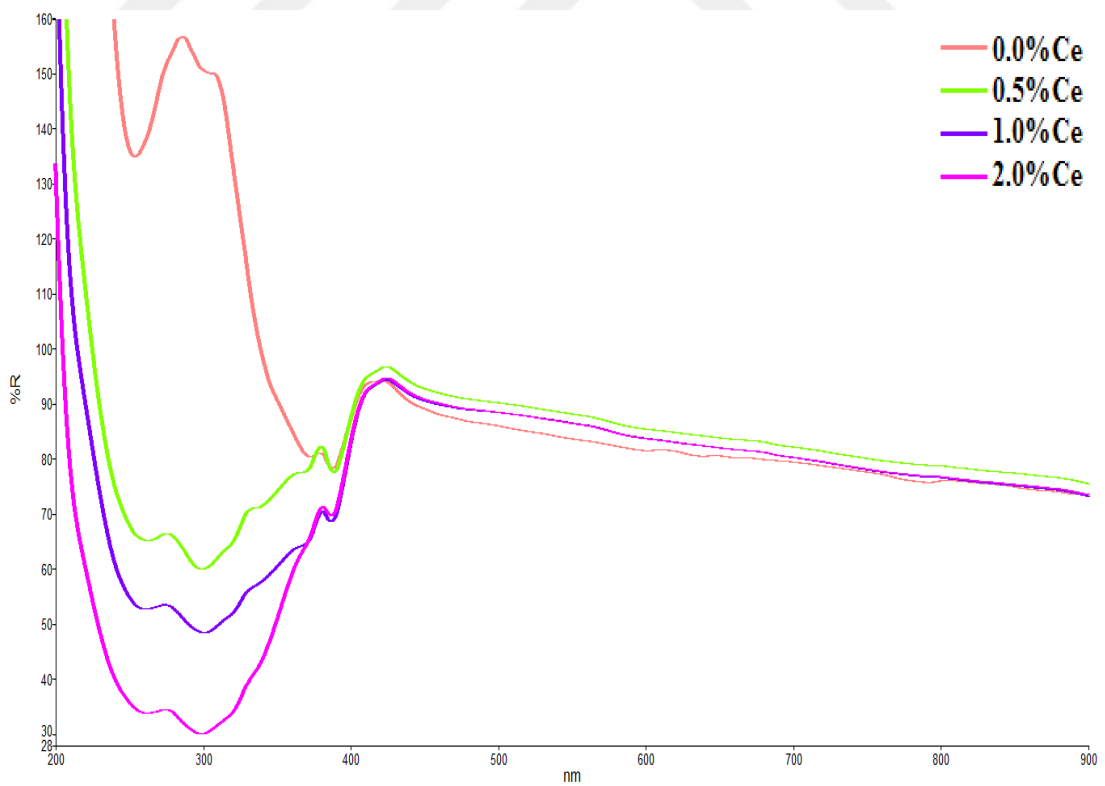


Figure 4.39. UV-VIS Reflectance Spectra of Ce^{3+} Doped $\text{Sr}_2\text{B}_2\text{O}_5$ at 900°C

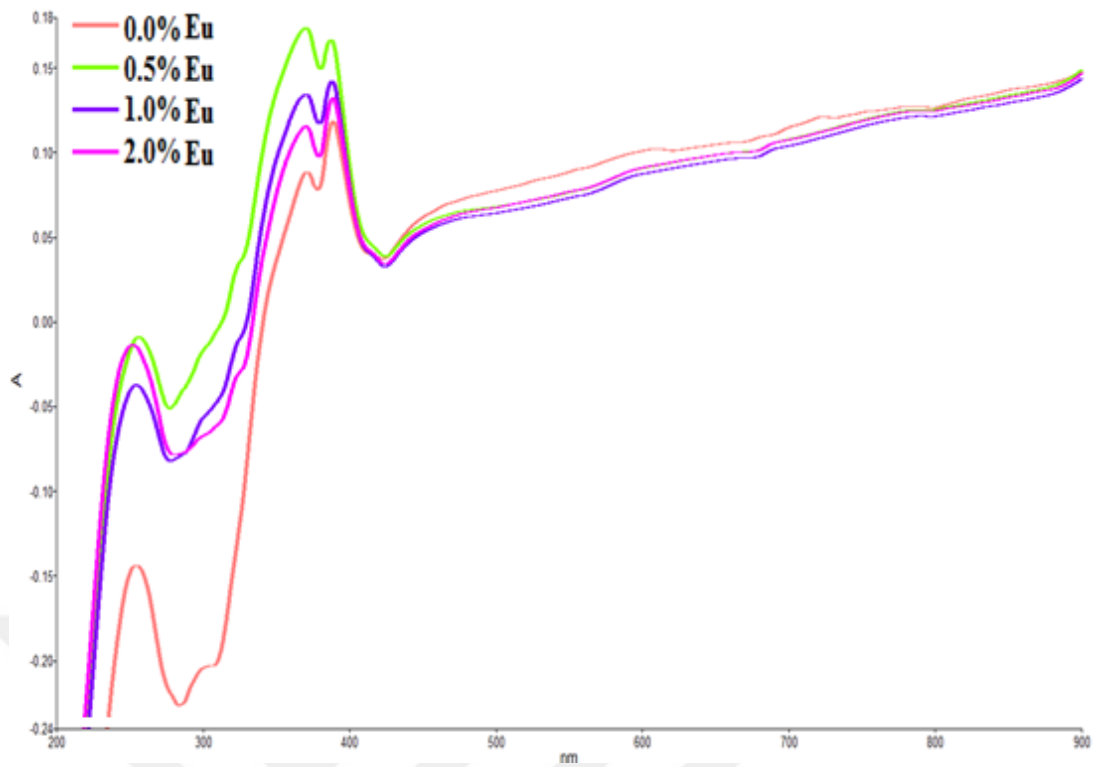


Figure 4.40. UV-VIS Absorbance Spectra of Eu^{3+} Doped $\text{Sr}_2\text{B}_2\text{O}_5$ at 800°C

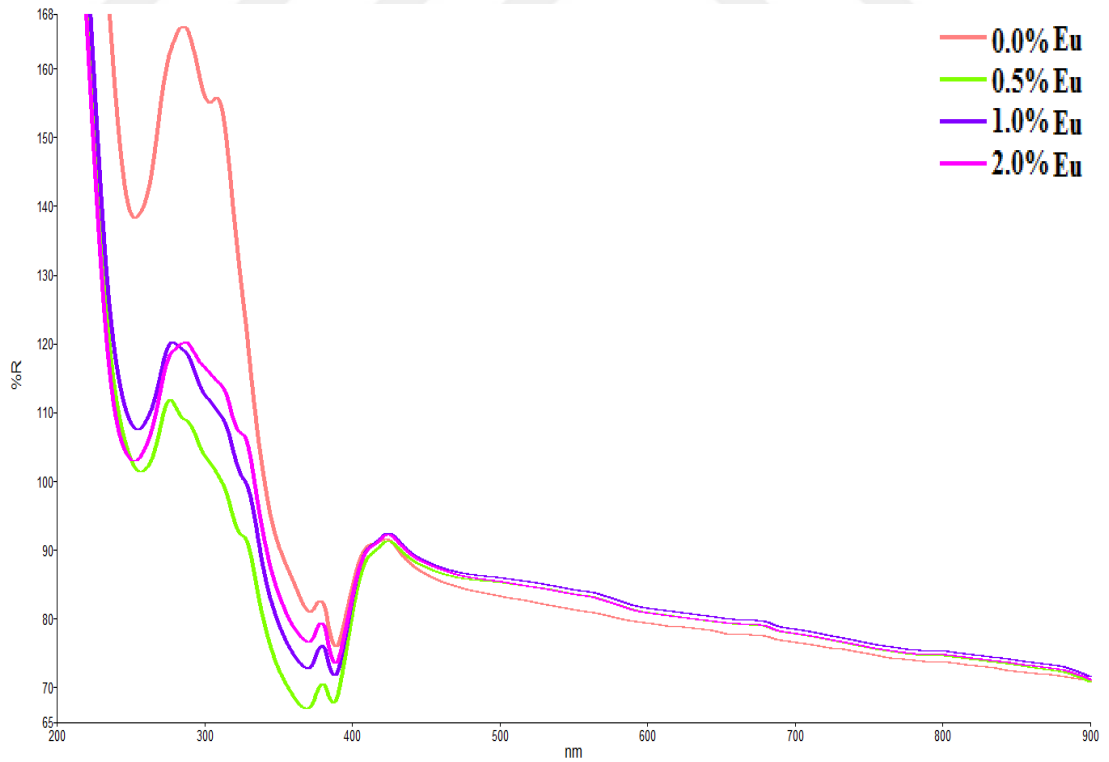


Figure 4.41. UV-VIS Reflectance Spectra of Eu^{3+} Doped $\text{Sr}_2\text{B}_2\text{O}_5$ at 800°C

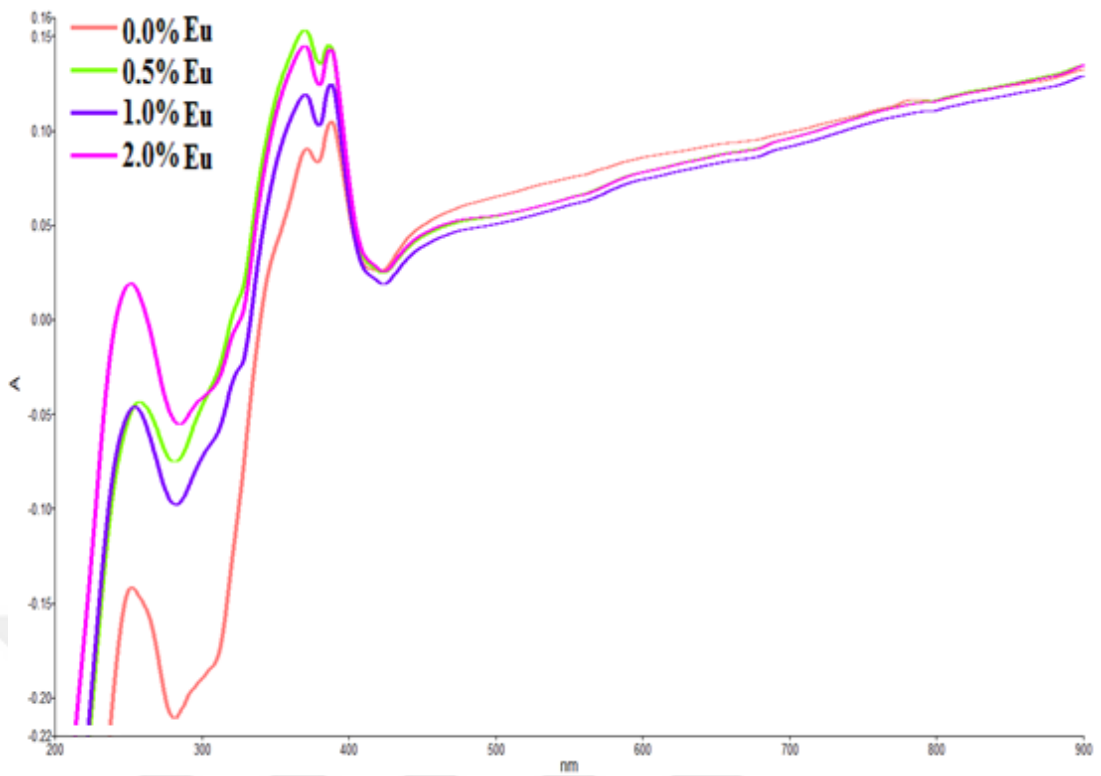


Figure 4.42. UV-VIS Absorbance Spectra of Eu^{3+} Doped $\text{Sr}_2\text{B}_2\text{O}_5$ at 900°C

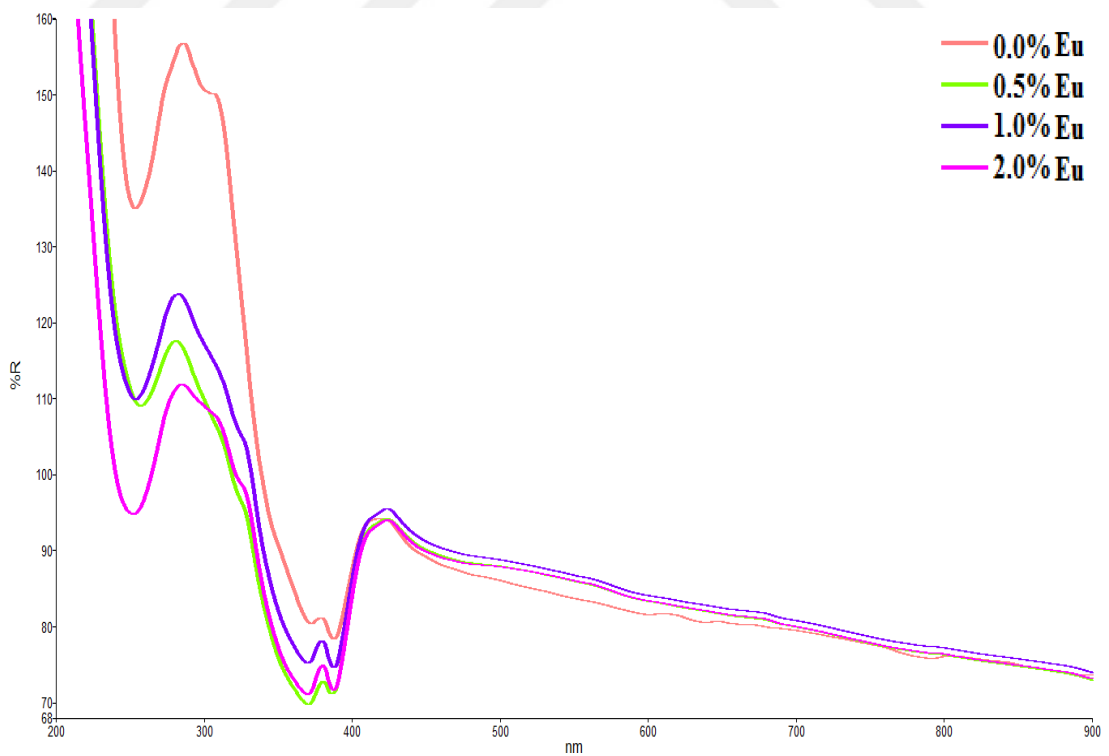


Figure 4.43. UV-VIS Reflectance Spectra of Eu^{3+} Doped $\text{Sr}_2\text{B}_2\text{O}_5$ at 900°C

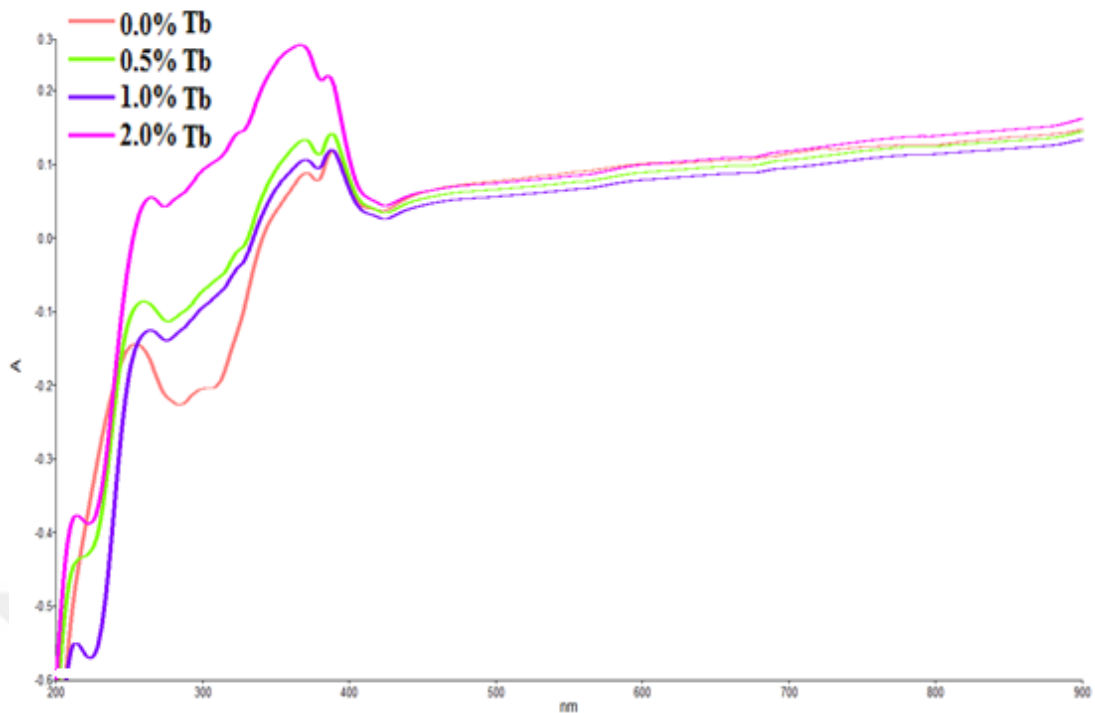


Figure 4.44. UV-VIS Absorbance Spectra of Tb^{3+} Doped $Sr_2B_2O_5$ at $800^\circ C$

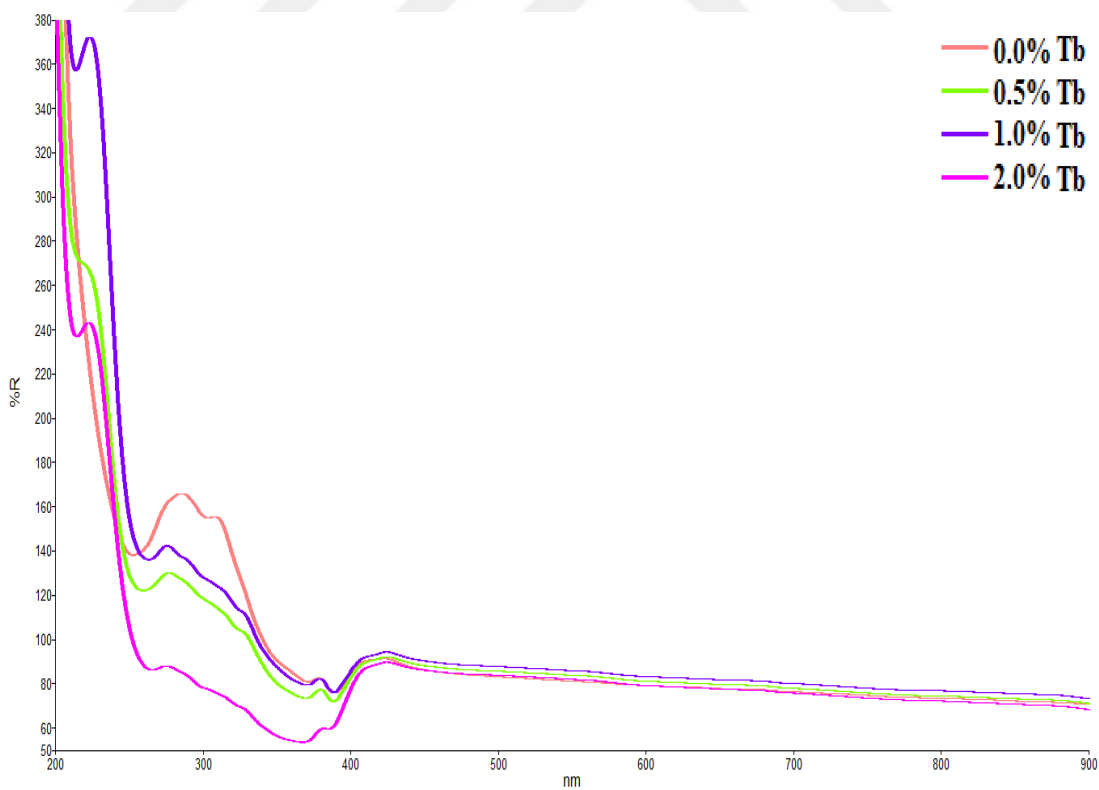


Figure 4.45. UV-VIS Reflectance Spectra of Tb^{3+} Doped $Sr_2B_2O_5$ at $800^\circ C$

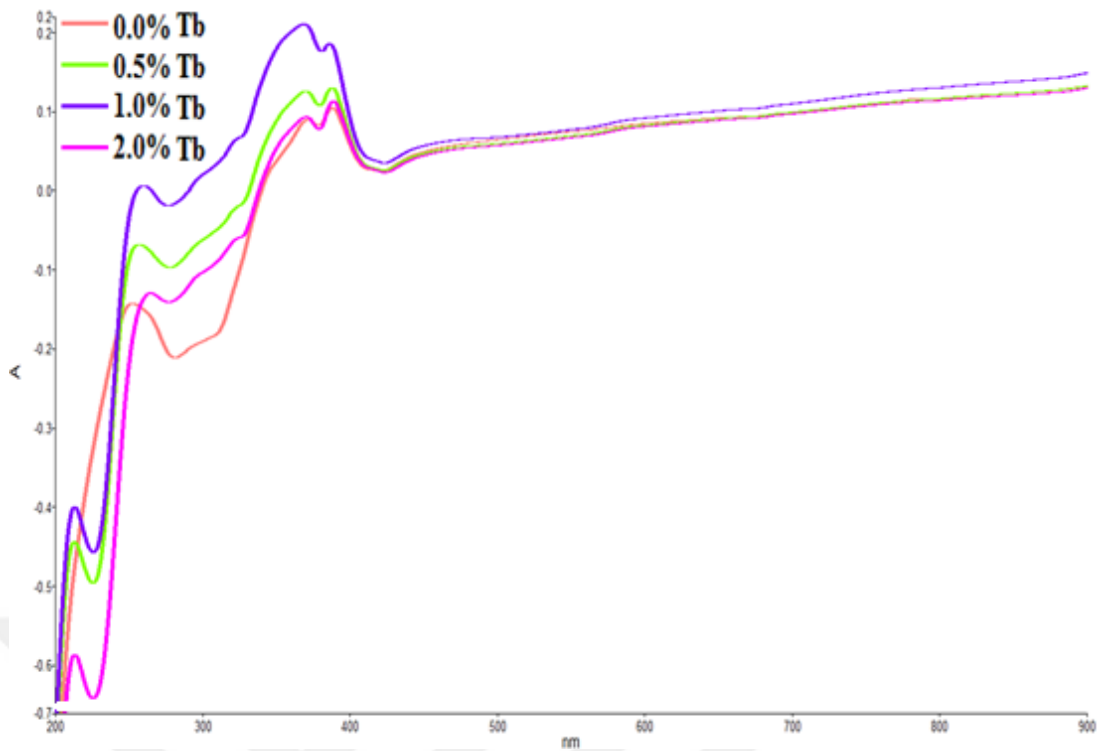


Figure 4.46. UV-VIS Absorbance Spectra of Tb^{3+} Doped $Sr_2B_2O_5$ at $900^\circ C$

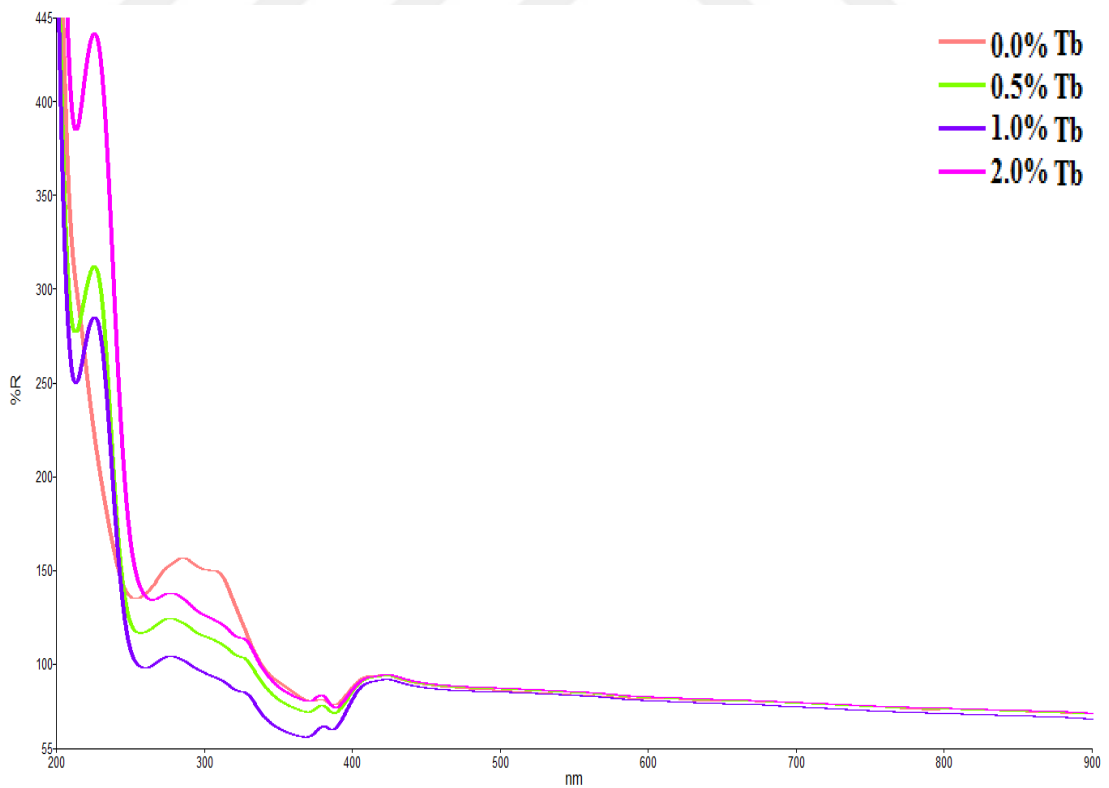


Figure 4.47. UV-VIS Reflectance Spectra of Tb^{3+} Doped $Sr_2B_2O_5$ at $900^\circ C$

The optical band gap energy of as-prepared product at 800°C and 900°C were determined using UV-VIS absorbance data by taking the intercept of the curve on the energy in the x-axis and all results are shown in Table 4.7.

Table 4.7. Optical Band Gap Energy of Undoped and Ln Doped Sr₂B₂O₅

Strontium Pyroborates	Band Gap (eV)	
	800 °C	900 °C
Undoped	4.88	4.88
2.0% Ce ³⁺	5.70	5.99
1.0% Ce ³⁺	5.54	5.83
0.5% Ce ³⁺	5.46	5.66
2.0% Eu ³⁺	5.27	5.08
1.0% Eu ³⁺	5.17	5.00
0.5% Eu ³⁺	5.22	5.02
2.0% Tb ³⁺	5.35	5.45
1.0% Tb ³⁺	5.04	5.36
0.5% Tb ³⁺	5.24	5.40

The band gap energy of undoped and lanthanide element doped strontium pyroborates were examined by using Tauc Plot. The effects of temperatures and dopants concentrations were also determined. The results showed that, the band gap energies are increasing by temperature except for europium ion doped Sr₂B₂O₅ which decrease in their band gap energy. According to the dopant concentrations, band gap energies are by the types of dopant. For Ce³⁺ doped Sr₂B₂O₅, the decrease in band gap energy was observed by decreasing the concentrations as shown in Figure 4.48 and Figure 4.49 for the product that was obtained at 800°C and 900°C, respectively. However, Eu³⁺ and Tb³⁺ ions doped products have different behavior with Ce³⁺ where the lowest band gap energy was observed with 1.0% dopant concentration. The Tauc Plot of Eu³⁺ ion doped products were given in Figure 4.50 and Figure 4.51 (800°C and 900°C). Lastly, Figure 4.52 and Figure 4.53 belong to the Tauc plot of Tb³⁺ ion doped products which were obtained at 800°C and 900°C, respectively.

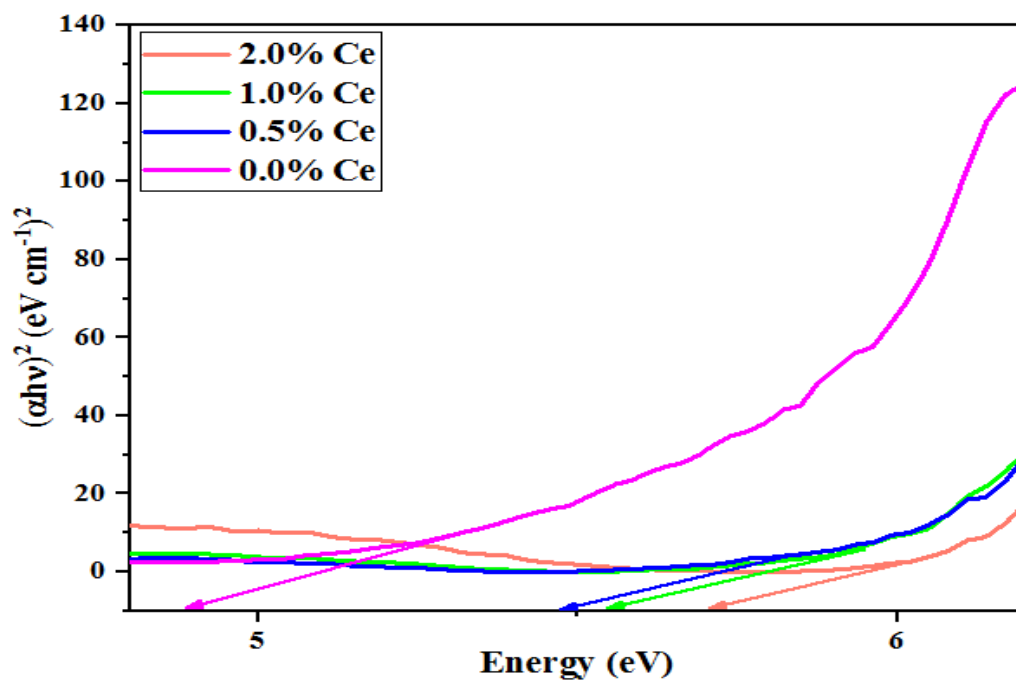


Figure 4.48. Optical Band Gap Energy of Ce^{3+} Doped $\text{Sr}_2\text{B}_2\text{O}_5$ at 800°C

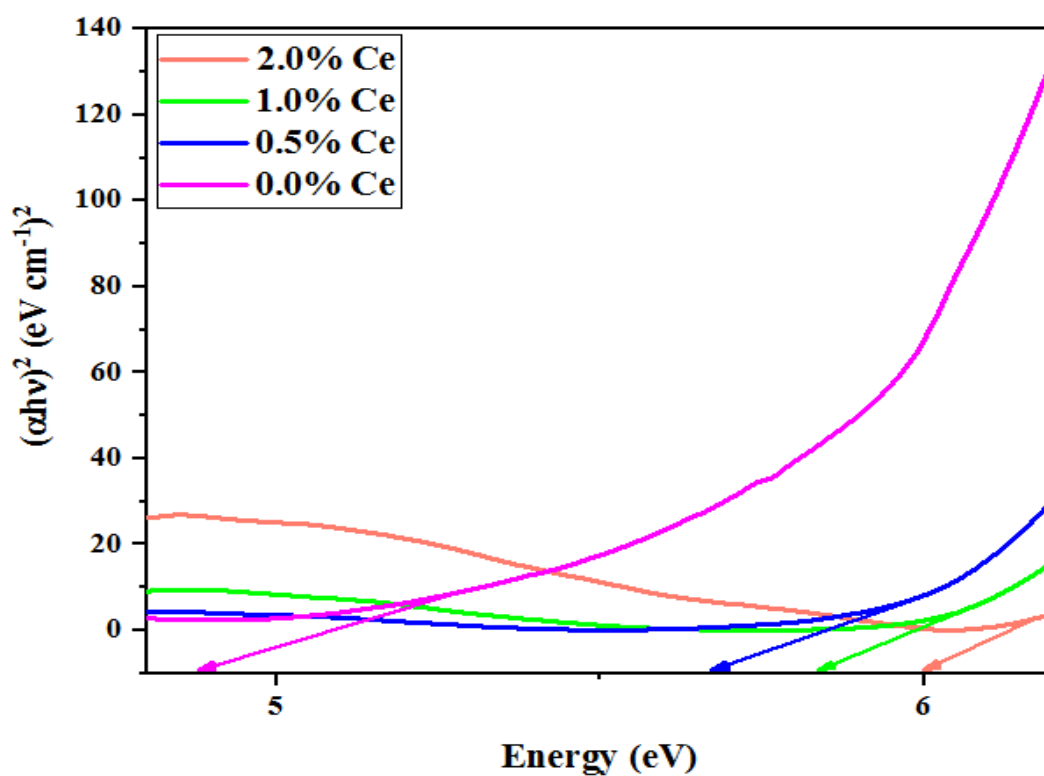


Figure 4.49. Optical Band Gap Energy of Ce^{3+} Doped $\text{Sr}_2\text{B}_2\text{O}_5$ at 900°C

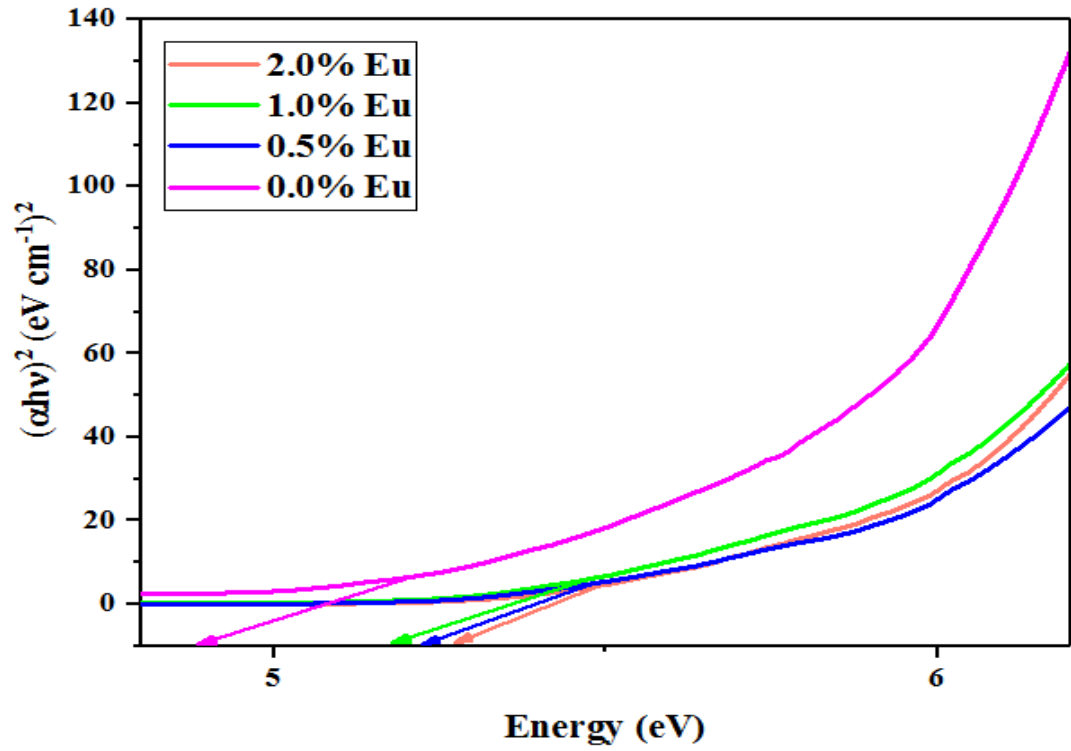


Figure 4.50. Optical Band Gap Energy of Eu^{3+} Doped $\text{Sr}_2\text{B}_2\text{O}_5$ at 800°C

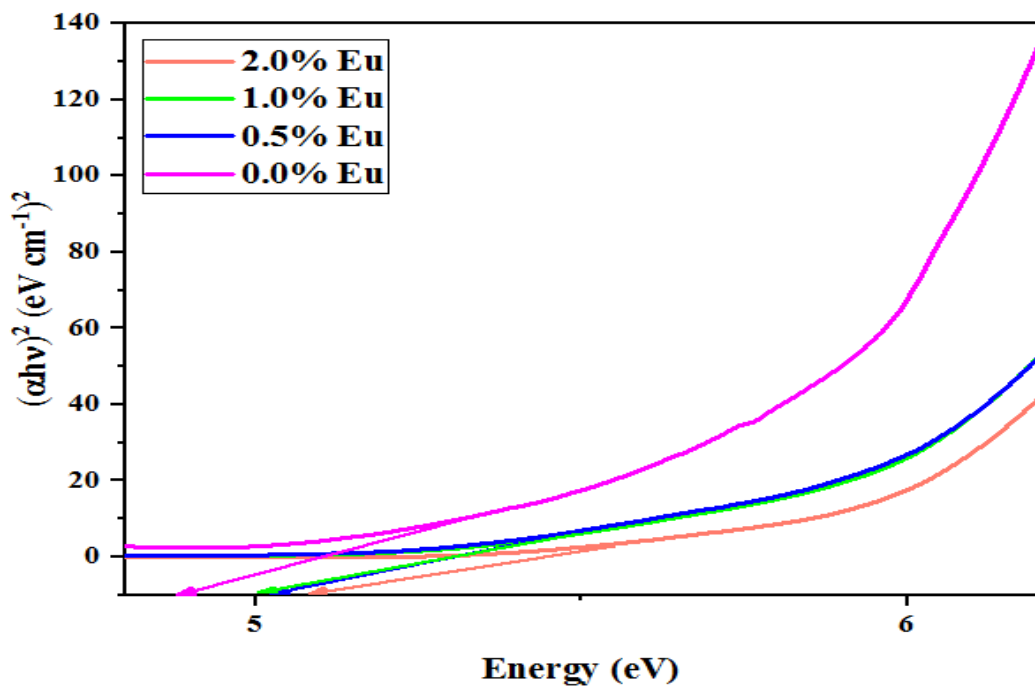


Figure 4.51. Optical Band Gap Energy of Eu^{3+} Doped $\text{Sr}_2\text{B}_2\text{O}_5$ at 900°C

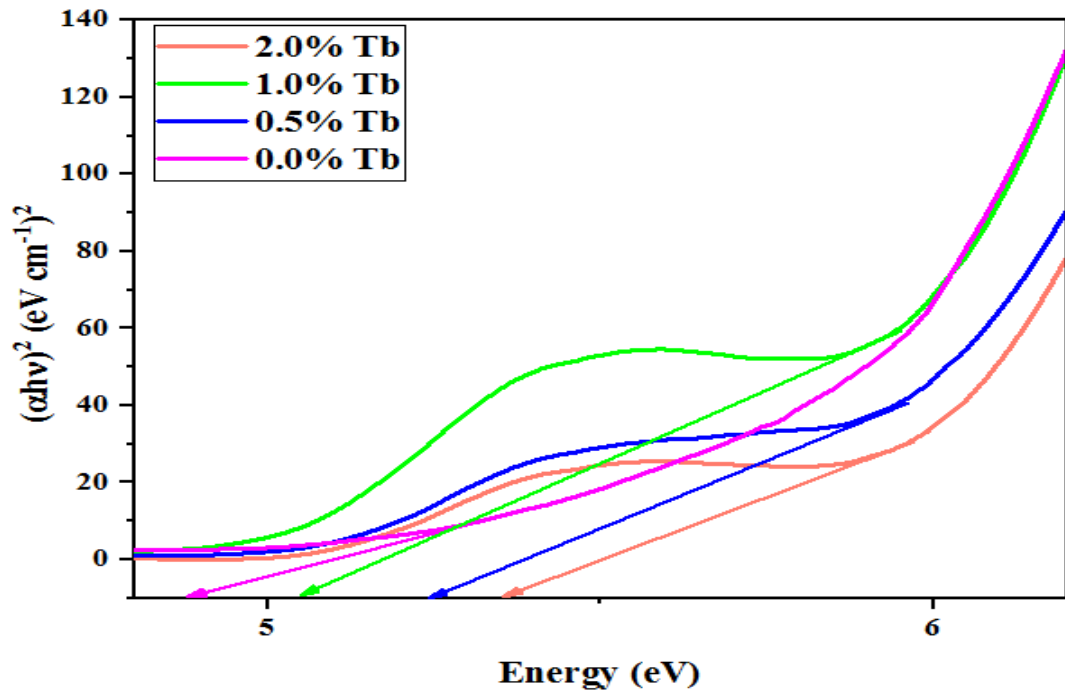


Figure 4.52. Optical Band Gap Energy of Tb^{3+} Doped $Sr_2B_2O_5$ at $800^\circ C$

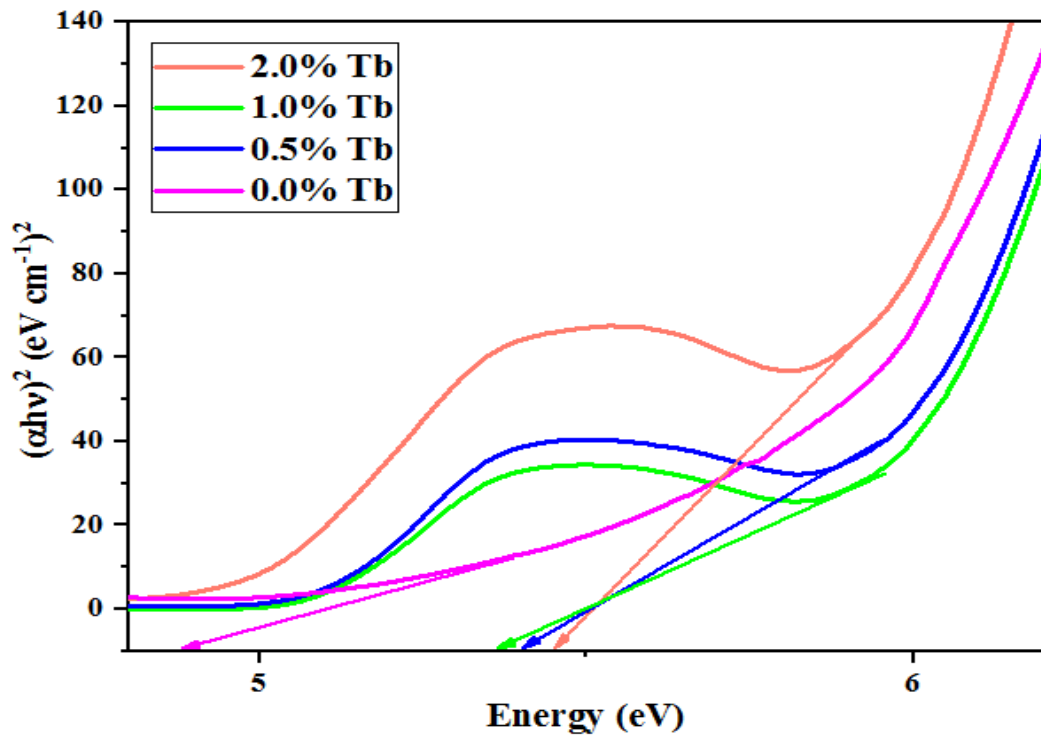


Figure 4.53. Optical Band Gap Energy of Tb^{3+} Doped $Sr_2B_2O_5$ at $900^\circ C$

5. CONCLUSION

Single phase undoped $\text{Sr}_2\text{B}_2\text{O}_5$ nanoparticles were synthesized by Solution Combustion Synthesis method, which is economical and effective. The pure products were obtained with a low synthesis temperature and short reaction time. The formation of $\text{Sr}_2\text{B}_2\text{O}_5$ was confirmed with FT-IR spectroscopy by analyzing the vibrational modes that occurred between 625 cm^{-1} to 1450 cm^{-1} . The stretching vibrational bands of B-O bond in BO_3 were found at 1450 cm^{-1} whereas BO_3 asymmetric stretching vibrations were observed at 1150 cm^{-1} and the modes at 732 cm^{-1} and 680 cm^{-1} was assigned to the BO_3 bending vibrations. The bands at 1376 cm^{-1} are corresponding to H-O-H bending vibrations.

In XRD analysis, the crystal structure of the products were determined as monoclinic. At the synthesis temperature, the small impurities were observed due to unreacted initial materials which were completely disappeared at 900°C . Moreover, by analyzing the XRD patterns of lanthanide element doped products, the effect of temperature and dopant concentrations on the crystallite size of $\text{Sr}_2\text{B}_2\text{O}_5$ were also studied. It was found that the crystallite size of the products are decreasing with increasing the heating temperature and they were also affected from the nature of the dopant and dopant concentration. Thus, the changed on crystallite size of each lanthanide element doped $\text{Sr}_2\text{B}_2\text{O}_5$ nanoparticles are showed different behaviors.

Through UV-VIS diffuse reflectance spectroscopic studies, the absorbance and reflectance spectra of the products were only observed in the ultraviolet region depending upon the host material, $\text{Sr}_2\text{B}_2\text{O}_5$. According to the temperature changed, it was found that the optical band gap energy of $\text{Sr}_2\text{B}_2\text{O}_5$ remains as the same value even though the temperature was increased. Whereas, the optical band gap energies of lanthanide element doped $\text{Sr}_2\text{B}_2\text{O}_5$ nanopowders showed different behavior where only the band gap energies of europium doped $\text{Sr}_2\text{B}_2\text{O}_5$ was decreasing by increasing temperature.

The effect of dopant concentration on optical band gap energies were also determined. The band gap energies of Ce^{3+} doped $\text{Sr}_2\text{B}_2\text{O}_5$ were observed to be decreased from 5.99-5.66 eV by decreasing the concentration at 900°C . The changed

in optical band gap energies of Eu^{3+} ion doped products were examined and it was found that it has similar behavior with Tb^{3+} ion doped $\text{Sr}_2\text{B}_2\text{O}_5$ which the lowest band gap was obtained at 1.0% concentration and was not decreasing with increasing of temperature.



6. REFERENCES

- Akella A, Keszler DA (1994) "Structure And Eu^{2+} Luminescence Of Dibarium Magnesium Orthoborate", 7.
- Alonso E, Sherman AM, Wallington TJ, Everson MP, Field FR, Roth R, Kirchain RE (2012) "Evaluating Rare Earth Element Availability: A Case with Revolutionary Demand from Clean Technologies" *Environmental Science & Technology*, 46: 3406-3414.
- Aloui-Lebbou O, Goutaudier C, Kubota S, Dujardin C, Cohen-Adad MTh, Pédrini C, Florian P, Massiot D (2001) "Structural and scintillation properties of new Ce^{3+} doped alumino-borate" *Optical Materials*, 16: 77-86.
- Badan C, Esenturk O, Yilmaz A (2012) "Microwave-assisted synthesis of Eu^{3+} doped lanthanum orthoborates, their characterizations and luminescent properties" *Solid State Sciences*, 14: 1710-1716.
- Bai JH, Liu JC (2010) "Solution combustion synthesis and sintering behavior of porous MgAl_2O_4 powders" *Science of Sintering*, 42: 133-141.
- Beatty R (2005) *The Elements: Boron*, Marshall Cavendish, New York.
- Bondzior B, Dereń PJ (2019) "The multi-site emission of Eu^{3+} in $\text{Ba}_2\text{M}(\text{BO}_3)_2$ (M = Mg, Ca) solid-solution" *Journal of Luminescence*, 213: 151-157.
- Boyer D, Bertrand G, Mahiou RA (2003) "Spectroscopic study of the vaterite form $\text{YBO}_3:\text{Eu}^{3+}$ processed by sol-gel technique" *Journal of Luminescence*, 104: 229-237.
- Bünzli JC (2013) *Lanthanides*, First Edition, 1-43, John Wiley & Sons, Inc., Hoboken.
- Cai L Ying L, Zheng J, Fan B, Chen R, Chen C (2014) "Luminescent properties of $\text{Sr}_2\text{B}_2\text{O}_5:\text{Tm}^{3+}, \text{Na}^+$ blue phosphor" *Ceramics International*, 40: 6913-6918.
- Chatterjee KK (2007) "Uses of metals and metallic minerals" New Age International (P) Ltd., Publishers, New Delhi.
- Chauhan AO, Pala, CB, Sawala NS, Omanwar SK (2017) "Combustion synthesis and photoluminescence study of UV emitting $\text{LaBaB}_9\text{O}_{16}$ phosphors" *Journal of Materials Science: Materials in Electronics*, 28: 7643-7649.
- Cheng WD, Zhang H, Zheng FK, Chen JT, Zhang QE, Pandey R (2000) "Electronic Structures and Linear Optics of $\text{A}_2\text{B}_2\text{O}_5$ (A=Mg,Ca,Sr) Pyroborates" *Chemistry of Materials*, 12: 3591-3594.

- Cotton S (2006) Lanthanide and Actinide Chemistry, First Edition, 280, Wiley, Chichester.
- Diaz A, Keszler DA (1996) "Red, green, and blue Eu^{2+} luminescence in solid-state borates: A structure-property relationship" *Materials Research Bulletin*, 31: 147-151.
- Dinçer O, Ege A (2013) "Synthesis and luminescence of Tb^{3+} doped lithium borate (LiBO_2)" *Journal of Luminescence*, 138: 174-178.
- Elssfah EM, Elsanousi A, Zhang J, Song HS, Tang C (2007) "Synthesis of magnesium borate nanorods" *Materials Letters*, 61: 4358-4361.
- Greenwood NN, Earnshaw A (1997) *Chemistry of The Elements*, 2nd Edition, Butterworth-Heinemann, Oxford, Boston.
- Guo X, Wu H, Pan S, Yang Z, Yu H, Zhang B, Han J, Zhang F (2014) "Synthesis, Crystal Structure, and Characterization of a Congruent Melting Compound Magnesium Strontium MgSrB_2O_5 : Congruent Melting Compound MgSrB_2O_5 " *Zeitschrift für anorganische und allgemeine Chemie*, 640: 1805-1809.
- Hara H, Takeshita S, Isobe T, Nanai Y, Okuno T, Sawayama T, Niikura S (2013) "Glycothermal synthesis and photoluminescent properties of Ce^{3+} doped YBO_3 mesocrystals" *Journal of Alloys and Compounds*, 577: 320-326.
- Hassan F (2011) *Lanthanides and Actinides Chemistry*, 124, Aswan University, Aswan.
- Helvacı C (2005) "MINERALS | Borates, in: *Encyclopedia of Geology*" Elsevier, 510-522.
- Husted R (2000) "A Periodic Table of the Elements at Los Alamos National Laboratory" <https://www.cdc.gov/niosh/docs/2004-101/pdfs/periodic.pdf>, 27 July 2019
- Jiang LH, Zhang YL, Li CY, Hao JQ, Su Q (2007) "Thermoluminescence properties of Ce^{3+} doped $\text{LiSr}_4(\text{BO}_3)_3$ phosphor" *Materials Letters*, 61: 5107-5109.
- Kar Y, Şen N, Demirbaş A (2006) "Boron Minerals in Turkey, Their Application Areas and Importance for the Country's Economy" *Minerals & Energy - Raw Materials Report*, 20: 2-10.
- Kichanov SE, Shevchenko GP, Malashkevich GE, Ivlieva IYu, Bokshyts YuV, Kozlenko DP, Nguyen CT, Lukin EV, Savenko BN, Podurets KM (2018) "Colloidal chemical synthesis, structural and luminescent properties of $\text{YAl}_3(\text{BO}_3)_4:\text{Ce}^{3+}$ phosphors" *Journal of Alloys and Compounds*, 749: 511-516.
- Kistler RB, Helvacı C (1994) "Boron and borates" *Industrial minerals and rocks*, 6: 171-186.

- Klassen NV, Shmurak SZ, Shmyt'ko IM, Strukova GK, Derenzo SE, Weber MJ (2005) "Structure and luminescence spectra of lutetium and yttrium borates synthesized from ammonium nitrate melt" *Nuclear Instruments and Methods in Physics Research Section A: Accelerators, Spectrometers, Detectors and Associated Equipment*, 537: 144-148.
- Koo HY, Jung DS, Ju SH, Hong SK, Kang YC (2006) "Effect of preparation temperature on the characteristics of Eu-doped borate phosphor particles in the spray pyrolysis" *Materials Letters*, 60: 3091-3095.
- Kumar RS, Ponnusamy V, Sivakumar V, Jose MT (2014) "Role of monovalent co-dopants on the PL emission properties of $\text{YAl}_3(\text{BO}_3)_4:\text{Ce}^{3+}$ phosphor" *Journal of Rare Earths*, 32: 927-932.
- Kwon IE, Yu BY, Bae H, Hwang YJ, Kwon TW, Kim CH, Pyun CH, Kim SJ (2000) "Luminescence properties of borate phosphors in the UV/VUV region" *Journal of Luminescence*, 87-89: 1039-1041.
- Li Y, Fan Z, Lu JG, Chang RPH (2004) "Synthesis of Magnesium Borate ($\text{Mg}_2\text{B}_2\text{O}_5$) Nanowires by Chemical Vapor Deposition Method" *Chemistry of Materials*, 16: 2512-2514.
- Lin Q (1999) "Crystal and Electronic Structures and Linear Optics of Strontium Pyroborate" *Journal of Solid State Chemistry*, 144: 30-34.
- Liu Q, Zheng Z, Zhang X, Bai Z (2015) "Structure, properties and luminescence mechanism of $\text{Sr}_{1.93}\text{B}_2\text{O}_5:0.07\text{Eu}^{3+}$ red phosphors" *Journal of Alloys and Compounds*, 628: 298-302.
- Liu QS, Zheng ZY, Cheng LQ, Zhang XY, Song Y, Liu JW, Cui T (2013) "CRYSTAL STRUCTURE AND LUMINESCENT PROPERTIES OF $\text{Sr}_2\text{B}_2\text{O}_5:\text{Eu}^{2+}$ BLUE PHOSPHORS" *Functional Materials Letters*, 06: 1350034.
- Lu CH, Godbole SV, Natarajan V (2005) "Luminescence characteristics of strontium borate phosphate phosphors" *Materials Chemistry and Physics*, 94: 73-77.
- Lu CH, Godbole SV, Qureshi M (2006) "Luminescence and Energy Transfer Characteristics of Tb^{3+} and Ce^{3+} Co-doped BaBPO_5 Phosphors" *Japanese Journal of Applied Physics*, 45: 2606-2611.
- Lucas F, Jaulmes S, Quarton M, Le Mercier T, Guillen F, Fouassier C (2000) "Crystal Structure of $\text{SrAl}_2\text{B}_2\text{O}_7$ and Eu^{2+} Luminescence" *Journal of Solid State Chemistry*, 150: 404-409.
- Malandrino G, Nigro RL, Fragalà IL (2007) "Magnesium hydrotris (1-pyrazolyl) borate as a promising single source MOCVD precursor of magnesium borate phases" *Inorganica Chimica Acta*, 360: 1138-1142.

- Mansuy C, Nedelec JM, Dujardin C, Mahiou R (2007) “Concentration effect on the scintillation properties of sol–gel derived LuBO₃ doped with Eu³⁺ and Tb³⁺” *Optical Materials*, 29: 697-702.
- Mansuy C, Nedelec JM, Dujardin C, Mahiou R (2004) “Scintillation of Sol-Gel Derived Lutetium Orthoborate Doped with Ce³⁺ Ions” *Journal of Sol-Gel Science and Technology*, 32: 253-258.
- Mehmood M (2018) “Rare Earth Elements- A Review” *Journal of Ecology & Natural Resources* 2.
- Mukasyan AS, Epstein P, Dinka P (2007) “Solution combustion synthesis of nanomaterials” *Proceedings of the Combustion Institute*, 31: 1789-1795.
- Nair RG, Nigam S, Sudarsan V, Vatsa RK, Jain VK (2018) “YBO₃ versus Y₃BO₆ host on Tb³⁺ luminescence” *Journal of Luminescence*, 195: 271–277.
- Narlikar AV (2005) “Frontiers in Magnetic Materials” Springer Science & Business Media.
- Panse VR, Kokode NS, Yerpude AN, Dhoble SJ (2016) “Combustion synthesis of Sr₂B₂O₅:Tb³⁺ green emitting phosphor for solid state lighting” *Optik*, 127: 1603-1606.
- Schaffers KI, Keszler DA (1994) “Tetrahedral Triangular 3-D Framework and Europium Luminescence in the Borate BaBe₂(BO₃)₂” *Inorganic Chemistry*, 33: 1201-1204.
- Shan F, Zhang G, Zhang X, Xu T, Wu Y, Fu Y, Wu Y (2015) “Growth and spectroscopic properties of Tb³⁺ doped Na₃La₉O₃(BO₃)₈ crystal” *Journal of Crystal Growth*, 424: 1–4.
- Shyichuk A, Lis S, Meinrath G (2014) “Structure modeling of terbium doped strontium-lanthanum borate” *Journal of Rare Earths*, 32: 248-253.
- Sun J, Lai J, Zhu J, Xia Z, Du H (2012) “Luminescence properties and energy transfer investigations of Sr₂B₂O₅: Ce³⁺, Tb³⁺ phosphors” *Ceramics International*, 38: 5341-5345.
- Sun JY, Lai JL, Sun YN, Xia ZG, Du HY (2012) “Luminescence Properties of Ce³⁺ and Tb³⁺ Doped Strontium Pyroborate Phosphors” *Advanced Materials Research*, 502: 140-143.
- Ternane R, Cohen-Adad MT, Panczer G, Goutaudier C, Dujardin C, Boulon G, Kbir-Ariguib N, Trabelsi-Ayedi M (2002) “Structural and luminescent properties of new Ce³⁺ doped calcium borophosphate with apatite structure” *Solid State Sciences*, 4: 53–59.

- Volkov S, Dušek M, Bubnova R, Krzhizhanovskaya M, Ugolkov V, Obozova E, Filatov S (2017) “Orientational order-disorder $\gamma \leftrightarrow \beta \leftrightarrow \alpha' \leftrightarrow \alpha$ phase transitions in $\text{Sr}_2\text{B}_2\text{O}_5$ pyroborate and crystal structures of β and α phases” *Acta Crystallographica Section B Structural Science, Crystal Engineering and Materials*, 73:1056-1067.
- Wang F, Song H, Pan G, Fan L, Dong B, Liu L, Bai X, Qin R, Ren X, Zheng Z, Lu S (2008) “Luminescence properties of Ce^{3+} and Tb^{3+} ions co-doped strontium borate phosphate phosphors” *Journal of Luminescence*, 128: 2013-2018.
- Wang JF, Liang P (2019) “Thermochemical properties of alkaline-earth metals borates of a series of $\text{MB}_8\text{O}_{11}(\text{OH})_4 \cdot x\text{H}_2\text{O}$ ($\text{M}=\text{Ca}, \text{Sr}, \text{Ba}; x=0,3$)” *The Journal of Chemical Thermodynamics*, 134: 1-4.
- Wang R, Xu J, Chen C (2012) “Luminescent characteristics of $\text{Sr}_2\text{B}_2\text{O}_5:\text{Tb}^{3+}, \text{Li}^+$ green phosphor” *Materials Letters*, 68: 307-309.
- Woods WG (1994) “An Introduction to Boron: History, Sources, Uses, and Chemistry” *Environmental Health Perspectives*, 102: 7.
- Yang F, Pan SK, Ding DZ, Chen XF, Feng H, Ren GH (2010) “Crystal growth and luminescent properties of the Ce-doped $\text{Li}_6\text{Lu}(\text{BO}_3)_3$ ” *Journal of Crystal Growth*, 312: 2411-2414.
- Yang F, Pan SK, Ding DZ, Ren GH (2009) “Problems in the growth of Ce^{3+} doped $\text{Li}_6\text{Gd}(\text{BO}_3)_3$ crystals by Czochralski method” *Crystal Research and Technology*, 44: 141-145.
- Yang L, Wan Y, Weng H, Huang Y, Chen C, Seo HJ (2016) “Luminescence and color center distributions in $\text{K}_3\text{YB}_6\text{O}_{12}:\text{Ce}^{3+}$ phosphor” *Journal of Physics D: Applied Physics*, 49: 325303.
- Yazici AN, Doğan M, Kafadar VE, Toktamiş H (2006) “Thermoluminescence of undoped and Ce-doped BaB_4O_7 ” *Nuclear Instruments and Methods in Physics Research Section B: Beam Interactions with Materials and Atoms*, 246: 402-408.
- Yildiz E, Erdoğan E (2018) “Investigation of luminescence properties of Pb^{2+} doped $\text{Sr}_2\text{B}_2\text{O}_5$ phosphor” *International Journal of Applied Ceramic Technology*, 15: 1287-1291.
- Yıldız E, Erdoğan E (2018) “Luminescence concentration quenching of Pb^{2+} single doped and $\text{Pb}^{2+}/\text{Dy}^{3+}$ co-doped strontium tetraborate phosphor” *Journal of Luminescence*, 204: 1-4.
- Ying LL, Zheng SS, Zheng JH, Cai LH, Chen C (2014) “Characterization and Photoluminescence of $\text{Sr}_2\text{B}_2\text{O}_5:\text{Eu}^{3+}, \text{Na}^+$ Red Phosphor”, *Advanced Materials Research*, 1003: 7-10.

Zhang X, Lang H, Jin Seo H (2011) “On the Luminescence of Ce^{3+} , Eu^{3+} , and Tb^{3+} in Novel Borate $LiSr_4(BO_3)_3$ ” *Journal of Fluorescence*, 21: 1111-1115.

Zhi-Gang D, You-Fen L, Gang L, Ru Y (2016) “Preparation and Down-conversion Luminescent Properties of Tb^{3+} , Yb^{3+} co-doped $Sr_2B_2O_5$ ” *Journal of Inorganic Materials*, 31: 1081.

Zhou B, Li Z, Chen C (2017) “Global Potential of Rare Earth Resources and Rare Earth Demand from Clean Technologies” *Minerals*, 7: 203.



7. CURRICULUM VITAE

Name SURNAME : Fatma YALÇIN

Place and Date of Birth : Çankırı, TURKEY, 27.07.1993

Adress : Feneryolu Mah. Mashar Osman Sok. Ferah
Apt. No:24 Kadıköy İSTANBUL, TURKEY

e-mail : fatmayalciin@gmail.com

Education

Bachelor's Degree : Bolu Abant İzzet Baysal University